



1 **The CAMS interim Reanalysis of Carbon Monoxide, Ozone**  
2 **and Aerosol for 2003–2015**

3 **J. Flemming<sup>1</sup>, A. Benedetti<sup>1</sup>, A. Inness<sup>1</sup>, R. Engelen<sup>1</sup>, L. Jones<sup>1</sup>, V. Huijnen<sup>2</sup>, S.**  
4 **Remy<sup>3</sup>, M. Parrington<sup>1</sup>, M. Suttie<sup>1</sup>, A. Bozzo<sup>1</sup>, V.-H. Peuch<sup>1</sup>, D. Akritidis<sup>4</sup> and E.**  
5 **Katragkou<sup>4</sup>**

6 [1] European Centre for Medium-Range Weather Forecasts, Reading, UK

7 [2] Royal Netherlands Meteorological Institute, De Bilt, The Netherlands

8 [3] Laboratoire de météorologie dynamique, UPMC/CNRS, Paris, France

9 [4] Department of Meteorology and Climatology, Aristotle University of Thessaloniki, School  
10 of Geology, Thessaloniki, Greece

11

12

13

14 Correspondence to: J. Flemming (Johannes.Flemming@ecmwf.int)

15

16

17

18

19



20 **Abstract**

21 A new global reanalysis data set of atmospheric composition (AC) for the period 2003–2015  
22 has been produced by the Copernicus Atmosphere Monitoring Service (CAMS). Satellite  
23 observations of total column (TC) carbon monoxide (CO) and aerosol optical depth (AOD) as  
24 well as several TC and profile observation of ozone have been assimilated with the Integrated  
25 Forecasting System for Composition (C-IFS) of the European Centre for Medium-Range  
26 Weather Forecasting. Compared to the previous MACC reanalysis (MACCRA), the new  
27 CAMS interim reanalysis (CAMSIRA) is of a coarser horizontal resolution of about 110 km  
28 compared to 80 km but covers a longer period with the intent to be continued to present day.  
29 This paper compares CAMSiRA against MACCRA and a control experiment (CR) without  
30 assimilation of AC retrievals. CAMSiRA has smaller biases than CR with respect to  
31 independent observations of CO, AOD and stratospheric ozone. However, ozone at the  
32 surface could not be improved by the assimilation. The assimilation of AOD led to a global  
33 reduction of sea salt and desert dust as well as an exaggerated increase in sulphate. Compared  
34 to MACCRA, CAMSiRA had smaller biases for AOD, surface CO and TC ozone as well as  
35 for upper stratospheric and tropospheric ozone. Finally, the temporal consistency of  
36 CAMSiRA was clearly better than the one of MACCRA. This was achieved by using a  
37 revised emission data set as well as by applying a careful selection and bias-correction of the  
38 assimilated retrievals. CAMSiRA is therefore better suited than MACCRA for the study of  
39 inter-annual variability than MACCRA as demonstrated for trends in surface CO.  
40



## 41 1 Introduction

42 Exploiting the multitude of satellite observations of atmospheric composition (AC) is a key  
43 objective of the Copernicus Atmosphere Monitoring Service (CAMS). For its global  
44 component CAMS uses the four-dimensional variational (4D-VAR) data assimilation  
45 technique to combine satellite observations with chemistry-aerosol modelling to obtain a  
46 gridded continuous representation (analysis) of the mass mixing ratios of atmospheric trace  
47 gases and aerosols.

48 The global CAMS system is built on the heritage of the EU-funded GEMS (Hollingsworth et  
49 al., 2008) and series of MACC projects at the European Centre for Medium-Range Weather  
50 Forecasts (ECMWF). During these projects the Integrated Forecasting System (IFS) of  
51 ECMWF was extended by modules for atmospheric chemistry, aerosols and greenhouse gases  
52 in such a way that the 4D-VAR data assimilation system, which had been developed for the  
53 analysis of the meteorological fields, could be used for the assimilation of AC retrievals.

54 Assimilating satellite AC retrievals into an AC model has advantages to the sole use of the  
55 AC retrievals because of their specific limitations. First, only a small subset of the trace gases  
56 or only total aerosol is directly observable with sufficient accuracy. Second, AC satellite  
57 retrievals have incomplete horizontal coverage because of the orbital cycle, viewing  
58 geometry, the presence of clouds and other factors such as surface properties. Third, the  
59 vertical distribution of the trace species can often not or only rather coarsely be retrieved from  
60 the satellite observations, while the measurement sensitivity towards the surface is generally  
61 low.

62 The AC analyses are used to (i) initialise AC model forecasts and (ii) for the retrospective  
63 analysis (reanalysis) of AC for air quality and climate studies. The reanalysis of the  
64 meteorological fields has been an important activity at ECMWF (ERA-40, Uppala et al.,  
65 2005, ERA interim Dee et al., 2011) and other meteorological centres such as NCEP (CFSR,  
66 Saha et al., 2010, JMA (JRA-55, JRA-25, Onogi et al., 2007) and NASA/DAO (MERRA,  
67 Rienecker, et al., 2011). An important application of these reanalysis data sets is the  
68 estimation of the inter-annual variability and the trends of climate variables over the last  
69 decades up to the present day. The complete spatial and temporal coverage makes the trend  
70 analysis of reanalyses more robust and universal than the trend analysis of individual  
71 observing systems. However, constructing a data set which is suited for this purpose is a  
72 complex task because of the developing and changing observing system, which can introduce



73 spurious trends and sudden shifts in the reanalysis data record. Careful quality control of the  
74 assimilated observations and techniques (e.g. Dee et al., 2004) to address inter-instrument  
75 biases are applied to mitigate this problem.

76 Most meteorological reanalyses contain stratospheric ozone but other traces gases, apart from  
77 water vapour, are not included. In the last decade chemical and aerosol data assimilation has  
78 matured (Bocquet et al., 2015) and dedicated reanalysis data sets for AC have emerged. The  
79 Multi-Sensor-Reanalysis of total ozone (van der A et al., 2015) for 1970–2012 used ground  
80 based Brewer observations to inter-calibrate satellite retrievals. The MERRAero reanalysis  
81 (2002–present, <http://gmao.gsfc.nasa.gov/reanalysis/merra/MERRAero/>) assimilated AOD  
82 retrievals from the two Moderate Resolution Imaging Spectroradiometer (MODIS) instruments  
83 in the GOCART aerosol module of the GEOS-5 model system using the meteorological  
84 variables of the MERRA meteorological analysis. Its next version, the MERRA2 reanalysis, is  
85 a joint meteorological and aerosol reanalysis covering the period from 1979 to present.  
86 Miyazaki et al. (2015) put together a tropospheric chemistry reanalysis using a Kalman filter  
87 approach for the years 2005–2012. They use the CHASER Chemical transport model (CTM)  
88 to assimilate retrievals of tropospheric ozone and CO profiles, NO<sub>2</sub> tropospheric columns and  
89 HNO<sub>3</sub> stratospheric columns. Their approach tackles two specific challenges of AC data  
90 assimilation. First, they not only correct atmospheric concentrations but also alter the surface  
91 emissions which control the tracer distributions to a large extent. Second, the Kalman filter  
92 develops co-variances of the errors between observed and un-observed species, which are used  
93 to correct un-observed species based on the observations increments.

94 The MACC reanalysis (MACCRA) of reactive gases (Inness et al., 2013) and aerosols for the  
95 period 2003–2012 is an AC reanalysis that covers tropospheric and stratospheric reactive gases  
96 and aerosols as well as the meteorological fields in one consistent data set. MACCRA has  
97 proved to be a realistic data set as shown in several evaluation studies for reactive gases  
98 (Elguindi et al., 2010, Inness et al., 2013, Katragkou et al., 2015 and Gaudel et al., 2015) and  
99 aerosols (Cesnulyte et al., 2014 and Cuevas et al., 2015, ). MACCRA is widely used, for  
100 example, as boundary condition for regional models (Schere et al., 2012, Im et al., 2014,  
101 Giordano et al., 2015), to construct trace gas climatologies for the IFS radiation schemes  
102 (Bechtold et al., 2009), to estimate aerosol radiative forcing (Bellouin et al., 2013), as input to  
103 solar radiation schemes for solar energy applications and to report the current state of aerosol  
104 and CO as part of the climate system (Benedetti et al., 2014., Flemming and Inness, 2014).



105 CAMS is committed to produce a comprehensive high-resolution AC reanalysis in the next  
106 years. The CAMS interim Reanalysis (CAMSiRA) presented here has an interim status  
107 between MACCRA and this planned analysis data set. It was produced at a lower horizontal  
108 resolution (110 km) than the resolution of MACCRA (80 km), and the number of archived  
109 AC fields was limited to selected key species only.

110 The reasons for producing CAMSiRA before the more comprehensive reanalysis are as  
111 follows: The MACCRA for reactive gases was produced using a coupled system consisting of  
112 the IFS and the MOZART-3 (Kinnison et al., 2007) chemical transport model (CTM) as  
113 described in Flemming et al. (2009). This coupled system was replaced by the much more  
114 computationally efficient on-line coupled model C-IFS (Flemming et al., 2015), which uses  
115 the chemical mechanism CB05 of the TM5 CTM (Huijnen et al., 2010). With the  
116 discontinuation of the coupled system it was not possible to extend the MACC reanalysis to  
117 the present day. For the AC monitoring service of CAMS it is however important to be able to  
118 compare the present conditions with previous years in a consistent way. Another motivation  
119 for producing CAMSiRA was that the aerosol module used for the MACCRA had undergone  
120 upgrades (Morcrette et al., 2011) in recent years. Finally, MACCRA suffered from small but  
121 noticeable shifts because of changes in the assimilated observations, the emission data and the  
122 bias correction approach. These spurious shifts undermine the usefulness of the MACCRA for  
123 the reliable estimation of trends. The lessons learnt from the evaluation of CAMSiRA will  
124 feed into the setup of the planned CAMS reanalysis.

125 Reanalyses of AC are generally less well-constrained by observations than meteorological  
126 reanalyses because of the aforementioned limitations of the AC observations and because of  
127 the strong impact of the emission, which are in many cases not constrained by observations. It  
128 is therefore good scientific practise to investigate the impact of the AC assimilation by  
129 comparing the AC reanalysis to a control experiment that did not assimilate AC observations.  
130 The control run (CR) to CAMSiRA was carried out using the same emission data as well as  
131 the meteorological fields produced by CAMSiRA.

132 The purpose of this paper is firstly to document the model system, the emissions and the  
133 assimilated observations used to produce CAMSiRA, and to highlight the differences to the  
134 setup of the MACCRA. As the emissions are an important driver for variability of AC, a  
135 presentation of the totals and the inter-annual variability of the emission data used in  
136 CAMSiRA and CR is given in a supplement to the paper.



137 In the remainder of the paper, CO, aerosol as well as tropospheric and stratospheric ozone of  
138 CAMSiRA, CR and MACCRA are inter-compared and evaluated with independent  
139 observations in a separate section for each species. The comparison of CAMSiRA with  
140 MACCRA has the purpose to report progress and issues of CAMSiRA for potential users of  
141 the data sets. The comparison of CAMSiRA with CR shows the impact of the data  
142 assimilation and is helpful to better understand deficiencies of the C-IFS model and its input  
143 data.

144 Each section starts with a discussion of the spatial differences of CAMSiRA, CR and  
145 MACCRA of the considered species. Next, the temporal variability is investigated using time  
146 series of monthly mean values averaged over selected regions. We present global burdens and  
147 discuss changes in the speciation of the aerosol fields introduced by the assimilation. Finally,  
148 the three data sets are compared against independent observations, which were not used in the  
149 assimilation. A summary and recommendations for future AC reanalysis will be given in the  
150 last section.

151



## 152 **2 Description of CAMSiRA setup**

### 153 **2.1 Overview**

154 CAMSiRA is a data set of 6 hourly reanalyses of AC for the period 2003–2015. A 3 hourly data  
155 set consistent with the AC analysis is available from forecasts linking the analyses. The  
156 horizontal resolution is about 110 km on a reduced Gaussian grid (T159) and the vertical  
157 discretisation uses 60 levels from the surface to a model top of 0.1 hPa. Total columns of CO  
158 (TC CO) of the Measurements Of Pollution In The Troposphere (MOPITT) instrument, MODIS  
159 AOD and several ozone TC and stratospheric profile retrievals (see Table 2) were assimilated  
160 together with meteorological in-situ and satellite observations.

161 The description of MACCRA for reactive gases can be found in Inness et al. (2013). Important  
162 commonalities and differences between the two AC reanalyses are given in Table 1.

163 The control run is a forward simulation of C-IFS in monthly segments. The meteorological  
164 simulation is relaxed using the approach by Jung et al. (2008) to the meteorological reanalysis  
165 produced by the CAMSiRA. The emission input fields are the same as used for CAMSiRA.

### 166 **2.2 C-IFS model**

167 C-IFS is documented and evaluated in Flemming et al. (2015). C-IFS applies the chemical  
168 mechanism CB05, which describes tropospheric chemistry with 55 species and 126 reactions.  
169 Stratospheric ozone chemistry in C-IFS is parameterized by the “Cariolle-scheme” (Cariolle  
170 and Dèquè, 1986 and Cariolle and Teyssède, 2007). Chemical tendencies for stratospheric and  
171 tropospheric ozone are merged at an empirical interface of the diagnosed tropopause height in  
172 C- IFS. C-IFS benefits from the detailed cloud and precipitation physics of the IFS for the  
173 calculation of wet deposition and lightning NO emission. Wet deposition modelling for the  
174 chemical species is based on Jacob (2000) and accounts for the sub-grid scale distribution of  
175 clouds and precipitation. Dry deposition is modelled using pre-calculated monthly-mean dry  
176 deposition velocities following Wesely (1989) with a superimposed diurnal cycle. Surface  
177 emissions and dry deposition fluxes are applied as surface boundary conditions of the diffusion  
178 scheme. Lightning emissions of NO were calculated based on convective precipitation (Meijer  
179 et al., 2001).

180 The aerosol module (Morcrette et al., 2009) is a bulk/bin scheme simulating desert dust, sea  
181 salt at 80% relative humidity (RH), hydrophilic and hydrophobic organic carbon and black



182 carbon as well as sulphate aerosol based on the LMDZ aerosol model (Reddy et al., 2005). Sea  
183 salt and desert dust are represented in 3 size-bins. The radii ranges of the dust bins are 0.030–  
184 0.55, 0.55–0.9 and 0.9–20  $\mu\text{m}$  (DD1, DD2, and DD3) and of the sea salt at 80% RH bins 0.03–  
185 0.5, 0.5–5 and 5–20  $\mu\text{m}$  (SS1, SS2, and SS3). There is no consideration of the aerosol growth,  
186 which would transfer aerosol mass from one size bin to another. Hygroscopic growth of  
187 hydrophilic species is taken into account in the computation of the aerosol optical properties  
188 only. Following the emission release, the aerosol species are subject to wet and dry deposition  
189 and the largest size bins of sea salt and dust also to sedimentation. The chemical source of  
190 sulphate is modelled by climatological conversion rates using a  $\text{SO}_2$  tracer, which is  
191 independent of the  $\text{SO}_2$  simulated in CB05. The  $\text{SO}_2$  tracer is driven by prescribed  $\text{SO}_2$  and  
192 DMS emissions. Its loss is simulated by wet and dry deposition as well as the climatological  
193 chemical conversion to  $\text{SO}_4$ .

194 The aerosol and chemistry modules used to simulate source and sink terms are not coupled.  
195 Also, wet and dry deposition are modelled with different parameterisations but with the same  
196 meteorological input such as precipitations fields. Aerosol and chemistry have in common that  
197 they are advected and vertically distributed by diffusion and convection in the same way. A  
198 proportional mass fixer as described in Diamantakis and Flemming (2014) is applied for all  
199 tracers in C-IFS.

### 200 **2.3 Emission data sets**

201 This section only references the origin of the emission data. The emitted totals and the linear  
202 trends of the anthropogenic, biomass burning and natural emissions as well as the modelled  
203 desert dust and sea salt emissions used in CAMSiRA and CR are presented in a supplement.

204 The anthropogenic surface emissions for the chemical species were taken from the MACCity  
205 inventory (Granier et al., 2011), which covers the period 1960–2010. MACCity emissions are  
206 based on the ACCMIP (Lamarque et al., 2013) inventory but have improved seasonal  
207 variability. The changes from 2000–2005 and for 2010 are obtained using the representative  
208 concentration pathways (RCP) scenarios version 8.5. For the production of CAMSiRA the  
209 MACCity data set was extended to 2015 by also applying the RCP 8.5 scenario. The  
210 anthropogenic CO emissions were increased following Stein et al. (2014). Time series of the  
211 anthropogenic CO emissions for Europe, North America, East Asia (see Table 3) and the globe  
212 are shown in Figure S2 of the supplement.





213 The anthropogenic emissions of organic matter, black carbon and aerosol precursor SO<sub>2</sub> are  
214 retrieved from AEROCOM data base, which is compiled using EDGAR and SPEW data  
215 (Dentener et al., 2006). In contrast to the anthropogenic gas emissions, the aerosol  
216 anthropogenic emissions did not account for trends but only for the seasonal cycle.

217 The biogenic emissions for the chemical species were simulated off-line by the MEGAN2.1  
218 model (Guenther et al., 2006) for the 2000–2010 period (MEGAN-MACC, Sindelarova et al.,  
219 2014). For the remaining years 2011–2015 a climatology of the MEGAN-MACC data was put  
220 together. Natural emissions from soils and oceans for NO<sub>2</sub>, DMS and SO<sub>2</sub> were taken from  
221 POET database for 2000 (Granier et al., 2005; Olivier et al., 2003).

222 Daily biomass burning emissions for reactive gases and aerosols were produced by the Global  
223 Fire Assimilation System (GFAS) version 1.2, which is based on satellite retrievals of fire  
224 radiative power (Kaiser et al., 2012). This is an important difference with respect to the  
225 MACCRA, which used an early version of the GFED 3.1 data from 2003 until the end 2008  
226 and daily GFAS v1.0 data from 2009 to 2012. The GFED 3.1 is on average 20% lower than  
227 GFAS v1.2 (Inness et al., 2013). Time series of the biomass burning CO emissions for Tropical  
228 Africa, South America and Maritime South East Asia (see Table 3) and the globe are shown in  
229 Figure S3 of the supplement.

#### 230 **2.4 C-IFS data assimilation**

231 C-IFS uses an incremental 4D-VAR algorithm (Courtier et al., 1994), which minimizes a cost  
232 function for selected control variables to combine the model and the observations in order to  
233 obtain the best possible representations of the atmospheric fields. The mass mixing ratios of O<sub>3</sub>,  
234 CO and total aerosol are incorporated into the ECMWF variational analysis as additional  
235 control variables and are minimized together with the meteorological control variables. The  
236 assimilation of satellite retrieval of the chemical species and total aerosol optical depth is  
237 documented in Inness et al. (2015) and Benedetti et al. (2009). The assimilation of aerosol  
238 differs from the assimilation of CO and ozone because only the total aerosol mass can be  
239 constrained by the observations and information about the speciation must be obtained from the  
240 model.

241 The assimilation of AOD retrievals uses an observation operator that translates the aerosol mass  
242 mixing ratios and humidity fields of C-IFS to the respective AOD (550 nm) values using pre-  
243 computed optical properties. Total aerosol mass mixing ratio is included in the 4D-VAR cost



244 function and the analysis increments are repartitioned into the individual aerosol components  
245 according to their fractional contribution to the total aerosol mass. This is an approximation  
246 which is assumed to be only valid over the 12 hour of the assimilation window. In reality, the  
247 relative fraction of the aerosol components is not conserved during the whole assimilation  
248 procedure because of differences in the efficiency of the removal processes. Aerosol  
249 components with a longer atmospheric lifetime will retain relatively longer the change imposed  
250 by the increments and may thereby change the relative contributions.

251 The background error statistics for the chemical species and for total aerosol are univariate in  
252 order to minimize the feedback effects of the chemical fields on the meteorological variables.  
253 Correlations between the background errors of different chemical species are also not accounted  
254 for (Inness et al., 2015).

255 In the ECMWF data assimilation system the background error covariance matrix is given in a  
256 wavelet formulation (Fisher, 2004, 2006). This allows both spatial and spectral variations of  
257 the horizontal and vertical background error covariances. The background errors for AC are  
258 constant in time.

259 The background errors for ozone are the same as the ones used for MACCRA (Inness et al.,  
260 2013). Only the vertical correlations of the ozone background errors have been modified and  
261 restricted to  $\pm 5$  levels around a model level, to avoid correlations between the lower  
262 troposphere and upper tropospheric and stratospheric levels that affected near-surface ozone  
263 adversely. The background errors of total aerosol for both MACCRA and CAMSiRA were  
264 calculated using the method described in Benedetti and Fisher (2008). The aerosol background  
265 errors for CAMSiRA were updated using a more recent C-IFS model version. The background  
266 errors for CO are newly calculated for the CAMSiRA from an ensemble of C-IFS forecast runs  
267 (Inness et al., 2015).

## 268 **2.5 Assimilated observations**

269 Table 2 shows the AC composition data sets for CO, ozone and AOD that were assimilated in  
270 CAMSiRA. The time line of the assimilation for the different retrievals is shown in Figure 1.  
271 CO is assimilated from MOPITT V5 TIR only whereas the MACCRA assimilated the V4 TIR  
272 product and additionally IASI TC CO retrievals after April 2008. The biases between the  
273 retrievals (George et al., 2015) of the two instruments in mid and higher latitudes could not be  
274 reconciled with the variational bias correction and led to a discontinuity in the time series of



275 CO in MACCRA, which consequently could not be used for trend analyses (see Figure 4  
276 below). It was therefore decided to only use the MOPITT V5 CO data set in CAMSiRA because  
277 it covers the whole period from 2003–2015. The MOPITT V5 product has better long term  
278 stability and a smaller SH bias than V4 (Deeter et al., 2013). V4 suffered from a positive  
279 temporal bias drift and a positive bias in SH.

280 An additional ozone data set in CAMSiRA were the Michelson Interferometer for Passive  
281 Atmospheric Sounding (MIPAS) ozone profiles, which were assimilated from 2005 until the  
282 end of the ENVISAT mission in April 2012. After the end of 2012 the version of the assimilated  
283 Microwave Limb Sounder (MLS) data set changed from V2 to V3.4. Information about the  
284 differences between the two versions can be found in  
285 [https://mls.jpl.nasa.gov/data/v3\\_data\\_quality\\_document.pdf](https://mls.jpl.nasa.gov/data/v3_data_quality_document.pdf)

286 Averaging kernels were used for the calculation of the model's first-guess fields in the  
287 observation operators for the MOPITT data.

288 The AC satellite retrievals were thinned to a horizontal resolution of  $1^\circ \times 1^\circ$  by randomly  
289 selecting an observation in the grid box to avoid oversampling and correlated observation  
290 errors. Variational quality control (Andersson and Järvinen, 1999) and background quality  
291 checks were applied. Only 'good' data were used in the analysis and data flagged as 'bad' by  
292 the data providers were discarded.

293 Variational bias correction (Dee, 2004, McNally et al., 2006, Auligné et al., 2007, Dee and  
294 Uppala, 2009) was applied to the MODIS AOD data, as well as to ozone column data from the  
295 Ozone Monitoring Instrument (OMI), the SCanning Imaging Absorption spectroMeter for  
296 Atmospheric CHartographY (SCIAMACHY) and the Global Ozone Monitoring Experiment 2  
297 (GOME-2). The partial column of the Solar Backscatter Ultraviolet Radiometer 2 (SBUV/2),  
298 MLS and MIPAS were used to anchor the bias correction. Experience from the MACC  
299 reanalysis had shown that it was important to have an anchor for the bias correction to avoid  
300 drifts in the fields (Inness et al., 2013).

301



### 302 **3 Carbon monoxide**

303 Global CTMs tend to underestimate the observed CO values (Shindell et al., 2006) but data  
304 assimilation (Inness et al., 2013 and 2015, Miyazaki et al., 2015, Gaubert et al., 2016) of satellite  
305 retrieval is able to successfully reduce the biases of the simulated CO fields. The correct  
306 representation of vertical CO profiles by the assimilation remains a challenge (Gaudel et al.,  
307 2015). An important next step will be the correct representation of the global CO trends by  
308 means of CO reanalyses such as CAMSiRA.

#### 309 **3.1 Spatial patterns of total column CO**

310 Figure 2 shows the seasonal mean of TC CO over the period 2003–2015 of CAMSiRA and the  
311 differences with CR and MACCRA (2003–2012). Overall, the assimilation of TC CO in  
312 CAMSiRA led to an increase in the northern hemisphere (NH) and a decrease in the Southern  
313 hemisphere (SH) and most of the tropics. CAMSiRA was about 2–5% higher than CR in NH  
314 and up to 20% lower in the SH. The reduction was especially large in the tropical and sub-  
315 tropical outflow regions of the biomass burning regions in South America, Central Africa and  
316 Maritime South East Asia. The largest reduction in these regions occurred in DJF. The largest  
317 negative bias of CR with respect to CAMSiRA occurred over NH in December–February (DJF)  
318 and March–May (MAM). Overall the zonal patterns of the biases throughout all seasons were  
319 rather uniform indicating an underestimation of the hemispheric CO gradient in CR and could  
320 point to deficiencies in the simulation of the global chemical loss and production of CO as well  
321 as problems with the large scale transport. Biases in the amount of the emissions seem to play  
322 a smaller role for the problem with the hemispheric gradient.

323 However, more emission related differences occurred in September–November (SON) and to  
324 a smaller extent in June–August (JJA), when CR had (i) higher values in the biomass burning  
325 regions and the respective outflow regions in Central Africa, Maritime South East Asia and  
326 South America and (ii) lower values in the outflow regions of the emissions in North America  
327 and East Asia in the Eastern and Western Northern Pacific. This suggests that GFAS biomass  
328 burning emissions were too high whereas the anthropogenic emissions in North America and  
329 East Asia were too low. On the other hand, CR had higher values than CAMSiRA in South  
330 Asia, which indicates that the anthropogenic emissions are too high in India.

331 Compared to MACCRA, CAMSiRA was up to 10% higher in the Northern high latitudes and  
332 up to 20% higher above the tropical biomass burning regions and above the parts of East



333 Asia. The differences over the biomass burning regions can be attributed to the different biomass  
334 burning emissions data sets (see section 2.3). Over the oceans in NH and the tropics, apart from  
335 biomass burning outflow regions, CAMSiRA CO is slightly lower (3%) than MACCRA. The  
336 differences in the NH high latitudes are mainly caused by the reduction in MACCRA CO in  
337 this region introduced by the assimilation of IASI CO retrieval after 2008 (see also Figure 4  
338 below).

339 Figure 3 shows the average zonal mean cross section of the average CO mass mixing ratio of  
340 CAMSiRA and the relative difference to CR and MACCRA. The overestimation of CR in the  
341 tropics and SH extratropics was found throughout the troposphere. It was most pronounced in  
342 relative terms at about 500 hPa. Stratospheric CO in CAMSiRA was much lower than in  
343 MACCRA. This might be an improvement as Gaudel et al. (2015) report an overestimation in  
344 the MACCRA over this region. In the upper troposphere CAMSiRA had higher CO than  
345 MACCRA most notably in the tropics and SH where values are up to 40% higher. CO was  
346 lower in the mid and lower troposphere in SH and higher in NH. These differences in the  
347 vertical distribution might be caused by (i) a more consistent modelling approach of the  
348 stratosphere-troposphere exchange with the on-line coupled C-IFS, (ii) the fact that C-IFS  
349 CB05 has a very different chemistry treatment compared to MOZART and (iii) updated  
350 background error statistics for CO (see Table 1).

### 351 **3.2 Inter-annual variability of CO burden**

352 Figure 4 shows time series of the monthly mean CO burden from CAMSiRA, MACCRA and  
353 CR for selected areas (see Table 3). Then modelled global CO burden (CR) was reduced by the  
354 assimilation by about 3% at the start and by about 7% at the end of the period. CAMSiRA  
355 showed a stepwise decrease of the global CO burden from 2008 and 2009 which corresponds  
356 to a significant negative linear trend of  $-0.86\%/yr$  over the whole period. This figure is in good  
357 agreement with the results of Worden et al. (2013) who estimates trends of  $-1\%$  per year for  
358 both the globe and NH over the last decade by studying different satellite-based instruments.  
359 CR also showed the largest decrease in the period from 2007–2009 but the CO burden increased  
360 slightly after that period. The resulting linear trend of CR was still negative ( $-0.36\%/yr$ ) but less  
361 strong than the trend of CAMSiRA.

362 The higher global CO burdens of CR with respect to CAMSiRA originated mainly from the  
363 tropics and the SH mid-latitudes, which are strongly influenced by biomass burning emissions



364 in tropical Africa and South America. CO was reduced by the assimilation in CAMSiRA  
365 especially after the start of the biomass burning season. The reduction of the biomass burning  
366 emissions of -7.4%/yr (see supplement Table S1) over South America led to a significant  
367 negative trend of the CO burden of -1.23%/yr in CAMSiRA and -0.83%/yr in CR over that  
368 region. The overestimation of CR with respect to CAMSiRA increased slightly during the  
369 period.

370 2015 was an exceptional year because the global CO burden reached the highest values in the  
371 whole period for both CAMSiRA and CR despite the overall decadal negative trend. The  
372 increase was caused by exceptionally high biomass burning emissions in Indonesia because of  
373 El Niño related dry conditions. The El Niño controlled inter-annual variability of CO over  
374 Maritime South East Asia was reproduced in a very similar way in CAMSiRA and CR but the  
375 assimilation reduced the burden by about 1 Tg (10%).

376 In the regions of high anthropogenic emissions the temporal variability at a monthly scale was  
377 very similar between CR and CAMSiRA. Both in North America and Europe CR  
378 underestimated the CO maximum of CAMSiRA in early spring by less than 5% up to the year  
379 2010 but the biases almost disappeared in later years. This means that the negative total CO  
380 trend in these regions was larger in CAMSiRA, which contains the MOPITT observations, than  
381 in CR. It could indicate that the anthropogenic emissions were biased low at the beginning of  
382 the period but less so towards the end. Over East Asia the difference between CR and  
383 CAMSiRA was generally very small indicating a high degree of realism of the emissions in the  
384 area. A further explanation for this agreement is the fact that this area covers both the  
385 underestimation of CAMSiRA by CR in NH mid-latitudes and the overestimation in the tropics.  
386 Both CAMSiRA and CR had a negative but not a significant trend over East Asia.

387 Stroden et al. (2016) also find good agreement between MOPITT-based and modelled negative  
388 trends for the 2000-2010 period of total column CO over Europe and North America but  
389 disagreement in the sign of the trend over Eastern China, where their model, using  
390 MACCity emissions, simulates a positive trend but MOPITT has a negative trend. Over Eastern  
391 China also CR (2003-2015) had a small positive linear trends whereas CAMSiRA had a  
392 negative trend but both trends were not statistically significant. The positive trend over Eastern  
393 China in CR was mainly driven by directly emitted CO at the surface. Owing to the hemispheric  
394 influence, the CO trend in CR became negative in the middle troposphere, where the MOPITT  
395 sensitivity to CO is highest.



396 In the Arctic, which is influenced by the long-range transport from North America, Europe and  
397 Asia (Emmons et al., 2015), no MOPITT observations were assimilated (see Table 2). Also in  
398 this region the variability of the CR and CAMSiRA CO burden matched well but the bias was  
399 much reduced after 2012.

400 The time series of the global CO burden of CAMSiRA and MACCRA agree better than  
401 CAMSiRA and CR. The global burden of MACCRA is slightly lower than in CAMSiRA (1%)  
402 until 2010 but starts to exceed CAMSiRA in 2011 and 2012. Hence, larger differences occur at  
403 the beginning and end of the MACCRA period.

404 The CO burden of MACCRA above the biomass burning regions of South America and  
405 Tropical Africa was lower than CAMSiRA for the period 2003–2010. This is most likely  
406 because of the use of the GFED biomass burning emissions until 2008, which are on average  
407 20% lower than GFAS, which was used for CAMSiRA. In the years 2011–2012 MACCRA  
408 had higher values, which even led to a reversal in the sign of the trend over the two regions in  
409 MACCRA in comparison to CAMSiRA. MACCRA and CAMSiRA agreed well above the  
410 anthropogenic source regions. Only from 2008 onwards MACCRA was slightly lower which  
411 led to enhanced negative trends.

412 Over the Arctic, CAMSiRA is higher from 2008 whereas MACCRA was higher at the start.  
413 This is consistent with the respective trends over Europe and North America. All data sets  
414 showed a step-like reduction the CO burden at mid-2008 but it was most pronounced in  
415 MACCRA.

416

### 417 **3.3 Evaluation with MOZAIC/IAGOS aircraft CO observations**

418 Measurements of O<sub>3</sub>, water vapour, carbon monoxide and nitrogen oxides by in-service  
419 Airbus aircraft (MOZAIC) and In-service Aircraft for a Global Observing System (IAGOS) are  
420 subsequent programmes of AC observations mounted on commercial aircraft. The MOZAIC  
421 CO data have an accuracy of  $\pm 5$  ppbv, a precision of  $\pm 5\%$ , and a detection limit of 10 ppbv  
422 (Nédélec et al., 2003). De Laat et al. (2014) compare MOZAIC/IAGOS profile with the  
423 MOPITT v5 NIR retrievals, which were assimilated in CAMSiRA. They find good agreement  
424 and no drift of the biases of the two data sets in their study period 2002–2010.



425 We use the CO profiles obtained during take-off and landing to evaluate the CO fields averaged  
426 over airports in different regions from 2003–2012. The number of MOZAIC/IAGOS CO  
427 profiles fluctuated considerably over the years. They have decreased from 2003–2014 by about  
428 50% and certain airports had many more observations than others. Since the aircraft used in  
429 MOZAIC were based in Frankfurt, the majority of the CO profiles were observed at this airport.  
430 Therefore the observations from Frankfurt dominate the European mean values. Observations  
431 from Tokyo and other Japanese cities were the largest contribution to the mean over East Asia.  
432 Atlanta, Toronto and Vancouver had the largest number of observation in the North American  
433 domain. Windhoek had by far the largest number of observations in Tropical Africa and Caracas  
434 in South America. The mean of Maritime South East Asia sea salt is mainly calculated from  
435 observations over Jakarta and Kuala Lumpur in 2005, 2006, and 2012 with an unbalanced  
436 coverage of the difference months.

437 Profiles of the mean relative bias of CAMSiRA, MACCRA and CR against MOZAIC/IAGOS  
438 CO observations for different regions (see Table 3) averaged over the period 2003–2012 are  
439 shown in Figure 5. We discuss here only the annual biases since the seasonal relative biases did  
440 not differ to a large extent from the annual relative biases.

441 All three data sets underestimated the observed CO values throughout the troposphere in  
442 Europe, North America and East-Asia. At the surface and the lower PBL up to 900 hPa, i.e.  
443 where the highest CO concentrations are observed, CAMSiRA and CR had a relative biases of  
444 about -10% in Europe and North America and up to -20% in East Asia, whereas MACCRA had  
445 larger relative biases of -20 –30% at this level and the largest biases occurred in DJF. On the  
446 other hand, MACCRA had smaller biases than CAMSiRA and CR in the middle and upper  
447 troposphere. The smaller biases of MACCRA may be caused by the more realistic simulation  
448 of the chemical CO production by the MOZART chemical mechanism as well as by the change  
449 in the CO background error statistic. The assimilation of MOPITT in CAMSiRA reduced the  
450 biases relative to CR in the troposphere over Europe and North America but had only little  
451 effect at the surface. Over East Asia the assimilation did not lead to changes between CR and  
452 CAMSiRA.

453 Whereas CR had the largest underestimation in NH it was generally higher than CAMSiRA and  
454 MACCRA in the tropics. This led to better agreement with the MOZAIC observation in South  
455 America and Tropical Africa but also to an overestimation of 20–30% in Maritime South East  
456 Asia. The limited number of observations in that region makes this result less robust. MACCRA





457 and CAMSiRA showed little differences over South America and Tropical Africa. The 10%  
458 negative bias of MACCRA and CAMSiRA in Tropical Africa is consistent with the 10%  
459 underestimation of MOPITT v5 against MOZAIC/IAGOS over Windhoek reported by de Laat  
460 et al. (2014, their Figure 3). Over MSEA below 700hPa CAMSiRA and MACCRA  
461 overestimated CO whereas MACCRA underestimated the observations. This could be the  
462 consequence of the different fire emissions and the different chemistry schemes but the limited  
463 number of available profiles makes this result less representative.

#### 464 **3.4 Evaluation with NOAA GMD surface observations**

465 NOAA Global Monitoring Division (GMD) network of flask CO surface observations (Novelli  
466 and Masarie, 2010) has a good global coverage, which also includes the high latitudes of SH  
467 and NH, to observe the background concentrations. The tropical stations represent the maritime  
468 background because they are mainly located on islands in the tropical oceans. The station  
469 density is higher in North America and Europe. The uncertainty of the NOAA/GMD CO  
470 observations is estimated to be 1–3 ppm (Novelli et al., 2003).

471 We calculated the mean and linear trend at each station for the period 2003–2014 or 2003–2012  
472 (MACCRA). The overall bias averaged over all stations of CAMSiRA and CR was 3.0 ppb for  
473 the whole period but CAMSiRA had a slighter lower RMSE (13 ppb) than CR (15 ppb). For  
474 the 2003–2012 period MACCRA had a bias of 6 ppb whereas CAMSiRA and CR had a bias of  
475 3.1 and 3.9 ppb respectively.

476 Figure 6 shows the zonal means of the observed averages and the corresponding model values  
477 at station location as well as the median of the estimated linear trend from the observations and  
478 the model results. The graphs were constructed by calculating the mean concentrations and  
479 median trends of all stations in 15° wide latitude bins. The errors bars indicate the range of the  
480 observed values in the latitude bin.

481 In the SH high and mid-latitudes the typical observed annual mean surface concentration was  
482 50 ppbv. The background levels started to rise in the SH extra tropics and reached a maximum  
483 of 145 ppbv in the NH mid- latitudes. The values then decreased to about 130 ppb in the Arctic.  
484 The general structure of the zonal variation was well represented by all data sets. CR  
485 overestimated the SH mid and high values by 15 ppb whereas CAMSiRA and MACCRA had  
486 a bias of 7 ppb. In the tropics CAMSiRA had slightly lower (3 ppb) values than the observations  
487 whereas MACCRA and CR overestimated by about 5 ppb. CAMSiRA had the highest values



488 of all three data sets in the NH mid-latitudes but still underestimated the mean of the  
489 observations by 7 ppb. However the observed means at the station locations in this latitude band  
490 varied in a range of about 100 ppb. CR had a slightly larger underestimation than CAMSiRA.  
491 MACCRA underestimated the observations by more than 20 ppb in the mid and high latitudes.  
492 The reduction towards the NH high latitudes in CR and CAMSiRA was similar to the  
493 observations.

494 The observations in the SH showed essentially no linear trend in the 2003–2014 period. Starting  
495 in the tropics a negative linear trend gradually occurred which reached values of about -2.2  
496 ppb/yr in the NH mid- and high latitudes. CAMSiRA and CR had a small but still significant  
497 (95% confidence level) negative trend in SH of -0.3 and -0.5 ppb/yr respectively. The negative  
498 trends of CAMSiRA and CR started to become more pronounced from 20°S onwards. The trend  
499 in CAMSiRA was generally stronger than the trend in CR. This meant a better fit with the  
500 observed trends in the tropics for CR and a better fit in the NH mid- and high latitudes for  
501 CAMSiRA. In this region the median of the trends was -2.1ppb/yr for CAMSiRA and -2.0  
502 ppb/yr for CR. While the trends of CAMSiRA and CR agreed reasonably well with the  
503 observations, MACCRA suffered from unrealistically strong negative trends in the mid- and  
504 high latitudes of both hemispheres. This negative trend in MACCRA was caused by the  
505 reduction in the values related to assimilation of IASI data from 2008 onwards (Inness et al.,  
506 2013).

507

508

#### 509 **4 Aerosols**

510 In contrast to the assimilation of individual chemical gases, the assimilation of AOD  
511 observations is “underdetermined” because different combinations of the aerosol components  
512 can led to the same extinction, i.e. AOD value. A further complicating factor is that each aerosol  
513 component has different optical properties, which depend on relative humidity for the  
514 hydrophilic components such as sea salt, sulphate and organic matter. The correction of the  
515 speciation of the assimilated aerosol mass mixing ratio fields is therefore a big challenge despite  
516 good success in reproducing independent AOD observations with the aerosol analysis.



#### 517 **4.1 Global aerosol burden, speciation and AOD**

518 In this section the global averages of burdens and AOD are presented. Spatial patterns of AOD  
519 will be discussed in section 4.2. Global area-weighted averages of AOD at 550nm and the total  
520 global burden in Tg for the different aerosol components are shown in Figure 7. The figure also  
521 shows the median of the global AOD average and burdens simulated by the models of the  
522 AeroCom inter-comparison study (Kinne et al., 2006 and Textor et al., 2006). CR had the  
523 highest total global average aerosol burden of 46 Tg compared to MACCRA and CAMSiRA,  
524 which had both 33 Tg. This number was very similar to the AeroCom median of 29 Tg.

525 The global sea salt burden was about twice as high in CR (15.1 Tg) than in CAMSiRA (8.3  
526 Tg), and it was 16.1 Tg for MACCRA. In comparison, the median of the sea salt burden from  
527 the AeroCom models is 6.3 Tg. Another study of different emission schemes by Spada et al.  
528 (2013) found sea salt burdens in the range from 5.0 to 7.2 Tg. In the light of these studies as  
529 well as the applied correction by the assimilation in CAMSiRA, the simulated sea salt burden  
530 of CR as well as the assimilated burden of MACCRA appears to be too high. The simulated sea  
531 salt emissions of C-IFS were at the upper end of, but still within, the reported range in the  
532 literature (see supplement). This suggests that the high sea salt burden of CR can not entirely  
533 be explained by exaggerated emissions. The underestimation of the loss with respect to other  
534 models must have played an important role too. On the other hand, the high sea salt burden  
535 of MACCRA was probably caused by an exaggeration of the sea salt emission with an earlier  
536 version of the emissions module.

537 The desert dust burden in CR was 27 Tg, which was higher than the AeroCom median of 20  
538 Tg. It was strongly reduced by the assimilation in CAMSiRA to 18 Tg. MACCRA had an even  
539 lower desert dust burden of 12 Tg because of the underestimation of the desert dust emissions  
540 scheme used in MACCRA. As in the case of the sea salt, the underestimation of the desert dust  
541 loss by deposition and sedimentation may play an important role in the overestimation of dust  
542 burden in CR.

543 The strongest relative change in the global burden by the assimilation occurred for sulphate,  
544 which was 1.2 Tg in CR but was 4.7 Tg in CAMSiRA and 3.3 Tg in MACCRA. The respective  
545 AeroCom median value is 2 Tg. Because of the larger extinction per unit mass of sulphate, this  
546 increase in sulphate had a large impact on total AOD, which will be discussed further below.



547 The organic matter and black carbon burden of CR (0.2 Tg and 2.0 Tg) was increased by the  
548 assimilation to 0.36 Tg and 2.4 Tg respectively. The values agreed reasonably well with the  
549 AeroCom median of 0.21 Tg and 1.76 Tg.

550 In contrast to the global burden, CR had the lowest global AOD average of 0.13. CAMSiRA  
551 and MACCRA had values of 0.16 and 0.18. The values for CR was close to the median of the  
552 AeroCom models (0.12) but the two reanalyses had a higher value than the highest global  
553 average AOD value of the AeroCom models of 0.15.

554 The largest fraction of the CAMSiRA AOD came from sulphate, which was strongly increased  
555 by the assimilation. The contribution of sulphate AOD to total AOD was 13% in CR and 43%  
556 in CAMSiRA. Sulphate was also the largest AOD contribution in MACCRA. The global  
557 average of sulphate AOD of CR (0.018) was about half of the AeroCom median (0.034), which  
558 could suggest an underestimation in the global sulphate burden and AOD in CR. On the other  
559 hand, global sulphate AOD of CAMSiRA was 0.06, which was higher than the highest value  
560 of the AeroCom model ensemble (0.051).

561 As already discussed for the respective burdens, global desert dust AOD and sea salt AOD were  
562 strongly reduced in CAMSiRA compared to CR. In CR sea salt and desert dust AOD  
563 contributed each about 30% to the total AOD, whereas in CAMSiRA the contribution was  
564 reduced to 15% and 19%. The reduction of sea salt by the assimilation was reasonable as the  
565 sea salt burden was above the reported range by Textor (2006) and Spada et al. (2012).  
566 However, the reduction in sea salt was compensated by the increase in sulphate, which became  
567 the most important contribution to total AOD over many parts of the oceans.

568 The global sea salt burden of MACCRA was higher than in CAMSiRA but similar to CR.  
569 However, a different distribution of the mass within the size classes meant that the resulting sea  
570 salt AOD of MACCRA was 20% higher than CR. MACCRA had the lowest desert dust burden  
571 but differences in the size distribution towards smaller particles meant that the resulting AOD  
572 was slightly higher than CR and 20% higher than CAMSiRA. Black carbon and organic matter  
573 AOD and burden were similar among CAMSiRA, CR and MACCRA.

574

575



## 576 **4.2 Spatial patterns of AOD**

577 Figure 8 shows the annual mean of total AOD and AOD for desert dust, sea salt, sulphate, black  
578 carbon and organic matter for period 2003–2015 from CAMSiRA and the differences with CR  
579 and MACCRA (2003–2012). The global maxima of the total AOD ( $>0.5$ ) in CAMSiRA were  
580 found over areas of desert dust emissions such as the Sahara, the Arabian Peninsula and the  
581 deserts of Central Asia. High emissions of black carbon and organic matter from biomass  
582 burning sources in tropical Africa and anthropogenic sources in Eastern China and Northern  
583 India also produced to AOD maxima on the global scale.

584 The increase of the global average AOD in CAMSiRA with respect to CR by the assimilation  
585 (see section 4.1) occurred in most parts of the globe, in particular over the areas of industrial  
586 activity in North America, Europe and East Asia (20–30%) as well as in the polar regions ( $>$   
587 50%), where AOD is generally low. The differences between CR and CAMSiRA, although  
588 varying in magnitude, exhibit similar spatial patterns in all seasons, with the largest differences  
589 occurring throughout NH in MAM. As discussed in section 4.1 the increase is mostly caused  
590 by a wide-spread increase in sulphate AOD. Sulphate AOD was increased in relative terms  
591 more strongly over the oceans and higher latitudes. In areas of higher modelled sulphate AOD  
592 such as the North America, Europe and Northern Asia and the Arctic the contribution to total  
593 AOD changed from 40% to 90%, which made sulphate the by far the most abundant aerosol  
594 species in these areas as well as over the Antarctic, which seems unrealistic.

595 The identified reduction of global desert dust in CAMSiRA with respect to CR was mainly  
596 confined to the main desert dust region, where AOD was reduced by to 0.2. As total AOD was  
597 dominated by desert dust, total AOD was strongly reduced in these regions, whereas total AOD  
598 of CAMSiRA was always higher than CR in the other parts of the globe. The largest relative  
599 reduction of desert dust AOD occurred in the remote outflow regions from Australia, Tropical  
600 Africa and Eurasia. The reduction of desert dust occurred throughout all seasons with the largest  
601 reduction in JJA.

602 The strongest reduction in sea salt occurred in CAMSiRA with respect to CR occurred over the  
603 oceans proportional to the sea salt AOD. Because of the increase in sulphate, the sea salt  
604 reduction led only to a small reduction of total AOD over the area of the highest sea salt  
605 emissions in the North Atlantic in DJF and over the Southern Ocean in JJA and MAM. The  
606 contribution of sea salt AOD to total AOD over most of the ocean was changed from more than



607 80% in CR to 50% in CAMSiRA in mid- and high latitudes of SH and to 30% over the rest of  
608 the maritime area by the assimilation.

609 Black carbon and organic matter AOD were reduced in CAMSiRA over tropical Africa where  
610 biomass burning is the largest source on the global scale and also the CO biomass burning  
611 emissions were too high. The black carbon and organic matter AOD values were higher in  
612 CAMSiRA away from the sources where values are generally low. The differences of black  
613 carbon and organic matter AOD between CAMSiRA and CR showed a strong reduction directly  
614 over the areas of intense fire emission in tropical Africa and boreal forest of NH and an increase  
615 in the adjacent outflow regions. This could indicate that the GFAS emissions, as in the case of  
616 CO (see section 3.1), were too high but the atmospheric residence times of the aerosol species  
617 were too short.

618 Compared to CAMSiRA, MACCRA AOD values were up to 50% (-0.2– -0.3) lower in the  
619 desert dust dominated areas over the Sahara and Central Asia. The largest differences over  
620 North-Africa occurred in JJA and MAM and are an indication that MODIS AOD retrievals are  
621 not available over this regions because of their bright surface (Hsu et al., 2013). The higher  
622 AOD values of CAMSiRA than MACCRA in the desert dust regions might be an improvement  
623 as Cuevas et al. (2015) reported a general underestimation with respect to AERONET  
624 observations in the dust dominated regions of MACCRA.

625 On the other hand, sea salt AOD over all oceans was much higher in MACCRA than CAMSiRA  
626 and it even exceeded the high sea salt AOD of CR. Despite the higher sea salt AOD, the total  
627 AOD of MACCRA over the oceans was lower than in CAMSiRA because of the overall smaller  
628 sulphate AOD in maritime regions.

629 In the regions of boreal fire emissions MACCRA was lower during the JJA fire season as well  
630 as in the South American fire season in SON. For the rest of the globe the CAMSiRA, was  
631 about 0.05 lower than the MACCRA, which meant a large relative reduction (>50%) in  
632 particular over the oceans.

633 The differences between MACCRA and CAMSiRA can mainly be explained with the changes  
634 in the underlying modelling approach and the emissions since the same MODIS AOD retrievals  
635 were assimilated in both reanalyses. Differences in the back ground error statistics may have  
636 contributed to the differences, particularly in the high latitudes.



637 Figure 9 shows a zonally averaged cross section of the total aerosol mixing ratio of CAMSiRA  
638 and its relative differences of CR and MACCRA. The highest zonal average occurred over the  
639 southern ocean because of the continuous sea salt production, and over the latitudes of the  
640 regions with large desert dust and anthropogenic emissions. Despite the mostly higher AOD  
641 values, CAMSiRA had lower mass mixing ratios than CR throughout the troposphere with the  
642 largest relative differences occurring over the SH mid-latitudes and in the region of intense  
643 convection in the tropics. This is related to a change in the speciation, which was discussed in  
644 section 4.1. CAMSiRA had up to 90% higher values in the stratosphere and Antarctica. The  
645 higher aerosol mixing ratios of CAMSiRA in the upper troposphere were dominated by sulphate  
646 aerosol. MACCRA mixing ratios were considerably higher in relative terms than CAMSiRA  
647 throughout the troposphere with the exception of NH extra-tropical mid- troposphere, caused  
648 by the lower dust emissions in MACCRA, and the SH and tropical stratosphere related to high  
649 sulphate concentrations in CAMSiRA.

#### 650 **4.3 Inter-annual variability of AOD**

651 Figure 10 shows time series of average AOD from CAMSiRA, CR and MACCRA for different  
652 regions. To better distinguish the impact of sea salt, the regional AOD is averaged over land  
653 points only. The global average AOD time series are shown separately for land and sea points.  
654 CR and CAMSiRA did not have any significant trends in AOD over the whole globe or any of  
655 the considered regions. There was a good agreement between CAMSiRA and CR in their inter-  
656 annual variability with respect to specific years with higher maxima over South and North  
657 America as well as over Maritime South East Asia and North-Africa. This demonstrates that  
658 despite biases the model was able to reproduce the variability related to fire emissions and wind  
659 driven desert dust suspension. A large relative difference between CR and CAMSiRA occurred  
660 in the Arctic. The CAMSiRA and MACCRA AOD values were almost twice as high as CR and  
661 had a much more pronounced seasonality.

662 In contrast to the lack of significant trends in CR and CAMSiRA, MACCRA had significant  
663 positive trend over all sea points leading to an increase over 10 years, which was as large as the  
664 seasonal variation over all sea points. Averaged over all land points, the seasonal variation is  
665 much larger than over sea. The agreement in AOD in the monthly means time series was  
666 generally high but MACCRA also showed a significant increasing trend, which was not present  
667 in the other two data sets. Most of this trend in MACCRA was caused by dust AOD, which



668 increased by 3.7%/yr, and by sea salt AOD, which increased by 1.7%/yr over sea points. We  
669 consider this trend in MACCRA as spurious. It is probably caused by an accumulation of  
670 aerosol mass, which could not be corrected by the assimilation. A reason for the mass  
671 accumulation could be the fact that the MACCRA model did not apply a global mass fixer.

672 Even if CR and CAMSiRA did not show significant trends in total AOD, sulphate AOD of  
673 CAMSiRA increased significantly by 0.55%/yr and both CR and CAMSiRA had a positive  
674 trend in sea salt AOD of 0.3%/yr. This suggests an artificial accumulation of sulphate by the  
675 assimilation considering that SO<sub>2</sub> emissions for aerosol sulphate precursor were constant.

#### 676 **4.4 Evaluation with AERONET AOD observations**

677 The AOD at 550 nm was evaluated with observations of the AErosol RObotic NETwork  
678 (AERONET) network. The AERONET is a network of about 400 stations measuring spectral  
679 AOD aerosol with ground based sun-photometers (Holben et al., 1998). The stations are mostly  
680 located over land with a high number of stations situated in North America and Europe. The  
681 global number of stations contributing observations for the evaluation increased from about 60  
682 in 2003 to about 250 in 2014 before it reduced strongly to only a couple of stations at the end  
683 of 2015.

684 Figure 11 shows time series of the monthly biases of CAMSiRA, MACCRA and CR for the  
685 globe and different regions. Over North America, an area with a high density of AERONET  
686 stations, CR underestimated AOD in general by 0.05 on average. On the other hand, the two  
687 analyses overestimated AOD by about 0.02 but CAMSiRA has marginally smaller biases than  
688 MACCRA. In South America a similar pattern was found only that the average underestimation  
689 of CR and overestimation of CAMSiRA and MACCRA was -0.05 and 0.05 respectively. The  
690 overestimation of CAMSiRA and MACCRA and the underestimation of CR over America  
691 leads to the conclusion that the assimilated MODIS retrievals were biased high against the  
692 AERONET observations in this region as also pointed out in Levy et al. (2010). The underlying  
693 model does not seem to be the cause of the overestimation in CAMSiRA.

694 Over Europe CAMSiRA had the smallest biases and MACCRA overestimated slightly whereas  
695 CR underestimated the observations. The bias of CR was -0.07 at the beginning of the period  
696 and almost zero at the end. More research is needed to understand this trend in the bias, which  
697 is also apparent in CAMSiRA and MACCRA, but it might be caused by the reduced number of  
698 available stations.





699 MACCRA had the lowest biases over South East Asia because of small biases in Northern India  
700 and Indochina. It was higher, as almost everywhere, than CAMSiRA and CR. CAMSiRA  
701 underestimated the observations in this region by about 0.05. The underestimation by CR was  
702 bigger and showed a pronounced seasonal cycle. The largest negative biases occurred at the  
703 time of the seasonal minimum in DJF.

704 The performance for desert dust and sea salt was more difficult to evaluate with AERONET  
705 stations in a robust way because only few stations are available in these regions. The average  
706 bias over Africa showed a strong reduction of the CR peak values, which occurred because of  
707 desert dust outbreaks, by the assimilation. A good example of the successful reduction of dust  
708 by the assimilations was Lake Argyle (16.11.S, 128.75E) in Australia (Figure 11, left).

709 The AOD AERONET observations over the oceans show generally an overestimation of all  
710 runs, in particular for MACCRA. The bias of the MODIS retrievals with respect to AERONET  
711 (Shi et al., 2011) may be a reason for this overestimation. The comparison with AOD  
712 observation at Mauna Loa Station (19.54 N, 155.58 W, not shown) in the Eastern Pacific  
713 suggests that the low AOD values of CR reproduced the observations best, although still  
714 overestimating them. At Nauru Station (0.52 ° S, 166.9 ° E, Figure 11, right) in the Western  
715 Pacific CAMSiRA match the observations well whereas CR underestimated and MACCRA  
716 overestimated them.

## 717 **5 Stratospheric ozone**

718 The experience from the assimilation of TC and stratospheric profiles retrievals (Inness et al.,  
719 2013, van der A et al., 2015 and Levefer et al., 2015) shows that these observations are sufficient  
720 to constrain stratospheric ozone in the reanalysis. Because almost the same ozone retrievals  
721 were assimilated in CAMSiRA as in MACCRA (see Table 2) most of the differences in the  
722 ozone analyses can be attributed to differences in the ozone simulation of the assimilating  
723 model. For CAMSiRA the Cariolle parameterization (Cariolle and Teyssèdre, 2007) of  
724 stratospheric ozone chemistry and the chemical mechanism CB05 for the troposphere were  
725 used. The tropospheric and stratospheric chemical scheme of the MOZART CTM (Kinnison et  
726 al., 2007) was used for MACCRA.

### 727 **5.1 Spatial patterns of TC ozone**

728 Figure 13 shows the seasonal average TC ozone from CAMSiRA and the difference between  
729 this data set and CR and MACCRA. The differences between CAMSiRA and CR had a



730 meridional pattern. The assimilation in CAMSiRA increased the total ozone columns in the  
731 tropics and subtropics by up to 25 DU (8%) and it decreased them by 50–70 DU in the NH mid  
732 and high latitudes. The largest reduction occurred in DJF and MAM. Also over Antarctica the  
733 assimilation led to lower values in austral winter (JJA), when TC ozone was reduced by up to  
734 30 DU.

735 CAMSiRA was about 3–5 DU (1%) lower than MACCRA throughout the globe. Larger  
736 differences of up to 10 DU (2%) were located mainly over tropical land areas. Their shape  
737 suggest that they were partially caused by differences in tropospheric ozone (see section 6.1).  
738 On the seasonal scale, CAMSiRA was about 10 DU lower over Antarctica and the Arctic in the  
739 respective spring seasons MAM and SON.

740 Figure 14 shows the average ozone partial pressure cross section of CAMSiRA and the relative  
741 differences with CR and MACCRA. The tropospheric part of the figure will be discussed in  
742 section 6.1. The overestimation of CR in the high latitudes of NH and SH was located  
743 predominately in the mid and upper stratosphere at around 20 hPa. The underestimation in the  
744 tropics had the largest values at around 50 hPa.

745 In the lower and middle stratosphere, i.e. from 70 to 20 hPa, CAMSiRA and MACCRA differed  
746 by less than 5%. Larger differences occurred above 10 hPa where MACCRA was up to 30%  
747 higher than CAMSiRA.

## 748 **5.2 Inter-annual variability of TC ozone**

749 Figure 15 shows area-weighted averages of the monthly TCs for the whole globe, the tropics,  
750 SH and NH mid-latitudes, Antarctica and the Arctic.

751 In the tropics, CAMSiRA had a significant trend of +0.15%/yr. Although the period of 13 years  
752 is too short to estimate total ozone trends with respect to ozone recovery it is worth noticing  
753 that the number is in good agreement with the estimate of the ozone trend for the period 1995–  
754 2013 by Coldewey-Egbers et al. (2014, see their figure 1), which varies in the tropics between  
755 0.5 to 1.5%/decade. No trends could be found in CR, probably because the climatological  
756 approach applied in the Cariolle scheme is not able to simulate long-term trends. The tropical  
757 trend in MACCRA was 0.25%/yr, which seems too high and there was also a significant trend  
758 in the SH mid-latitudes of 0.65%/yr.



759 The seasonal range, i.e. the difference between annual maximum and minimum, of TC ozone  
760 in CAMSiRA increased from 10 DU in the tropics to up 150 DU in the Arctic and 100 DU in  
761 Antarctica. As already mentioned in section 5.1, CR was 20% higher than CAMSiRA in NH  
762 mid-latitudes and Antarctica. However, the inter-annual variability agreed reasonably well  
763 between CAMSiRA and CR in SH and MH high and mid-latitudes. For example, the reduced  
764 Arctic ozone spring in 2011 (Manney et al., 2011) and the year-to-year differences in mid-  
765 latitudes found in CAMSiRA were well reproduced by CR.

766 The ozone hole in Austral spring is the most important feature of seasonal variability over  
767 Antarctica. Remarkably CR, which uses the Cariolle scheme, reproduced the ozone loss during  
768 the ozone hole periods with respect to minimum value and inter-annual variability of TC ozone  
769 very well without assimilating any observations. 2015, 2003 and 2006 were the years with the  
770 deepest ozone holes and 2011, 2013 and 2004 with the shallowest ozone hole both in  
771 CAMSiRA and CR. On the other hand, CR overestimated the average TC ozone during winter  
772 by about 30 DU.

773 There was generally good agreement between CAMSiRA and MACCRA over all parts of the  
774 globe but MACCRA was on average about 5–10 DU (2%) higher than CAMSiRA. The strong  
775 positive trend of MACCRA in the tropics together with a significant positive trend in the SH  
776 mid-latitudes led to increasing differences of the global average at the end of the MACC period.  
777 Larger difference between MACCRA and CAMSiRA occurred in winter (JJA) over Antarctica,  
778 when MACCRA was up to 25 DU lower than CAMSiRA. The depth of the ozone hole was  
779 slightly deeper in CAMSiRA than in MACCRA.

### 780 **5.3 Evaluation with total ozone retrievals from Dobson sun-photometers**

781 Ozone TCs are observed from the ground with Dobson, Brewer, Point Filter and FTIR  
782 spectrometers. The Dobson instruments provide the longest and best spatial coverage and we  
783 use this data set to evaluate the TC of CAMSiRA, MACCRA and CR. The Dobson instruments  
784 of the WOUDC network are well calibrated and their precision is 1% (Basher, 1982). Factors  
785 that influence the accuracy of the Dobson spectrometer are the temperature dependency of the  
786 ozone absorption coefficient and the presence of SO<sub>2</sub>.

787 Figure 16 shows time series of the monthly bias against the Dobson photometer observations  
788 for different regions. Observations of about 50–60 stations were available until 2013 but the  
789 number of stations dropped steadily to about 10 Stations at the end of 2015. CAMSiRA



790 overestimated the observations in the tropics and the mid-latitudes of both hemisphere on  
791 average by 2 DU whereas the mean bias of MACCRA was about 5 DU larger. In Antarctica  
792 and the Arctic the biases showed a more pronounced seasonal cycle mostly between -10 and 20  
793 DU.

794 The biases of MACCRA increased in the tropics and the SH-mid latitudes from 2003 to 2008  
795 whereas CAMSiRA and CR did not show an obvious change in the biases until 2012. The  
796 variability of the bias of CAMSiRA amplified at the start of 2013 in NH. As this change in the  
797 bias is not seen at individual stations reporting until the end of 2015, we conclude that the  
798 change is caused by the reduction in stations available after 2013. However, the change of the  
799 assimilated MLS data set (from V2 to V3.4) at the beginning of 2013 (see Table 2).

800 The biases of CR were much larger than the ones of CAMSiRA, and they had a strong seasonal  
801 cycle. In the tropics CR underestimated the TC by 10 DU in DJF and 0 DU in MAM. The NH  
802 biases were positive and varied between 20–50 DU and in the Arctic between 20–70 DU. Over  
803 Antarctica CR overestimated the observation by 40–60 DU in JJA but the bias was close to zero  
804 or even slightly negative during the time of the ozone hole.

#### 805 **5.4 Evaluation with ozone sondes in the stratosphere**

806 The global network of ozone sondes is the most comprehensive independent data set for the  
807 evaluation of the 3D ozone fields from the surface to about 10 hPa, which is the level with the  
808 highest stratospheric ozone volume mixing ratios. The observation error of the sondes is about  
809  $\pm 5\%$  in the range between 200 and 10 hPa and  $-7$ – $17\%$  below 200 hPa (Beekmann et al., 1994,  
810 Komhyr et al., 1995 and Steinbrecht et al., 1996). The number of soundings varied for the  
811 different stations used here. Typically, the sondes are launched once a week but in certain  
812 periods such as during ozone hole conditions launches are more frequent. Sonde launches are  
813 carried out mostly between 9 and 12 hours local time. The global distribution of the launch sites  
814 is even enough to allow meaningful averages over larger areas such North America, Europe,  
815 the tropics, the Arctic and Antarctica.

816 Figure 17 shows the profiles of the relative biases of CAMSiRA, MACCRA and CR over the  
817 tropics, Antarctica, the Arctic and the NH and SH mid-latitudes for the period 2003–2012. All  
818 available observations were included in the average.

819 In the tropics, CAMSiRA had a relative bias of mostly below 10% in most of the stratosphere.  
820 MACCRA underestimated the ozone sondes strongly (up to 30%) in the lower stratosphere but



821 the relative bias of MACCRA was similar or slightly smaller than the bias of CAMSiRA in  
822 most parts of the stratosphere, i.e. in the pressure range from 70 to 20 hPa. CR underestimated  
823 the ozone sondes by up to 20% in the stratosphere up to 30 hPa. The largest underestimation of  
824 CR occurred in the lower and mid stratosphere, where the maximum in ozone partial pressure  
825 is located. In the upper stratosphere above 20 hPa, where the maximum of ozone volume mixing  
826 ratio is located, the relative biases of all data sets were smaller than in the levels below. CR had  
827 almost no bias whereas MACCRA overestimated by up to 10%.

828 Over the Arctic and NH mid-latitudes CAMSiRA and MACCRA agreed well with the sondes  
829 in the whole stratosphere with relative biases below 5%. The absolute biases of CAMSiRA  
830 were slightly smaller than the biases of MACCRA in particular in the lower stratosphere and  
831 upper troposphere. CR overestimated the ozone observations by up to 25% in the stratosphere  
832 and upper troposphere over the Arctic and up to 20% in the NH mid-latitudes. The relative  
833 biases of CR tended to be slightly smaller in the mid stratosphere (50 hPa) than in the upper  
834 and lower stratosphere.

835 Over SH-mid latitudes and Antarctica the annual biases in the stratosphere were slightly smaller  
836 in CAMSiRA than MACCRA but for both reanalyses they were below 10%. As over the Arctic,  
837 the absolute tropospheric biases, with the exception of the surface values, were smaller in  
838 MACCRA since CAMSiRA showed an underestimation of about 10%. CR had a stronger  
839 underestimation in the lower and upper stratosphere.

840 As the process of the ozone-hole formation cannot easily be demonstrated with annual means,  
841 Figure 18 shows the monthly mean profile from August to November over Neumayer Station  
842 (70.7° S, 8.3° W). The two reanalysis agreed very well with the observations: vertical level and  
843 magnitude of the ozone profile at the end of the austral winter in August, the ozone depletion  
844 in September and October and the closure of the ozone hole starting in the upper stratosphere  
845 were well captured because of the assimilation of TC and limb-sounders profiles.

846 In contrast, CR showed a strong overestimation in August in the middle and lower stratosphere.  
847 Ozone in the upper stratosphere in September was underestimated in CR because of an  
848 exaggerated depletion whereas ozone was overestimated in the lower stratosphere. In the  
849 following months CR ozone remained too high in the lower stratosphere and too low in the  
850 upper troposphere but the resulting TCs matched the observations in a reasonable way (see  
851 Figure 16)



## 852 **5.5 Evaluation with the GOZCARDS ozone product in the upper stratosphere**

853 Ozone sondes do not provide accurate measurements above 10 hPa. The ozone bias profiles  
854 shown in Figure 17 indicate higher values of MACCRA in the upper stratosphere and  
855 mesosphere, i.e. from above 10 hPa to the model top of 0.1 hPa. Although the ozone mass in  
856 this region is relatively small, the high values of the mixing ratios have a large impact on the  
857 radiative transfer and the associated heating rates. To investigate the biases in that region we  
858 used the Global OZone Chemistry And Related trace gas Data records for the Stratosphere  
859 (GOZCARDS) product (Froidevaux et al., 2015). It consists of merged SAGE I, SAGE II,  
860 HALOE, UARS and Aura MLS, and ACE-FTS data from late 1979 to 2012. SAGE II is used  
861 as the primary reference in the merging procedure for the instruments. For most of the  
862 CAMSiRA period, i.e. from 2004 onwards, Aura MLS and ACE-FTS are the dominating  
863 instruments in the upper stratosphere. Tegtmeier et al. (2013) showed that ozone retrievals from  
864 various instruments show a considerable spread in the upper stratosphere. ACE-FTS is biased  
865 high above 10 hPa and biased low below 10 hPa against the median of various retrievals.

866 Figure 19 shows cross sections of the GOZCARDS product and relative bias of CAMSiRA,  
867 MACCRA and CR in the vertical range from 50–0.3 hPa. In the region from 10–5 hPa  
868 MACCRA had a positive bias of 10–15% in the tropics and mid-latitudes, which has already  
869 been reported in Inness et al. (2013). About half of the 10 DU higher TCs in MACCRA  
870 compared to CAMSiRA were caused by this overestimation in the levels above 10 hPa. The  
871 biases of CAMSiRA in that region were smaller and vary between 2.5 and -2.5%. CAMSiRA  
872 underestimated the GOZCARDS data between 5 and 1 hPa by up to 7%, whereas MACCRA  
873 slightly overestimated. In the lower mesosphere MACCRA underestimated the ozone  
874 concentrations by up to 30%.

875 CR had very similar biases as CAMSiRA above 5 hPa in the tropics and mid-latitudes. This  
876 means that the assimilation of observations had already little influence in this region even if no  
877 increments were added during the CAMSiRA assimilation above 1 hPa. Below 10 hPa the cross  
878 section of the bias shows the already discussed strong overestimation of CR in the mid and  
879 higher latitudes, which was largest in relative terms at around 20–15 hPa and the  
880 underestimation in the tropics, which was largest at around 50 hPa.



## 881 **6 Tropospheric ozone**

882 Correcting tropospheric ozone by the assimilation of TC and stratospheric ozone profiles  
883 remains a challenge because the observations are dominated by the high stratospheric mixing  
884 ratios (Wagner et al., 2015). The modelled ozone fields as well as the specification of the  
885 vertical background error correlation have therefore a large impact on the analysed tropospheric  
886 ozone fields (Inness et al., 2015).

### 887 **6.1 Spatial patterns of ozone at 850 hPa**

888 We focus the discussion of the seasonal spatial patterns of monthly mean tropospheric ozone  
889 mole fraction to the 850 hPa pressure level values but we also discuss tropospheric ozone at  
890 500 and 200 hPa in the section 6.2 and comparisons with ozone sondes for different  
891 tropospheric layers in section 6.3. Figure 20 shows the seasonal means of CAMSiRA and the  
892 differences with CR and MACCRA at 850 hPa. Extratropical NH ozone values of CAMSiRA  
893 were mostly in the range from 35–55 ppb. The season of the maximum was MAM, when values  
894 were about 20 ppb higher than in the seasonal minimum in DJF. Regional maxima of over 60  
895 ppb were situated over the East Asia and the Arabian Peninsula. JJA was the season when the  
896 highest values occurred over the areas of the regional maxima. In this season an additional  
897 regional maxima occurred over tropical Africa. The SH values were generally below 35 ppb.  
898 The seasonal maximum was in Austral spring (SON) and the minimum in Austral summer and  
899 late autumn (SON).

900 CR was about 2–4 ppb higher than CAMSiRA in most parts of the globe. Only in the higher  
901 latitudes of SH as well as over the biomass burning regions in Africa, South America and  
902 Maritime South East Asia, CAMSiRA was up to 4 ppb lower than CR. The biggest large-scale  
903 reduction by the assimilation in NH occurred in DJF and the biggest increase in SH in SON.  
904 The largest absolute increases of CAMSiRA of up to 10 ppb occurred over the Southern end of  
905 the Arabian Peninsula at the time of the seasonal maximum in JJA. This was the only local  
906 maximum in CAMSiRA that was increased by the assimilation.

907 Tropospheric ozone was the only considered species for which the differences between  
908 CAMSiRA and MACCRA were larger than the difference between CAMSiRA and CR. This  
909 indicates the importance of the chemistry model parameterization and the limitations of the data  
910 assimilation in this respect. In the extra-tropics of NH and SH, CAMSiRA was 2–5 ppb lower  
911 than MACCRA with an increasing difference towards the poles. The largest difference occurred



912 in NH summer in JJA. CAMSiRA was up to 10 ppb lower than MACCRA over the continents  
913 in the tropics. On the other hand, CAMSiRA had higher values than MACCRA over the tropical  
914 oceans, the Sahara as well as at the location of the strong maximum over the Arabian Peninsula,  
915 which was not present in MACCRA. The strong land-sea contrast in the differences could be  
916 caused by (i) a different efficiency of deposition over the oceans, (ii) the discussed differences  
917 in biomass burning emissions and (iii) differences in the chemistry treatment (e.g. the isoprene  
918 degradation scheme).

919 The vertical distribution (see Figure 14) of the mean ozone partial pressure in the troposphere  
920 shows that CAMSiRA was lower than CR in the whole troposphere apart from the tropical  
921 upper troposphere, where it was up to 10% higher, as well as below 500 hPa in the SH  
922 troposphere. Compared to MACCRA, CAMSiRA was up to 20% higher in the middle and  
923 upper troposphere in the tropics and subtropics but increasingly lower towards the surface.

## 924 **6.2 Inter-annual variability**

925 Estimating and understanding tropospheric ozone trends have been studied widely in the  
926 literature, as reviewed in Cooper et al. (2014) and Monks et al. (2015). Factors that influence  
927 the inter-annual variability and trends of tropospheric ozone are changes in anthropogenic and  
928 biomass burning emissions, the stratosphere-troposphere exchange and the variability of the  
929 meteorological fields. The observed trends vary strongly because these different factors are not  
930 uniform in space and time. Trends are often confined to specific seasons or levels. Positive  
931 trends are more common than negative trends and are found over Europe and North America  
932 during spring (Cooper et al., 2014).

933 Figure 21 shows time series of average ozone volume mixing ratios over selected regions and  
934 pressure levels at 850, 500 and 200 hPa. It is beyond the scope of the paper to investigate the  
935 robustness of the trends in CAMSiRA in detail. But it is worth noting that there were only  
936 positive trends in the considered region at 850, 500 and 200 hPa in CAMSiRA. The trends  
937 varied between 0-1.1%/yr, with a global mean of 0.5%/yr. Many of these trends were  
938 significant. CR also had mostly positive but much smaller trends with a global mean of  
939 0.17%/yr. The only significant trend in CR of 0.35%/yr was found over East-Asia and the  
940 corresponding trend in CAMSiRA had the same value. Focusing over Easter China, Verstraeten  
941 et al. (2015) find a trend of about 1.2%/yr between 2005 and 2010, which is considerably larger  
942 than the trend in CAMSiRA and CR.





943 The time series in Figure 21 show that the higher values in NH of CR with respect to CAMSiRA  
944 occurred in the entire troposphere. In the lower and mid troposphere CAMSiRA was lower than  
945 CR especially during the seasonal minimum. In the tropics, CR and CAMSiRA agreed well at  
946 850 hPa, CR was slightly higher at 500 hPa and about 5 ppb lower than CAMSiRA at 200 hPa.  
947 At this level CAMSiRA had a significant trend of 0.95%/yr in the tropics, which was not present  
948 in CR. More detailed studies are needed to confirm the realness of this upper tropospheric trend  
949 in CAMSiRA.

950 A more detailed inspection of the time series shows that from the start of 2013 CR and  
951 CAMSiRA agree to higher degree than before in the middle and upper part of the troposphere  
952 in NH. The agreement is most likely caused by a reduced correction by the assimilation in the  
953 NH troposphere in this period. In early 2013 the assimilated MLS ozone retrieval switched from  
954 version V2 to the NRT V3.4 product (see Table 2), which had different levels and observations  
955 errors. The discontinuation of the MIPAS in spring 2012 do not seem to be the reason for this  
956 behaviour.

957 The year-to-year variability of tropospheric ozone from MACCRA did often not resemble that  
958 of CAMSiRA. In NH at 850 hPa (most prominently seen in the Arctic) MACCRA had  
959 increasing values until 2008 after which they dropped to the values of CAMSiRA. This drift of  
960 MACCRA and the associated negative trends are not realistic (as confirmed in section 6.3).  
961 They were caused by applying the variational bias correction scheme to MLS data in MACCRA  
962 (see Inness et al. 2013 for more details). The agreement between CAMSiRA and MACCRA  
963 increases with increasing height in the extra-tropics but in the tropics MACCRA showed a  
964 much stronger trend at 200 hPa than CAMSiRA.

### 965 **6.3 Evaluation with ozone sondes in the troposphere**

966 Figure 22 show time series of seasonal biases in pressure ranges representing the lower, middle  
967 and upper troposphere from 6 different ozone sonde sites. The selected stations had at least one  
968 observations for each month of the 2003-2105 period and are examples for Europe (De Bilt),  
969 North America (Huntsville), the tropics (Nairobi), the Arctic (Ny-Ålesund) and Antarctica  
970 (Neumayer Station). To present South-Asia we chose Hong Kong Observatory, which had  
971 complete cover from 2003-2012. These individual time series depend on the specific  
972 characteristics of the individual stations and are therefore less representative than the averages  
973 over the gridded data sets shown in section 6.2.



974 In the lower troposphere (950-700 hPa) over DeBilt, Huntsville and Nairobi, CR and  
975 CAMSiRA had seasonal biases in the mostly in the range of -7-7 ppb. In the polar regions at  
976 Neumayer Station and Ny-Ålesund both CR and CAMSiRA underestimated the observations.  
977 At all locations CAMSiR was lower in the lower troposphere than CR, which meant that  
978 CAMASiRA had mostly a larger absolute bias than CR. At Hong Kong Observatory both  
979 CAMSiRA and CR overestimated the observations with biases in the range between 0-10 ppb.

980 In the middle troposphere the absolute biases of CAMSiRA and CR were of the same magnitude  
981 but of different signs. In the upper troposphere CR overestimated the observations by about 10  
982 ppb whereas the bias of CAMSiRA remained below 5 ppb. The overestimation of CR is  
983 probably caused by the influence of the stratosphere where CR was too high (see section 5.4).  
984 Over Nairobi the biases of CR and CAMSiRA were very similar in all levels but CAMSiRA  
985 had overall lower biases in the lower troposphere. In the pressure range 400-300 hPa in the  
986 tropics the impact of stratospheric biases on CR is less strong because of the higher tropopause  
987 height in this region.

988 The biases for all three data sets at Ny-Ålesund, Hunstville and Hong Kong Observatory  
989 showed a pronounced seasonality in the middle and upper troposphere. At Huntsville the spring  
990 maximum was especially overestimated, i.e. it occurred 2-3 month too early. At Ny-Ålesund  
991 the overestimation was caused by too high values in summer and autumn. Over Hong Kong  
992 Observatory the pronounced observed spring maximum was not well reproduced.

993 As already discussed in section 6.2, the characteristics of the bias of CAMSiRA changed at the  
994 start of 2013 mainly in the upper parts of the NH troposphere but also throughout the  
995 troposphere over higher latitudes. In this period the CAMSiRA biases resembles much more  
996 the bias of CR which often mean an increase in the average values, which could cause a spurious  
997 enhancement of positive trends.

998 At Neumayer Station CAMSiRA increased in a step-wise manner already at the start of 2012,  
999 which changed the bias from an underestimation to a slight overestimation together with an  
1000 increased seasonality. This behaviour could be caused by the discontinuation of MIPAS in  
1001 spring 2012 (see Table 2). Although the MIPAS retrievals were only stratospheric profiles, the  
1002 combined assimilation with total column retrievals can trigger a correction in the troposphere  
1003 (Flemming et al., 2011).



1004 MACCRA had a less stable bias than CAMSiRA. In the lower and mid-troposphere biases from  
1005 2006–2008 were much higher than in the rest of the period, when they resembled more the  
1006 biases of CAMSiRA and CR. This confirms that the discussed inter-annual variability of  
1007 MACCRA seem less realistic than that of CR and CAMSiRA.

1008 It should be noted that both MACCRA and CAMSiRA suffered from larger than typical  
1009 negative biases in the NH in the first half of 2003, which can probably be explained by biases  
1010 in the initial conditions.

#### 1011 **6.4 Evaluation with Airbase Ozone surface observations**

1012 The AirBase and EMEP databases host operational air quality observations from different  
1013 national European networks. All EMEP stations are located in rural areas, while Airbase  
1014 stations are designed to monitor pollution at different scales. Stations of the rural regime can  
1015 capture the larger scale signal in particular for O<sub>3</sub>, which is spatially well correlated (Flemming  
1016 et al., 2005). Therefore EMEP stations and only rural Airbase stations were used in the  
1017 evaluation to account for the model resolution of C-IFS.

1018 Figure 23 shows the average diurnal cycle for each season of the observed values and  
1019 CAMSiRA, CR and MACCRA. CR and CAMSiRA were very similar and matched well the  
1020 shape of the observed diurnal cycle. However there was a constant bias of about 5 ppb in MAM  
1021 and DJF. CR had slightly smaller biases than CAMSiRA in JJA in the afternoon. MACCRA  
1022 had a larger diurnal range because the day-time values were higher than the ones of CAMSiRA.  
1023 This meant smaller day-time biases in MAM and DJF and hence a smaller seasonal bias for  
1024 MACCRA. But it also led to a considerable (10 ppb) day time overestimation in JJA and a  
1025 smaller overestimation in SON as well as a less well fit with the shape of the observed diurnal  
1026 cycle in all seasons.

1027 The winter and spring underestimation of CAMSiRA and CR has already been reported in  
1028 Flemming et al. (2015). To investigate the possible causes of this seasonal bias Figure 24 shows  
1029 the average seasonal cycle at the surface at the EMEP-AirBase stations and in the lower  
1030 troposphere (950–750 hPa) over ozone sonde stations. The differences between CAMSiRA, CR  
1031 and MACCRA were more pronounced in the lower troposphere than at the surface. This  
1032 indicates again that the assimilation has little influence on the surface values. CR matched the  
1033 observations in the lower troposphere well in all seasons apart from SON, when it  
1034 overestimated. MACCRA had similar biases as CR but overestimated additionally in JJA and



1035 especially over southern Europe, as shown in Katragkou et al. (2015). CAMSiRA  
1036 underestimated throughout the year with the exception of SON. As the patterns of the seasonal  
1037 biases were different in the lower troposphere and at the surface, we conclude that the winter  
1038 and spring-time bias at the surface is not predominately caused by tropospheric biases. It is  
1039 more likely that the simulation of surface processes such dry deposition and titration by freshly  
1040 emitted NO are the reasons for this bias at the surface.

## 1041 **7 Summary and conclusions**

1042 CAMSiRA is a new reanalysis data set of aerosol, CO and ozone for the period 2003–2015. It  
1043 has been produced by assimilating satellite retrievals of AOD, TC CO as well as TC and  
1044 stratospheric ozone profile retrievals from various sensors in C-IFS using the ECMWF 4D-  
1045 VAR approach. A similar set of observations was assimilated in MACCRA, a previous  
1046 reanalysis data set for the period 2003–2012. A control run with C-IFS (CR) without the  
1047 assimilation of AC observations was carried to infer the impact of the assimilated observations.

### 1048 **7.1 CAMSiRA compared to MACCRA**

1049 Compared to its predecessor MACCRA, CAMSiRA had smaller biases of surface and lower  
1050 tropospheric CO as shown by the comparison with MOZAIC/IAGOS CO profiles and NOAA-  
1051 GMD CO flask observations. However, MACCRA had lower CO biases in NH mid and upper  
1052 troposphere with respect to the MOZAIC/IAGOS CO profiles. The biases of TC ozone against  
1053 the WOUDC Dobson sun photometers were reduced from 5–10 DU in MACCRA to 0–5 DU  
1054 in CAMSiRA. The biases of CAMSiRA against AERONET AOD observations were lower in  
1055 most parts of the globe with the exception of South East Asia. A larger improvement was the  
1056 elimination of the positive bias of upper stratospheric ozone in MACCRA as shown by the  
1057 comparison with the GOZCARDS ozone product. CAMSiRA also had a better agreement with  
1058 the shape of the mean observed diurnal cycle of AIRBASE ground-level ozone observations in  
1059 Europe in all seasons but winter and spring time seasonal values were still underestimated by 5  
1060 ppb. We attribute all the aforementioned differences between CAMSiRA and MACCRA, which  
1061 were mainly improvements, to the change of the assimilating model, which was the coupled  
1062 system IFS-MOZART for MACCRA and C-IFS with updated aerosol parameterizations for  
1063 CAMSiRA.

1064 Progress achieved by changes to the assimilated observations was a noteworthy improvement  
1065 of the temporal consistency of the tropospheric CO and ozone fields in CAMSiRA. The



1066 assimilation of IASI CO in MACCRA from 2008 onwards had led to a decrease in the TC CO  
1067 values because of the biases against the MOPITT data set, which was assimilated during the  
1068 whole period. Consequently, the MACCRA CO fields in the mid- and high latitudes of both  
1069 hemispheres showed strong negative trends which were not in agreement with linear trends  
1070 estimated from CO flask surface observations. On the other hand, the linear trends of  
1071 CAMSiRA agreed well with the observed trends, which were close to zero in SH and reached  
1072 values of about 2 ppb/yr in the NH mid and high latitudes. The mid and upper tropospheric  
1073 ozone fields of MACCRA suffered from an increase in the period 2004–2008 caused by a  
1074 applying disproportionate application of the inter-instrument bias correction to the MLS column  
1075 retrievals, which was corrected for CAMSiRA (Inness et al., 2015).

1076 A discontinuity in the upper and middle tropospheric ozone field was noted for CAMSiRA after  
1077 January of 2013 and was due to a change in version of the assimilated MLS ozone retrievals.  
1078 Although this change in CAMSiRA did not mean an increase in the bias, it has to be considered  
1079 when trends of tropospheric ozone fields are to be calculated from the CAMSiRA data set.

1080 The AOD in CAMSiRA was about 0.01 lower than MACCRA in most parts of the globe,  
1081 mainly because of a 50% lower burden of sea salt in CAMSiRA. CAMSiRA had higher AOD  
1082 values over the desert dust emitting regions in North-Africa and the global desert dust burden  
1083 was higher in CAMSiRA. CAMSiRA had 25% higher AOD contribution by sulphate than  
1084 MACCRA, which is currently under scrutiny.

## 1085 **7.2 CAMSiRA compared to CR**

1086 The comparison with CR showed that the assimilation led to a clear improvement for CO, AOD  
1087 and TC ozone as well as stratospheric and upper tropospheric ozone.

1088 The assimilation of MOPITT CO increased the values in the NH mid-latitudes more in the  
1089 beginning of the period, which could indicate a stronger underestimation of the anthropogenic  
1090 emissions in this period as well as an overestimation of the trend in the emissions. The tropical  
1091 and SH values were reduced by the assimilation, which may indicate an overestimation of the  
1092 biomass burning emissions in this region. However, the rather zonally homogeneous CO  
1093 differences between CR and CAMSiRA suggest that not only biases in the fire emissions but  
1094 also of the lifetime and the CO transport need to be investigated further.

1095 The Cariolle scheme for stratospheric ozone, which was used in C-IFS, suffered from a large  
1096 overestimation of NH mid-and high latitude stratospheric ozone (50–100DU) and an



1097 underestimation in the tropics (-20 DU). These biases were corrected by the assimilation and  
1098 the resulting biases of CAMSiRA were of 5 DU and lower. Also in the SH high-latitudes the  
1099 Cariolle scheme overestimated the mean TCs especially in JJA by up to 30 DU but the depth  
1100 and the year-to-year variability of the ozone hole was well reproduced by CR. Nevertheless,  
1101 CAMSiRA had more realistic TCs and profiles than CR during the annual ozone hole events.

1102 The assimilation had only little impact on the ozone values at the surface and in lower  
1103 troposphere, where the biases of CAMSiRA were sometimes even slightly larger than of CR.  
1104 The small influence could be explained by the fact, that dry deposition velocities and important  
1105 ozone precursors such as NO<sub>x</sub> were not constrained during the assimilation process. Also  
1106 contributing was the fact that no direct tropospheric ozone observations were assimilated. The  
1107 assimilation was more beneficial in the upper troposphere, where the stratospheric influence is  
1108 more important.

1109 CAMSiRA had about 0.05 higher AOD values than CR apart from the desert dust emission  
1110 regions, where the assimilation strongly reduced the modelled values. CAMSiRA tended to  
1111 slightly overestimate the AERONET AOD observations and CR to underestimate but the  
1112 overall biases of CAMSiRA were smaller.

1113 Despite moderate differences in AOD, CR and CAMSiRA had considerable differences in the  
1114 aerosol speciation. The global annual sea salt burden by C-IFS in CR of 15 Tg was considerably  
1115 higher than the result of other modelling studies (Textor et al., 2006 and Spada et al., 2012).  
1116 Less efficient loss processes may have played a large role in this overestimation. The  
1117 assimilation strongly reduced the sea salt burden in CAMSiRA to about half of the value in CR.  
1118 Also the global desert dust burden was reduced by 25% by the assimilation leading to lower  
1119 total AOD values over the desert dust emissions regions of Sahara, Australia and Middle Asia.  
1120 Despite the fact that CAMSiRA had a 30% smaller global aerosol burden, its average global  
1121 AOD was about 10% higher than the one of CAMSiRA. This was caused by a strong increase  
1122 in sulphate in CAMSiRA. The optical properties and assumed size distribution of sulphate make  
1123 extinction more efficient for the same amount of mass. Sulphate became the dominant  
1124 contribution to AOD in the regions away from the main aerosol emissions. The strong  
1125 contribution of sulphate may have partly compensated for the inadequate representation of other  
1126 secondary aerosols in C-IFS. However its magnitude and spread over the whole globe seems  
1127 excessive. It might be caused by the lack of strong loss processes in the free troposphere as well  
1128 as biases in the assimilated observations over the open oceans. As the CR underestimates the



1129 assimilated AOD, the aerosol mass is increased during the assimilation, initially by the same  
1130 relative amount for all components. However, a longer life-time of sulphate causes a longer  
1131 lasting change compared to the other aerosol species, which made sulphate the dominating  
1132 aerosol. This distortion of the speciation can not be corrected by the assimilated MODIS AOD  
1133 retrievals, which do not contain information about the speciation.

### 1134 **7.3 Recommendations for future AC reanalysis**

1135 CAMSIRA is considerable improvement over MACCRA especially with respect to the  
1136 temporal consistency. To further improve on this important aspect, one should make sure that  
1137 consistent input emission data sets and assimilated observations are used. Changes in the  
1138 assimilated observations, such as the version change in the MLS after 2012 should be avoided.  
1139 The use of MEGAN simulated biogenic emissions for the whole period is advisable even if no  
1140 related jumps were detected in this study. To ensure consistency between the aerosols and  
1141 chemistry components, the same SO<sub>2</sub> emissions should be used.

1142 As improvements to lower tropospheric ozone by assimilating current satellite observations are  
1143 difficult to achieve, emphasis needs to be put on the improved simulation of chemistry and dry  
1144 deposition. The assimilation of tropospheric ozone column retrievals as well as of tropospheric  
1145 NO<sub>2</sub> may further help to improve the ground level ozone in the reanalysis. To further develop  
1146 the C-IFS assimilation system to allow the correction of ozone-precursor emissions could be an  
1147 important next step towards an improved tropospheric ozone analysis.

1148 The high sulphate burden introduced by the assimilation can perhaps be avoided by (i) the  
1149 introduction of more intensive loss processes in the free troposphere, (ii) an increase of the  
1150 organic matter to better represent non-accounted SOA components and (iii) changes to the  
1151 vertical structure of the background errors to avoid the accumulation of aerosol mass away from  
1152 the surface. In general, any modelling improvements for a better speciation will reflect in a  
1153 more realistic aerosol analysis and a better exploitation of the available observations. If possible  
1154 the latest reprocesses MODIS AOD dataset should be used (collection 6).

1155 In CAMSIRA and MACCRA the aerosol and chemistry schemes were independent. A better  
1156 coupling between the two and the meteorological simulation is desirable. For example the use  
1157 of aerosol to modulate photolysis rates and heterogeneous uptake on aerosol as well as the  
1158 simulating the impact on aerosols and ozone within the radiation transfer calculation of IFS will  
1159 be important next steps.



1160

1161 **Data access**

1162 The CAMSiRA data are freely available. Please contact copernicus-[support@ecmwf.int](mailto:support@ecmwf.int)

1163

1164 **Acknowledgments**

1165 CAMS is funded by the European Union's Copernicus Programme. The GOZCARDS data

1166 were obtained from the NASA Goddard Earth Science Data and Information Services Centre.

1167 We are grateful to the World Ozone and Ultraviolet Radiation Data Centre (WOUDC) for

1168 providing ozone sonde and Dobsen-photometer observations. We thank the Global

1169 Atmospheric Watch programme for the provision of CO and ozone surface observations. We

1170 thank the European Environmental Agency for providing access to European ozone

1171 observations in the AirBase data base. We also thank the MOZAIC (Measurements of OZone,

1172 water vapour, carbon monoxide and nitrogen oxides by in-service Airbus aircraft) and IAGOS

1173 (In-Service Aircraft for a Global Observing System) programmes for providing CO profile

1174 observations.

1175

1176





1177 **References**

- 1178 Auligne, T., McNally, A. P., and Dee, D. P.: Adaptive bias correction for satellite data in a  
1179 numerical weather prediction system, *Q. J. Roy. Meteor. Soc.*, 133, 631–642, 2007.
- 1180 Basher, R. E. (1982), Review of the Dobson spectrophotometer and its accuracy, *Global Ozone*  
1181 *Res. Monit. Proj., Rep. 13*, World Meteorol. Organ., Geneva, Switzerland, Dec. (Available at  
1182 <http://www.esrl.noaa.gov/gmd/ozwv/dobson/papers/report13/report13.html>)
- 1183 Bechtold, P., Orr, A. Morcrette, J.-J., Engelen, R., Flemming, J. and Janiskova, M.:  
1184 Improvements in the stratosphere and mesosphere of the IFS, *ECMWF Newsletter No. 120–*  
1185 *Summer, 2009*.
- 1186 Beekmann M., Ancellet G., Megie G., Smit H. G. J., and Kley D.: Intercomparison campaign  
1187 for vertical ozone profiles including electrochemical sondes of ECC and Brewer-Mast type and  
1188 aground based UV-differential absorption radar, *J. Atmos. Chem.*, 10, 259–288, 1994.
- 1189 Bellouin, N., Quaas, J., Morcrette, J.-J., and Boucher, O.: Estimates of aerosol radiative forcing  
1190 from the MACC re-analysis, *Atmos. Chem. Phys.*, 13, 2045-2062, doi:10.5194/acp-13-2045-  
1191 2013, 2013.
- 1192 Benedetti, A., Morcrette, J.-J., Boucher, O., Dethof, A., Engelen, R. J., Fisher, M., Flentje, H.,  
1193 Huneus, N., Jones, L., Kaiser, J. W., Kinne, S., Mangold, A., Razinger, M., Simmons, A. J.,  
1194 Suttie, M., and the GEMS-AER team: Aerosol analysis and forecast in the European Centre  
1195 for Medium-Range Weather Forecasts Integrated Forecast System: 2. Data assimilation, *J.*  
1196 *Geophys. Res.*, 114, D13205, doi:10.1029/2008JD011115, 2009.
- 1197 Benedetti, A. Jones, L., Kaiser, J. W., Morcrette, J.-J. and Rémy, S.: [Global climate] Aerosols  
1198 [in “State of the Climate in 2013”]. *Bull. Amer. Meteor. Soc.*, 95 (7), S36-37, 2014.
- 1199 Bhartia, P. K. and Wellemeyer, C.: TOMS-V8 total O3 algorithm, in: *OMI Ozone Product*  
1200 *ATBD Volume II*, NASA Goddard Space Flight Center, Greenbelt, MD, USA, 2002.
- 1201 Bhartia, P. K., McPeters, R. D., Mateer, C. L., Flynn, L. E., and Wellemeyer, C., Algorithm for  
1202 the estimation of vertical ozone profiles from the backscattered ultraviolet technique, *J.*  
1203 *Geophys. Res.*, 101, 18793–18806, 1996.
- 1204 Bocquet, M., Elbern, H., Eskes, H., Hirtl, M., Žabkar, R., Carmichael, G. R., Flemming, J.,  
1205 Inness, A., Pagowski, M., Pérez Camaño, J. L., Saide, P. E., San Jose, R., Sofiev, M., Vira, J.,  
1206 Baklanov, A., Carnevale, C., Grell, G., and Seigneur, C.: Data assimilation in atmospheric



- 1207 chemistry models: current status and future prospects for coupled chemistry meteorology  
1208 models, Atmos. Chem. Phys., 15, 5325–5358, doi:10.5194/acp-15-5325-2015, 2015.
- 1209 Boucher, O.: Atmospheric Aerosols, Properties and Climate Impacts, Springer Netherlands,  
1210 10.1007/978-94-017-9649-1, 311p. 2015.
- 1211 Cariolle, D. and Dèquè, M.: Southern hemisphere medium-scale waves and total ozone  
1212 disturbances in a spectral general circulation model, J. Geophys. Res., 91D, 10825–10846,  
1213 1986.
- 1214 Cariolle, D. and Teyssère, H.: A revised linear ozone photochemistry parameterization for use  
1215 in transport and general circulation models: multi-annual simulations, Atmos. Chem. Phys., 7,  
1216 2183–2196, doi:10.5194/acp-7-2183-2007, 2007.
- 1217 Cesnulyte, V., Lindfors, A. V., Pitkänen, M. R. A., Lehtinen, K. E. J., Morcrette, J.-J., and  
1218 Arola, A.: Comparing ECMWF AOD with AERONET observations at visible and UV  
1219 wavelengths, Atmos. Chem. Phys., 14, 593–608, doi:10.5194/acp-14-593-2014, 2014.
- 1220 Coldewey-Egbers, M., Loyola R., D. G., Braesicke, P., Dameris, M., van Roozendaal, M.,  
1221 Lerot, C. and Zimmer, W.: A new health check of the ozone layer at global and regional scales,  
1222 Geophys. Res. Lett., 41, 4363–4372, doi:10.1002/2014GL060212, 2014.
- 1223 Cooper, O. R., Parrish, D. D., Ziemke, J., Balashov, N. V., Cupeiro, M., Galbally, I. E., Gilge,  
1224 S., Horowitz, L., Jensen, N. R., Lamarque, J.-F., Naik, V., Oltmans, S. J., Schwab, J., Shindell,  
1225 D. T., Thompson, A. M., Thouret, V., Wang, Y., and Zbinden, R. M.: Global distribution and  
1226 trends of tropospheric ozone: An observation-based review, Elementa: Science of the  
1227 Anthropocene, 2, 1–28, doi:10.12952/journal.elementa.000029, 2014.
- 1228 Courtier, P., Thépaut, J.-N., and Hollingsworth, A.: A strategy for operational implementation  
1229 of 4D-Var, using an incremental approach, Q. J. Roy. Meteorol. Soc., 120, 1367–1388, 1994.
- 1230 Cuevas, E., Camino, C., Benedetti, A., Basart, S., Terradellas, E., Baldasano, J. M., Morcrette,  
1231 J. J., Marticorena, B., Goloub, P., Mortier, A., Berjón, A., Hernández, Y., Gil-Ojeda, M., and  
1232 Schulz, M.: The MACC-II 2007–2008 reanalysis: atmospheric dust evaluation and  
1233 characterization over northern Africa and the Middle East, Atmos. Chem. Phys., 15, 3991–4024,  
1234 doi:10.5194/acp-15-3991-2015, 2015.



- 1235 Dee, D. P.: Variational bias correction of radiance data in the ECMWF system, in: Proceedings  
1236 of the ECMWF workshop on assimilation of high spectral resolution sounders in NWP,  
1237 Reading, UK, 28 June–1 July 2004, 97–112, 2004.
- 1238 Dee, D. P. and Uppala, S.: Variational bias correction of satellite radiance data in the ERA-  
1239 Interim reanalysis, *Q. J. Roy. Meteor. Soc.*, 135, 1830–1841, 2009.
- 1240 Dee, D.P., Uppala, S.M., Simmons, A.J., Berrisford, P., Poli, P., Kobayashi, S., Andrae, U.,  
1241 Balmaseda, M.A., Balsamo, G., Bauer, P., Bechtold, P., Beljaars, A.C.M., van de Berg, L.,  
1242 Bidlot, J., Bormann, N., Delsol, C., Dragani, R., Fuentes, M., Geer, A.J., Haimberger, L., Healy,  
1243 S.B., Hersbach, H., Hólm, E.V., Isaksen, L., Kållberg, P., Köhler, M., Matricardi, M., McNally,  
1244 A.P., Monge-Sanz, B.M., Morcrette, J.-J., Park, B.-K., Peubey, C., de Rosnay, P., Tavolato, C.,  
1245 Thépaut, J.-N., Vitart, F.: The ERA-Interim reanalysis: Configuration and performance of the  
1246 data assimilation system, *Quarterly Journal of the Royal Meteorological Society*, 2011.
- 1247 Deeter, M.N., MOPITT Version 5 Product User's Guide, Technical Report, NCAR, Boulder,  
1248 USA, [www.acom.ucar.edu/mopitt/v5\\_users\\_guide\\_beta.pdf](http://www.acom.ucar.edu/mopitt/v5_users_guide_beta.pdf) (last access 24.7.2016), 2011.
- 1249 Deeter, M. N., S. Martínez-Alonso, D. P. Edwards, L. K. Emmons, J. C. Gille, H. M. Worden,  
1250 J. V. Pittman, B. C. Daube, and S. C. Wofsy: Validation of MOPITT Version 5 thermal-  
1251 infrared, near-infrared, and multispectral carbon monoxide profile retrievals for 2000–2011, *J.*  
1252 *Geophys. Res. Atmos.*, 118, 6710–6725, doi:10.1002/jgrd.50272, 2013.
- 1253 de Laat, A. T. J., Aben, I., Deeter, M., Nédélec, P., Eskes, H., Attié, J.-L., Ricaud, P., Abida,  
1254 R., El Amraoui, L., and Landgraf, J.: Validation of nine years of MOPITT V5 NIR using  
1255 MOZAIC/IAGOS measurements: biases and long-term stability, *Atmos. Meas. Tech.*, 7, 3783-  
1256 3799, doi:10.5194/amt-7-3783-2014, 2014.
- 1257 Dentener, F., Kinne, S., Bond, T., Boucher, O., Cofala, J., Generoso, S., Ginoux, P., Gong, S.,  
1258 Hoelzemann, J. J., Ito, A., Marelli, L., Penner, J. E., Putaud, J.-P., Textor, C., Schulz, M., van  
1259 der Werf, G. R., and Wilson, J.: Emissions of primary aerosol and precursor gases in the years  
1260 2000 and 1750 prescribed data-sets for AeroCom, *Atmos. Chem. Phys.*, 6, 4321-4344,  
1261 doi:10.5194/acp-6-4321-2006, 2006.
- 1262 Diamantakis, M. and Flemming, J.: Global mass fixer algorithms for conservative tracer  
1263 transport in the ECMWF model, *Geosci. Model Dev.*, 7, 965-979, doi:10.5194/gmd-7-965-  
1264 2014, 2014.



- 1265 Elguindi, N., Clark, H., Ordóñez, C., Thouret, V., Flemming, J., Stein, O., Huijnen, V., Moinat,  
1266 P., Inness, A., Peuch, V.-H., Stohl, A., Turquety, S., Athier, G., Cammas, J.-P., and Schultz,  
1267 M.: Current status of the ability of the GEMS/MACC models to reproduce the tropospheric CO  
1268 vertical distribution as measured by MOZAIC, *Geosci. Model Dev.*, 3, 501-518,  
1269 doi:10.5194/gmd-3-501-2010, 2010.
- 1270 Emmons, L. K., Arnold, S. R., Monks, S. A., Huijnen, V., Tilmes, S., Law, K. S., Thomas, J.  
1271 L., Raut, J.-C., Bouarar, I., Turquety, S., Long, Y., Duncan, B., Steenrod, S., Strode, S.,  
1272 Flemming, J., Mao, J., Langner, J., Thompson, A. M., Tarasick, D., Apel, E. C., Blake, D. R.,  
1273 Cohen, R. C., Dibb, J., Diskin, G. S., Fried, A., Hall, S. R., Huey, L. G., Weinheimer, A. J.,  
1274 Wisthaler, A., Mikoviny, T., Nowak, J., Peischl, J., Roberts, J. M., Ryerson, T., Warneke, C.,  
1275 and Helmig, D.: The POLARCAT Model Intercomparison Project (POLMIP): overview and  
1276 evaluation with observations, *Atmos. Chem. Phys.*, 15, 6721-6744, doi:10.5194/acp-15-6721-  
1277 2015, 2015.
- 1278 Field, R.D., G.R. van der Werf, and S.S.P. Shen, Human amplification of drought-induced  
1279 biomass burning in Indonesia since 1960, *Nature Geoscience*, 2 (3), 185-188,  
1280 doi:10.1038/ngeo443, 2009.
- 1281 Flemming, J., Stern, R., and Yamartino, R. J.: A new air quality regime classification scheme  
1282 for O<sub>3</sub>, NO<sub>2</sub>, SO<sub>2</sub> and PM<sub>10</sub> observations sites, *Atmos. Environ.*, 39, 6121-6129, 2005.
- 1283 Flemming, J., Inness, A., Flentje, H., Huijnen, V., Moinat, P., Schultz, M. G., and Stein, O.:  
1284 Coupling global chemistry transport models to ECMWF's integrated forecast system, *Geosci.*  
1285 *Model Dev.*, 2, 253-265, doi:10.5194/gmd-2-253-2009, 2009.
- 1286 Flemming, J., Inness, A., Jones, L., Eskes, H. J., Huijnen, V., Schultz, M. G., Stein, O., Cariolle,  
1287 D., Kinnison, D., and Brasseur, G.: Forecasts and assimilation experiments of the Antarctic  
1288 ozone hole 2008, *Atmos. Chem. Phys.*, 11, 1961-1977, doi:10.5194/acp-11-1961-2011, 2011.
- 1289 Flemming J, and Inness, A.: [Global climate] Carbon Monoxide [in "State of the Climate in  
1290 2013"]. *Bull. Amer. Meteor. Soc.*, 95 (7), S43, 2014.
- 1291 Flemming, J., Huijnen, V., Arteta, J., Bechtold, P., Beljaars, A., Blechschmidt, A.-M.,  
1292 Diamantakis, M., Engelen, R. J., Gaudel, A., Inness, A., Jones, L., Josse, B., Katragkou, E.,  
1293 Marecal, V., Peuch, V.-H., Richter, A., Schultz, M. G., Stein, O., and Tsikerdekis, A.:  
1294 Tropospheric chemistry in the Integrated Forecasting System of ECMWF, *Geosci. Model Dev.*,  
1295 8, 975-1003, doi:10.5194/gmd-8-975-2015, 2015.



- 1296 Froidevaux, L., Anderson, J., Wang, H.-J., Fuller, R. A., Schwartz, M. J., Santee, M. L.,  
1297 Livesey, N. J., Pumphrey, H. C., Bernath, P. F., Russell III, J. M., and McCormick, M. P.:  
1298 Global Ozone Chemistry And Related trace gas Data records for the Stratosphere  
1299 (GOZCARDS): methodology and sample results with a focus on HCl, H<sub>2</sub>O, and O<sub>3</sub>, Atmos.  
1300 Chem. Phys., 15, 10471-10507, doi:10.5194/acp-15-10471-2015, 2015.
- 1301 Froidevaux, L., Jiang, Y. B., Lambert, A., Livesey, N. J., Read, W. G., Waters, J. W., Browell,  
1302 E. V., Hair, J. W., Avery, M. A., McGee, T. J., Twigg, L.W., Sunnicht, G. K., Jucks, K.W.,  
1303 Margitan, J. J., Sen, B., Stachnik, R. A., Toon, G. C., Bernath, P. F., Boone, C. D., Walker, K.  
1304 A., Filipiak, M. J., Harwood, R. S., Fuller, R. A., Manney, G. L., Schwartz, M. J., Daffer, W.  
1305 H., Drouin, B. J., Cofield, R. E., Cuddy, D. T., Jarnot, R. F., Knosp, B.W., Perun, V. S., Snyder,  
1306 W. V., Stek, P. C., Thurstans, R. P., and Wagner, P. A.: Validation of Aura Microwave  
1307 LimbSounder stratospheric ozone measurements, J. Geophys. Res., 113, D15S20,  
1308 doi:10.1029/2007JD008771, 2008.
- 1309 Gaubert, B., Arellano Jr. A. F., Barré, J., Worden, H. M., Emmons, L. K., Tilmes, S., Buchholz,  
1310 R. R., Vitt, F., Raeder, K., Collins, N., Anderson, J. L., Wiedinmyer, C., Martinez Alonso, S.,  
1311 Edwards, D. P., Andreae, M. O., Hannigan, J. W., Petri, C., Strong, K. and Jones, N.: Toward  
1312 a chemical reanalysis in a coupled chemistry-climate model: An evaluation of MOPITT CO  
1313 assimilation and its impact on tropospheric composition, J. Geophys. Res. Atmos., 121, 7310–  
1314 7343, doi:10.1002/2016JD024863, 2016.
- 1315 Gaudel, A., Clark, H., Thouret, V., Jones, L., Inness, A., Flemming, J., Stein, O., Huijnen, V.,  
1316 Eskes, H., Nédélec, and P. Boulangerand, D.: On the use of MOZAIC-IAGOS data to assess the  
1317 ability of the MACC reanalysis to reproduce the distribution of O<sub>3</sub> and CO in the UTLS over  
1318 Europe. Tellus B. 67, 27955. DOI: <http://dx.doi.org/10.3402/tellusb.v67.27955>, 2015.
- 1319 Giordano, L., Brunner, D., Flemming, J., Hogrefe, C., Im, U., Bianconi, R., Badia, A., Balzarini,  
1320 A., Baró, R., Chemel, C., Curci, G., Forkel, R., Jiménez-Guerrero, P., Hirtl, M., Hodzic, A.,  
1321 Honzak, L., Jorba, O., Knote, C., Kuenen, J. J. P., Makar, P. A., Manders-Groot, A., Neal, L.,  
1322 Pérez, J. L., Pirovano, G., Pouliot, G., San José, R., Savage, N., Schröder, W., Sokhi, R. S.,  
1323 Syrakov, D., Torian, A., Tuccella, P., Werhahn, J., Wolke, R., Yahya, K., Žabkar, R., Zhang,  
1324 Y., and Galmarini, S.: Assessment of the MACC reanalysis and its influence as chemical  
1325 boundary conditions for regional air quality modelling in AQMEII-2, Atmos. Environ., 115,  
1326 371–388, 2015.



- 1327 George, M., Clerbaux, C., Bouarar, I., Coheur, P.-F., Deeter, M. N., Edwards, D. P., Francis,  
1328 G., Gille, J. C., Hadji-Lazaro, J., Hurtmans, D., Inness, A., Mao, D., and Worden, H. M.: An  
1329 examination of the long-term CO records from MOPITT and IASI: comparison of retrieval  
1330 methodology, *Atmos. Meas. Tech.*, 8, 4313-4328, doi:10.5194/amt-8-4313-2015, 2015.
- 1331 Granier, C., J.F. Lamarque, A. Mieville, J.F. Muller, J. Olivier, J. Orlando, J. Peters, G. Petron,  
1332 G. Tyndall, S. Wallens, POET, a database of surface emissions of ozone precursors, available  
1333 on internet at <http://www.aero.jussieu.fr/projet/ACCENT/POET.php>, 2005.
- 1334 Granier, C., B. Bessagnet, T. Bond, A. D'Angiola, H.D.v.d. Gon, G.J. Frost, A. Heil, J.W.  
1335 Kaiser, S. Kinne, Z. Klimont, S. Kloster, J.-F. Lamarque, C. Liousse, T. Masui, F. Meleux, A.  
1336 Mieville, T. Ohara, J.-C. Raut, K. Riahi, M.G. Schultz, S.J. Smith, A. Thomson, J.v. Aardenne,  
1337 G.R.v.d. Werf, and D.P.v. Vuuren, Evolution of anthropogenic and biomass burning emissions  
1338 of air pollutants at global and regional scales during the 1980-2010 period, *Climatic Change*,  
1339 109(1-2), 163-190, doi:10.1007/s10584-011-0154-1, 2011.
- 1340 Grythe, H., Ström, J., Krejci, R., Quinn, P., and Stohl, A.: A review of sea-spray aerosol source  
1341 functions using a large global set of sea salt aerosol concentration measurements, *Atmos. Chem.*  
1342 *Phys.*, 14, 1277-1297, doi:10.5194/acp-14-1277-2014, 2014.
- 1343 Guenther, A. B., Karl, T., Harley, P., Wiedinmyer, C., Palmer, P. I., and Geron, C.: Estimates  
1344 of global terrestrial isoprene emissions using MEGAN (Model of Emissions of Gases and  
1345 Aerosols from Nature), *Atmos. Chem. Phys.*, 6, 3181-3210, doi:10.5194/acp-6-3181-2006,  
1346 2006.
- 1347 Hao, N., Koukouli, M. E., Inness, A., Valks, P., Loyola, D. G., Zimmer, W., Balis, D. S.,  
1348 Zyrichidou, I., Van Roozendaal, M., Lerot, C., and Spurr, R. J. D.: GOME-2 total ozone  
1349 columns from MetOp-A/MetOp-B and assimilation in the MACC system, *Atmos. Meas. Tech.*,  
1350 7, 2937-2951, doi:10.5194/amt-7-2937-2014, 2014.
- 1351 Holben B.N., Eck, T.F., Slutsker, I., Tanré, D., Buis, J.P., Setzer, A., Vermote, E., Reagan, J.A.  
1352 . Kaufman, Y., Nakajima, T., Lavenu, F., Jankowiak, I. and Smirnov, A.: AERONET - A  
1353 federated instrument network and data archive for aerosol characterization, *Rem. Sens.*  
1354 *Environ.*, 66, 1-16, 1998.
- 1355 Hollingsworth, A., Engelen, R.J., Textor, C., Benedetti, A., Boucher, O., Chevallier, F., Dethof,  
1356 A., Elbern, H., Eskes, H., Flemming, J., Granier, C., Kaiser, J.W., Morcrette, J.-J., Rayner, P.,  
1357 Peuch, V.H., Rouil, L., Schultz, M.G., Simmons, A.J and The GEMS Consortium: Toward a



- 1358 Monitoring and Forecasting System For Atmospheric Composition: The GEMS Project. Bull.  
1359 Amer. Meteor. Soc., 89, 1147-1164, 2008.
- 1360 Hsu N. C., Jeong M.-J., Bettenhausen C, Sayer A.M., Hansell R., Seftor C.S., Huang J., Tsay  
1361 S.-C.: Enhanced Deep Blue aerosol retrieval algorithm: The second generation, J. Geophys.  
1362 Res., VOL. 118, 120, doi:10.1002/jgrd.50712, 2013.
- 1363 Huneus, N., Schulz, M., Balkanski, Y., Griesfeller, J., Prospero, J., Kinne, S., Bauer, S.,  
1364 Boucher, O., Chin, M., Dentener, F., Diehl, T., Easter, R., Fillmore, D., Ghan, S., Ginoux, P.,  
1365 Grini, A., Horowitz, L., Koch, D., Krol, M. C., Landing, W., Liu, X., Mahowald, N., Miller,  
1366 R., Morcrette, J.-J., Myhre, G., Penner, J., Perlwitz, J., Stier, P., Takemura, T., and Zender, C.  
1367 S.: Global dust model intercomparison in AeroCom phase I, Atmos. Chem. Phys., 11, 7781-  
1368 7816, doi:10.5194/acp-11-7781-2011, 2011.
- 1369 Huijnen, V., Williams, J., van Weele, M., van Noije, T., Krol, M., Dentener, F., Segers, A.,  
1370 Houweling, S., Peters, W., de Laat, J., Boersma, F., Bergamaschi, P., van Velthoven, P., Le  
1371 Sager, P., Eskes, H., Alkemade, F., Scheele, R., Nédélec, P., and Pätz, H.-W.: The global  
1372 chemistry transport model TM5: description and evaluation of the tropospheric chemistry  
1373 version 3.0, Geosci. Model Dev., 3, 445-473, doi:10.5194/gmd-3-445-2010, 2010.
- 1374 Huijnen V., Wooster, M. J., Kaiser, J. W., Gaveau, D.L.A., Flemming, J., Parrington, M. Inness,  
1375 A., Murdiyarsa, D., Main, B. and van Weele, M.: Fire carbon emissions over maritime southeast  
1376 Asia in 2015 largest since 1997, Scientific Reports, 6:26886, DOI: 10.1038/srep26886, 2016.
- 1377 Im, U., Bianconi, R., Solazzo, E., Kioutsioukis, I., Badia, A., Balzarini, A., Baró, R., Bellasio,  
1378 R., Brunner, D., Chemel, C., Curci, G., Flemming, J., Forkel, R., Giordano, L., Jiménez-  
1379 Guerrero, P., Hirtl, M., Hodzic, A., Honzak, L., Jorba, O., Knote, C., Kuenen, J.J.P., Makar,  
1380 P.A., Manders-Groot, A., Neal, L., Pérez, J.L., Pirovano, G., Pouliot, G., San Jose, R., Savage,  
1381 N., Schroder, W., Sokhi, R.S., Syrakov, D., Torian, A., Tuccella, P., Werhahn, J., Wolke, R.,  
1382 Yahya, K., Zabkar, R., Zhang, Y., Zhang, J., Hogrefe, C., Galmarini, S.: Evaluation of  
1383 operational on-line-coupled regional air quality models over Europe and North America in the  
1384 context of AQMEII phase 2. Part I: Ozone, Atmospheric Environment, doi:  
1385 10.1016/j.atmosenv.2014.09.042, 2014.
- 1386 Inness, A., Baier, F., Benedetti, A., Bouarar, I., Chabrilat, S., Clark, H., Clerbaux, C., Coheur,  
1387 P., Engelen, R. J., Errera, Q., Flemming, J., George, M., Granier, C., Hadji-Lazaro, J., Huijnen,  
1388 V., Hurtmans, D., Jones, L., Kaiser, J. W., Kapsomenakis, J., Lefever, K., Leitão, J., Razinger,



- 1389 M., Richter, A., Schultz, M. G., Simmons, A. J., Suttie, M., Stein, O., Thépaut, J.-N., Thouret,  
1390 V., Vrekoussis, M., Zerefos, C., and the MACC team: The MACC reanalysis: an 8 yr data set  
1391 of atmospheric composition, *Atmos. Chem. Phys.*, 13, 4073-4109, doi:10.5194/acp-13-4073-  
1392 2013, 2013.
- 1393 Inness, A., Blechschmidt, A.-M., Bouarar, I., Chabrillat, S., Crepulja, M., Engelen, R. J.,  
1394 Eskes, H., Flemming, J., Gaudel, A., Hendrick, F., Huijnen, V., Jones, L., Kapsomenakis, J.,  
1395 Katragkou, E., Keppens, A., Langerock, B., de Mazière, M., Melas, D., Parrington, M.,  
1396 Peuch, V. H., Razinger, M., Richter, A., Schultz, M. G., Suttie, M., Thouret, V., Vrekoussis,  
1397 M., Wagner, A., and Zerefos, C.: Data assimilation of satellite retrieved ozone, carbon  
1398 monoxide and nitrogen dioxide with ECMWF's Composition-IFS, *Atmos. Chem. Phys.*, 15,  
1399 5275-5303, doi:10.5194/acp-15-5275-2015, 2015.
- 1400 Jacob, D.J. H. Liu, C.Mari, and R.M. Yantosca, Harvard wet deposition scheme for GMI,  
1401 Harvard University Atmospheric Chemistry Modeling Group, revised March 2000.  
1402 [http://acmg.seas.harvard.edu/geos/wiki\\_docs/deposition/wetdep.jacob\\_etal\\_2000.pdf](http://acmg.seas.harvard.edu/geos/wiki_docs/deposition/wetdep.jacob_etal_2000.pdf), 2000.
- 1403 Jung, T., T. N. Palmer, M. J. Rodwell, and S. Serrar: Diagnosing forecast error using relaxation  
1404 experiments. ECMWF Newsletter 82, ECMWF, Shinfield Park, Reading, Berkshire RG2 9AX,  
1405 UK, 2008.
- 1406 Kaiser, J. W., Heil, A., Andreae, M. O., Benedetti, A., Chubarova, N., Jones, L., Morcrette, J.-  
1407 J., Razinger, M., Schultz, M. G., Suttie, M., and van der Werf, G. R.: Biomass burning  
1408 emissions estimated with a global fire assimilation system based on observed fire radiative  
1409 power, *Biogeosciences*, 9, 527-554, doi:10.5194/bg-9-527-2012, 2012.
- 1410 Katragkou, E., Zanis, P., Tsikerdekis, A., Kapsomenakis, J., Melas, D., Eskes, H., Flemming,  
1411 J., Huijnen, V., Inness, A., Schultz, M. G., Stein, O., and Zerefos, C. S.: Evaluation of near  
1412 surface ozone over Europe from the MACC reanalysis, *Geoscientific Model Development*, 8,  
1413 2299-2314, 2015.
- 1414 Kinne, S., Schulz, M., Textor, C., Guibert, S., Balkanski, Y., Bauer, S. E., Berntsen, T., Berglen,  
1415 T. F., Boucher, O., Chin, M., Collins, W., Dentener, F., Diehl, T., Easter, R., Feichter, J.,  
1416 Fillmore, D., Ghan, S., Ginoux, P., Gong, S., Grini, A., Hendricks, J., Herzog, M., Horowitz,  
1417 L., Isaksen, I., Iversen, T., Kirkevåg, A., Kloster, S., Koch, D., Kristjansson, J. E., Krol, M.,  
1418 Lauer, A., Lamarque, J. F., Lesins, G., Liu, X., Lohmann, U., Montanaro, V., Myhre, G.,  
1419 Penner, J., Pitari, G., Reddy, S., Seland, O., Stier, P., Takemura, T., and Tie, X.: An AeroCom





- 1420 initial assessment – optical properties in aerosol component modules of global models, Atmos.  
1421 Chem. Phys., 6, 1815-1834, doi:10.5194/acp-6-1815-2006, 2006.
- 1422 Kinnison, D. E., Brasseur, G. P., Walters, S., Garcia, R. R., Marsh, D. R., Sassi, F., Harvey, V.  
1423 L., Randall, C. E., Emmons, L., Lamarque, J. F., Hess, P., Orlando, J. J., Tie, X. X., Randel,  
1424 W., Pan, L. L., Gettelman, A., Granier, C., Diehl, T., Niemeier, U. and Simmons, A. J.:  
1425 Sensitivity of Chemical Tracers to Meteorological Parameters in the MOZART-3 Chemical  
1426 Transport Model. J. Geophys. Res, 112, D03303, doi:10.1029/2008JD010739, 2007.
- 1427 Komhyr, W. D., Barnes, R. A., Borthers, G. B., Lathrop, J. A., Kerr, J. B., and Opperman, D.  
1428 P.: Electrochemical concentration cell ozonesonde performance evaluation during STOIC  
1429 1989, J. Geophys. Res., 100, 9231–9244, 1995.
- 1430 Lamarque, J.-F., Shindell, D. T., Josse, B., Young, P. J., Cionni, I., Eyring, V., Bergmann, D.,  
1431 Cameron-Smith, P., Collins, W. J., Doherty, R., Dalsoren, S., Faluvegi, G., Folberth, G., Ghan,  
1432 S. J., Horowitz, L. W., Lee, Y. H., MacKenzie, I. A., Nagashima, T., Naik, V., Plummer, D.,  
1433 Righi, M., Rumbold, S. T., Schulz, M., Skeie, R. B., Stevenson, D. S., Strode, S., Sudo, K.,  
1434 Szopa, S., Voulgarakis, A., and Zeng, G.: The Atmospheric Chemistry and Climate Model  
1435 Intercomparison Project (ACCMIP): overview and description of models, simulations and  
1436 climate diagnostics, Geosci. Model Dev., 6, 179-206, doi:10.5194/gmd-6-179-2013, 2013.
- 1437 Lefever, K., van der A, R., Baier, F., Christophe, Y., Errera, Q., Eskes, H., Flemming, J., Inness,  
1438 A., Jones, L., Lambert, J.-C., Langerock, B., Schultz, M. G., Stein, O., Wagner, A., and  
1439 Chabrilat, S.: Copernicus stratospheric ozone service, 2009–2012: validation, system  
1440 intercomparison and roles of input data sets, Atmos. Chem. Phys., 15, 2269-2293,  
1441 doi:10.5194/acp-15-2269-2015, 2015.
- 1442 Levelt, P. F., van den Oord, G. H. J., Dobber, M. R., Malkki, A., Visser, H., de Vries, J.,  
1443 Stammes, P., Lundell, J. O. V., and Saari, H.: The ozone monitoring instrument, IEEE T.  
1444 Geosci. Remote, 44, 1093–1101, 2006.
- 1445 Levy, R. C., Remer, L. A., Kleidman, R. G., Mattoo, S., Ichoku, C., Kahn, R., and Eck, T. F.:  
1446 Global evaluation of the Collection 5 MODIS dark-target aerosol products over land, Atmos.  
1447 Chem. Phys., 10, 10399-10420, doi:10.5194/acp-10-10399-2010, 2010.
- 1448 Liu, X., Bhartia, P. K., Chance, K., Spurr, R. J. D., and Kurosu, T. P.: Ozone profile retrievals  
1449 from the Ozone Monitoring Instrument, Atmos. Chem. Phys., 10, 2521–2537, 2010,  
1450 <http://www.atmos-chem-phys.net/10/2521/2010/>.



- 1451 Manney, G., Santee, M. L., Rex, M., Livesey, N. J., Pitts, M. C., Veefkind, P., Nash, R. R.,  
1452 Wohltmann, I., Lehmann, R., Froidevaux, L., Poole, L. R., Schoeberl, M. R., Haffner, D. P.,  
1453 Davies, J., Dorokhov, V., Gernandt, H., Johnson, B., Kivi, R., Kyr o, E., Larsen, N., Levelt, P.  
1454 F., Makshtas, A., McElroy, C. T., Nakajima, H., Parrondo, M. C., Tarasick, D.W., von der  
1455 Gathen, P., Walker, P. K. A., and Zinoviev, N. S.: Unprecedented Arctic ozone loss in 2011,  
1456 Arctic winter 2010/2011 at the brink of an ozone hole, *Nature*, 478, 469–475,  
1457 doi:10.1038/nature10556, 2011.
- 1458 McNally, A. P., Watts, P. D., Smith, J. A., Engelen, R. J., Kelly, G. A., Thépaut, J.-N., and  
1459 Matricardi, M.: The assimilation of AIRS radiance data at ECMWF, *Q. J. Roy. Meteor. Soc.*,  
1460 132, 935–957, 2006.
- 1461 Marengo, A., Thouret, V., Nédélec, P., Smit, H. G., Helten, M., Kley, D., Karcher, F., Simon,  
1462 P., Law, K., Pyle, J., Poschmann, G., Von Wrede, R., Hume, C., and Cook, T.: Measurement  
1463 of ozone and water vapour by Airbus in-service air-craft: The MOZAIC airborne programme,  
1464 an overview, *J. Geophys. Res.*, 103, 25631–25642, 1998.
- 1465 Meijer, E.W., P. F. J. van Velthoven, D. W. Brunner, H. Huntrieser and H. Kelder:  
1466 Improvement and evaluation of the parameterization of nitrogen oxide production by lightning,  
1467 *Physics and Chemistry of the Earth, Part C, Volume 26, Issue 8, Pages 577-583*, 2001.
- 1468 Miyazaki, K., Eskes, H. J., and Sudo, K.: A tropospheric chemistry reanalysis for the years  
1469 2005–2012 based on an assimilation of OMI, MLS, TES, and MOPITT satellite data, *Atmos.*  
1470 *Chem. Phys.*, 15, 8315–8348, doi:10.5194/acp-15-8315-2015, 2015.
- 1471 Monks, P. S., Archibald, A. T., Colette, A., Cooper, O., Coyle, M., Derwent, R., Fowler, D.,  
1472 Granier, C., Law, K. S., Mills, G. E., Stevenson, D. S., Tarasova, O., Thouret, V., von  
1473 Schneidemesser, E., Sommariva, R., Wild, O., and Williams, M. L.: Tropospheric ozone and  
1474 its precursors from the urban to the global scale from air quality to short-lived climate forcer,  
1475 *Atmos. Chem. Phys.*, 15, 8889–8973, doi:10.5194/acp-15-8889-2015, 2015.
- 1476 Morcrette, J.-J., Boucher, O., Jones, L., Salmond, D., Bechtold, P., Beljaars, A., Benedetti, A.,  
1477 Bonet, A., Kaiser, J. W., Razinger, M., Schulz, M., Serrar, S., Simmons, A. J., Sofiev, M.,  
1478 Suttie, M., Tompkins, A. M. and Untch, A.: Aerosol analysis and forecast in the ECMWF  
1479 Integrated Forecast System. Part I: Forward modelling, *J. Geophys. Res.*, 2009.



- 1480 Morcrette, J. J., Benedetti, A., Jones, L., Kaiser, J. W., Razinger, M., and Suttie, M.: Prognostic  
1481 Aerosols in the ECMWF IFS: MACC vs. GEMS Aerosols, ECMWF Technical Memorandum,  
1482 659, 2011.
- 1483 Nedelec, P., Cammas, J.-P., Thouret, V., Athier, G., Cousin, J.-M., Legrand, C., Abonnel, C.,  
1484 Lecoq, F., Cayez, G., and Marizy, C.: An improved infrared carbon monoxide analyser for  
1485 routine measurements aboard commercial Airbus aircraft: technical validation and first  
1486 scientific results of the MOZAIC III programme, *Atmos. Chem. Phys.*, 3, 1551–1564,  
1487 doi:10.5194/acp-3-1551-2003, 2003.
- 1488 Munro, R., R. Siddans, W. J. Reburn, and B. J. Kerridge, Direct measurements of tropospheric  
1489 ozone distributions from space, *Nature*, 392, 168–171, 1998.
- 1490 Munro, R., Eisinger, M., Anderson, C., Callies, J., Corpaccioli, E., Lang, R., Lefebvre, A.,  
1491 Livschitz, Y., and Albinana, A. P.: GOME-2 on MetOp, Proc. of The 2006 EUMETSAT  
1492 Meteorological Satellite Conference, Helsinki, Finland, 2006.
- 1493 Novelli, P.C. and Masarie, K.A.: Atmospheric Carbon Monoxide Dry Air Mole Fractions from  
1494 the NOAA ESRL Carbon Cycle Cooperative Global Air Sampling Network, 1988-2012,  
1495 Version: 2013-08-08, Path: [ftp://aftp.cmdl.noaa.gov/data/trace\\_gases/co/flask/surface/](ftp://aftp.cmdl.noaa.gov/data/trace_gases/co/flask/surface/), 2013.  
1496 (last access 6.5.2016)
- 1497 Novelli, P. C., Masarie, K. A., Lang, P. M., Hall, B. D., Myers, R. C., and Elkins, J. W.:  
1498 Reanalysis of tropospheric CO trends: effects of the 1997–1998 wildfires, *J. Geophys. Res.*,  
1499 108, 4464, doi:10.1029/2002JD003031, 2003.
- 1500 Olivier J., J. Peters, C. Granier, G. Petron, J.F. Muller, and S. Wallens: Present and future  
1501 surface emissions of atmospheric compounds, POET report #2, EU project EVK2-1999-00011,  
1502 2003.
- 1503 Onogi, K., Tsutsui, J., Koide, H., Sakamoto, M., Kobayashi, S., Hatsushika, H., Matsumoto,  
1504 T., Yamazaki, N., Kamahori, H., Takahashi, K., Kadokura, S., Wada, K., Kato, K., Oyama, R.,  
1505 Ose, T., Mannoji, N., and Taira, R.: The JRA-25 Reanalysis, *Q. J. Roy. Meteorol. Soc.*, 85,  
1506 369–432, 2007.
- 1507 Reddy M. S., Boucher O., Bellouin N., Schulz M., Balkanski Y., Dufresne J.-L., Pham M.:  
1508 Estimates of global multicomponent aerosol optical depth and direct radiative perturbation in  
1509 the Laboratoire de Mé té orologie Dynamique general circulation model, *J. Geophys. Res.*, 110,  
1510 D10S16, doi:10.1029/2004JD004757, 2005.



- 1511 Remer, L. A., Kaufman, Y. J. M., Tanré, D., Mattoo, S., Chu, D. A. M, Martins, J. V., Li, R.-  
1512 R., Ichoku, C., Levy, R. C., Kleidman, R. G., Eck, T. F., Vermote, E. and Holben, B. N.: The  
1513 MODIS Aerosol Algorithm, Products, and Validation Journal of the Atmospheric Sciences  
1514 2005 62:4, 947-973, 2005.
- 1515 Rienecker, M. M., Suarez, M. J., Gelaro, R., Todling, R., Bacmeister, J., Liu, E., Bosilovich,  
1516 M. G., Schubert, S. D., Takacs, L., Kim, G.- K., Bloom, S., Chen, J., Collins, D., Conaty, A.,  
1517 da Silva, A., Gu, W., Joiner, J., Koster, R. D., Lucchesi, R., Molod, A. M., Owens, T., Pawson,  
1518 S., Pegion, P., Redder, C. R., Reichle, R., Robertson, F. R., Ruddick, A. G., Sienkiewicz, M.,  
1519 and Woollen, J.: MERRA – NASA’s Modern- Era Retrospective, Anal. Res. Appl., J. Climate,  
1520 24, 3624–3648, doi:10.1175/JCLID-11-00015.1, 2011.
- 1521 Saha, S., Moorthi, S., Pan, H. L., Wu, X., Wang, J., Nadiga, S., Tripp, P., Kistler, R., Woollen,  
1522 J., Behringer, D., Liu, H., Stokes, D., Grumbine, R., Gayno, G., Hou, Y. T., Chuang, H. Y.,  
1523 Juang, H. M. H., Sela, J., Iredell, M., Treadon, R., Kleist, D., Van Delst, P., Keyser, D., Derber,  
1524 J., Ek, M., Meng, J., Wei, H., Yang, R., Lord, S., Van Den Dool, H., Kumar, A., Wang, W.,  
1525 Long, C., Chelliah, M., Xue, Y., Huang, B., Schemm, J. K., Ebisuzaki, W., Lin, R., Xie, P.,  
1526 Chen, M., Zhou, S., Higgins, W., Zou, C. Z., Liu, Q., Chen, Y., Han, Y., Cucurull, L., Reynolds,  
1527 R. W., Rutledge, G., and Goldberg, M.: The NCEP climate forecast system reanalysis, B. Am.  
1528 Meteorol. Soc., 91, 1015–1057, 2010.
- 1529 Schere, K., Flemming, J., Vautard, R., Chemel, C., Colette, A., Hogrefe, C., Bessagnet, B.,  
1530 Meleux, F., Mathur, R., Roselle, S., Hu, R.-M., Sokhi, R. S., Rao, S. T., and Galmarini, S.:  
1531 Trace gas/aerosol boundary concentrations and their impacts on continental-scale AQMEII  
1532 modeling domains, Atmos. Environ., 53, 38–50, doi:10.1016/j.atmosenv.2011.09.043, 2012.
- 1533 Schutgens, N. A. J., Nakata, M., and Nakajima, T.: Estimating aerosol emissions by  
1534 assimilating remote sensing observations into a Global transport model, Remote Sens., 4, 3528–  
1535 3543, 2012.
- 1536 Sindelarova, K., Granier, C., Bouarar, I., Guenther, A., Tilmes, S., Stavrakou, T., Müller, J.-F.,  
1537 Kuhn, U., Stefani, P., and Knorr, W.: Global data set of biogenic VOC emissions calculated by  
1538 the MEGAN model over the last 30 years, Atmos. Chem. Phys., 14, 9317-9341,  
1539 doi:10.5194/acp-14-9317-2014, 2014.



- 1540 Shi, Y., Zhang, J., Reid, J. S., Holben, B., Hyer, E. J., and Curtis, C.: An analysis of the  
1541 collection 5 MODIS over-ocean aerosol optical depth product for its implication in aerosol  
1542 assimilation, *Atmos. Chem. Phys.*, 11, 557-565, doi:10.5194/acp-11-557-2011, 2011.
- 1543 Shindell, D.T., G. Faluvegi, D.S. Stevenson, M.C. Krol, L.K. Emmons, J.-F. Lamarque, G.  
1544 Pétron, F.J. Dentener, K. Ellingsen, M.G. Schultz, O. Wild, M. Amann, C.S. Atherton, D.J.  
1545 Bergmann, I. Bey, T. Butler, J. Cofala, W.J. Collins, R.G. Derwent, R.M. Doherty, J. Drevet,  
1546 H.J. Eskes, A.M. Fiore, M. Gauss, D.A. Hauglustaine, L.W. Horowitz, I.S.A. Isaksen, M.G.  
1547 Lawrence, V. Montanaro, J.-F. Müller, G. Pitari, M.J. Prather, J.A. Pyle, S. Rast, J.M.  
1548 Rodriguez, M.G. Sanderson, N.H. Savage, S.E. Strahan, K. Sudo, S. Szopa, N. Unger, T.P.C.  
1549 van Noije, and G. Zeng: Multi-model simulations of carbon monoxide: Comparison with  
1550 observations and projected near-future changes. *J. Geophys. Res.*, 111, D19306,  
1551 doi:10.1029/2006JD007100, 2006.
- 1552 Spada, M., Jorba, O., Pérez García-Pando, C., Janjic, Z., and Baldasano, J. M.: Modeling and  
1553 evaluation of the global sea-salt aerosol distribution: sensitivity to size-resolved and sea-surface  
1554 temperature dependent emission schemes, *Atmos. Chem. Phys.*, 13, 11735-11755,  
1555 doi:10.5194/acp-13-11735-2013, 2013.
- 1556 Stein, O., Schultz, M. G., Bouarar, I., Clark, H., Huijnen, V., Gaudel, A., George, M., and  
1557 Clerbaux, C.: On the wintertime low bias of Northern Hemisphere carbon monoxide in global  
1558 model studies, *Atmos. Chem. Phys.*, 14, 9295–9316, doi:10.5194/acp-14-9295-2014, 2014
- 1559 Steinbrecht, W., Shwartz, R., and Claude, H.: New pump correction for the Brewer-Mast  
1560 ozonesonde: Determination from experiment and instrument intercomparisons, *J. Atmos.*  
1561 *Ocean. Tech.* 15, 144–156, 1998.
- 1562 Tegtmeier, S., Hegglin, M. I., Anderson, J., Bourassa, A., Brohede, S., Degenstein, D., Froide-  
1563 vaux, L., Fuller, R., Funke, B., Gille, J., Jones, A., Kasai, Y., Krüger, K., Kyrölä, E., Lingen-  
1564 felder, G., Lumpe, J., Nardi, B., Neu, J., Pendlebury, D., Remsberg, E., Rozanov, A., Smith, L.,  
1565 Toohey, M., Urban, J., von Clarmann, T., Walker, K. A., and Wang, R. H. J.: SPARC Data  
1566 Initiative: a comparison of ozone climatologies from international satellite limb sounders, *J.*  
1567 *Geophys. Res.*, 118, 12229–12247, doi:10.1002/2013JD019877, 2013.
- 1568 Textor, C., Schulz, M., Guibert, S., Kinne, S., Balkanski, Y., Bauer, S., Berntsen, T., Berglen,  
1569 T., Boucher, O., Chin, M., Dentener, F., Diehl, T., Easter, R., Feichter, H., Fillmore, D., Ghan,  
1570 S., Ginoux, P., Gong, S., Grini, A., Hendricks, J., Horowitz, L., Huang, P., Isaksen, I., Iversen,



- 1571 I., Kloster, S., Koch, D., Kirkevåg, A., Kristjansson, J. E., Krol, M., Lauer, A., Lamarque, J. F.,  
1572 Liu, X., Montanaro, V., Myhre, G., Penner, J., Pitari, G., Reddy, S., Seland, Ø., Stier, P.,  
1573 Takemura, T., and Tie, X.: Analysis and quantification of the diversities of aerosol life cycles  
1574 within AeroCom, Atmos. Chem. Phys., 6, 1777-1813, doi:10.5194/acp-6-1777-2006, 2006.
- 1575 Uppala, S., Kallberg, P., Simmons, A. J., Andrae, U., Bechtold, V. D. C., Fiorino, M., Gibson,  
1576 J. K., Haseler, J., Hernandez, A., Kelly, G. A., Li, X., Onogi, K., Saarinen, S., Sokka, N., Allan,  
1577 R. P., Andersson, E., Arpe, K., Balmaseda, M. A., Beljaars, A. C. M., van de Berg, L., Bidlot,  
1578 J., Bormann, N., Caires, S., Chevallier, F., Dethof, A., Dragosavac, M., Fisher, M., Fuentes,  
1579 M., Hagemann, S., Holm, E., Hoskins, B. J., Isaksen, L., Janssen, P. A. E. M., Jenne, R.,  
1580 McNally, A. P., Mahfouf, J. F., Morcrette, J. J., Rayner, N. A., Saunders, R. W., Simon, P.,  
1581 Sterl, A., Trenberth, K. E., Untch, A., Vasiljevic, D., Viterbo, P., and Woollen, J.: The ERA-  
1582 40 re-analysis, Q. J. R. Meteorol. Soc., 131, 2961–3012, 2005.
- 1583 Wagner, A., Blechschmidt, A.-M., Bouarar, I., Brunke, E.-G., Clerbaux, C., Cupeiro, M.,  
1584 Cristofanelli, P., Eskes, H., Flemming, J., Flentje, H., George, M., Gilge, S., Hilboll, A., Inness,  
1585 A., Kapsomenakis, J., Richter, A., Ries, L., Spangl, W., Stein, O., Weller, R., and Zerefos, C.:  
1586 Evaluation of the MACC operational forecast system – potential and challenges of global near-  
1587 real-time modelling with respect to reactive gases in the troposphere, Atmos. Chem. Phys., 15,  
1588 14005-14030, doi:10.5194/acp-15-14005-2015, 2015.
- 1589 Wesely, M.L.: Parameterization of Surface Resistances to Gaseous Dry Deposition in Regional-  
1590 Scale Numerical Models. Atmos. Environ., 23, 1293-1304, 1989.
- 1591 Worden, H. M., Deeter, M. N., Frankenberg, C., George, M., Nichitiu, F., Worden, J., Aben, I.,  
1592 Bowman, K. W., Clerbaux, C., Coheur, P. F., de Laat, A. T. J., Detweiler, R., Drummond, J.  
1593 R., Edwards, D. P., Gille, J. C., Hurtmans, D., Luo, M., Martínez-Alonso, S., Massie, S., Pfister,  
1594 G., and Warner, J. X.: Decadal record of satellite carbon monoxide observations, Atmos. Chem.  
1595 Phys., 13, 837-850, doi:10.5194/acp-13-837-2013, 2013.
- 1596 Van der A, R.J.; Allaart, M.A.F.; Eskes, H.J. Multi sensor reanalysis of total ozone. Atmos.  
1597 Chem.Phys. 2010, 10, 11277–11294.
- 1598 van der A, R. J., Allaart, M. A. F., and Eskes, H. J.: Extended and refined multi sensor reanalysis  
1599 of total ozone for the period 1970-2012, Atmos. Meas. Tech., 8, 3021-3035, doi:10.5194/amt-  
1600 8-3021-2015, 2015.



- 1601 Verstraeten, W. W., Neu, J. L., Williams, J. E., Bowman, K. W., Worden, J. R., Boersma, K.  
1602 F.: Rapid increases in tropospheric ozone production and export from China, *Nat. Geosci.*, 8,  
1603 690–695, doi:10.1038/ngeo2493, 2015.
- 1604 von Clarmann, T., Glatthor, N., Grabowski, U., Höpfner, M., Kellmann, S., Kiefer, M., Linden,  
1605 A., Mengistu Tsidu, G., Milz, M., Steck, T., Stiller, G. P., Wang, D. Y., Fischer, H., Funke, B.,  
1606 Gil-López, S., and López-Puertas, M.: Retrieval of temperature and tangent altitude pointing  
1607 from limb emission spectra recorded from space by the Michelson Interferometer for Passive  
1608 Atmospheric Sounding (MIPAS), *J. Geophys. Res.*, 108, 4736, doi:10.1029/2003JD003602,  
1609 2003.
- 1610 Waters, J.W., Froidevaux, L., Harwood, R. S., Jarnot, R. F., Pickett, H. M., Read, W. G., Siegel,  
1611 P. H., Cofield, R. E., Filipiak, M. J., Flower, D. A., Holden, J. R., Lau, G. K., Livesey, N. J.,  
1612 Manney, G. L., Pumphrey, H. C., Santee, M. L., Wu, D. L., Cuddy, D. T., Lay, R. R., Loo, M.  
1613 S., Perun, V. S., Schwartz, M. J., Stek, P. C., Thurstans, R. P., Boyles, M. A., Chandra, K. M.,  
1614 Chavez, M. C., Chen, G. S., Chudasama, B. V., Dodge, R., Fuller, R. A., Girard, M. A., Jiang,  
1615 J. H., Jiang, Y., Knosp, B. W., Labelle, R. C., Lam, J. C., Lee, A. K., Miller, D., Oswald, J. E.,  
1616 Patel, N. C., Pukala, D. M., Quintero, O., Scaff, D. M., Vansnyder, W., Tope, M. C., Wagner,  
1617 P. A., and Walch, M. J.: The Earth Observing System Microwave Limb Sounder (EOS MLS)  
1618 on the Aura Satellite, *IEEE T. Geosci. Remote*, 44, 1075–1092, 2006.
- 1619 Yarwood, G., Rao, S., Yocke, M., and Whitten, G.: Updates to the carbon bond chemical  
1620 mechanism: CB05. Final report to the US EPA, EPA Report Number: RT-0400675, available  
1621 at: [www.camx.com](http://www.camx.com), last access: 1 July 2014, 2005.

1622

	<b>MACCRA</b>	<b>CAMSiRA</b>
Period	01/2003–12/2012	01/2003–12/2015
Horizontal resolution	80 km (T255)	110 km (T159)
Vertical resolution	60 layers from surface to 0.1 hPa	as MACCRA
Anthropogenic Emissions	MACCity (trend: ACCMIP + RCP 8.5), AEROCOM	as MACCRA & CO emission upgrade (Stein et al., 2014)
Chemistry module	MOZART-3	C-IFS CB05 / Cariolle ozone
Assimilated observations	CO MOPITT (V4) & IASI (from 2008 onwards)	MOPITT (V5) & updated error statistics (Inness et al., 2015)



Assimilated ozone observations	SBUV-2, OMI, MLS, GOME-2, SCIAMACHY, GOME, MIPAS (01/2003–06/2004)	as MACCRA & MIPAS (2003–2012)
Ozone MLS bias correction	On	Off
Assimilated AOD observations	MODIS (Aqua and Terra) + VarBC	as MACCRA
Fire emissions	GFED (2003–2008) and GFAS v0 (2009–2012 )	GFAS v 1.2 (2003–2015)
IFS model version	CY36R2	CY40R2
Assimilation method and model	ECMWF 4D-VAR	as MACCRA
Meteorological observations assimilated	ECMWF RD setup (satellites, sondes, surface )	as MACCRA

1623

*Table 1 Important commonalities and differences between MACCRA and CAMSiRA*

1624

1625





1626

Instrument	References	Version	Period	Type	Data usage
MOPITT Terra	Deeter et al. (2011)	V5 TIR NRT	20030101– 20121218 From 20121219	CO TC	65N–65S QC=0
GOME ERS-2	Munro et al. (1998)		20030101– 20030531	O3 profile	80N–80S SOE>15, QC=0
GOME-2 Metop A	Hao et al. (2014)	NRT GDP4.4 NRT GDP4.7	20120901– 20130714 From 20130715	O3 TC	SOE>10 QC=0
GOME-2 Metop B	Hao et al. (2014)	NRT GDP4.7	From 20140101	O3 TC	SOE>10 QC=0
MIPAS Envisat	von Clarmann et al. (2003, 2009)	NRT CCI	20030101– 20040326 20050127– 20120331	O3 profile	QC=0
MLS Aura	Froidevaux et al. (2008)	V2 NRT V3.4	20040808– 20121231 From 20130107	O3 profile	QC=0
OMI Aura	Liu et al. (2010)	V003 NRT	20041001– 20121231 From 20130101	O3 TC	SOE>10 QC=0
SBUV/2 NOAA- 16	Bhartia et al. (1996)	V8	20040101– 20081020	O3 PC 6 layers	SOE>6 QC=0
SBUV/2 NOAA- 17	Bhartia et al. (1996)	V8	20030101– 20121130	O3 PC 6 layers	SOE>6 QC=0
SBUV/2 NOAA- 18	Bhartia et al. (1996)	V8	20050604– 20121217	O3 PC 6 layers	SOE>6 QC=0
SBUV/2 NOAA- 19	Bhartia et al. (1996)	V8	From 20090100	O3 PC 6 layers	SOE>6 QC=0
SCIAMACHY Envisat	Eskes et al. (2012)	CCI	20030101– 20120408	O3 TC	SOE>6 QC=0
MODIS / Terra	Remer et al. (2005)	Col.5 NRT Col.5	20030101– 20080731 From 20080801	AOD 550nm	70N–70S
MODIS / Aqua	Remer et al. (2005)	Col.5 NRT Col.5	20030101– 20080731 From 20080801	AOD 550nm	70N–70S

1627

Table 2 Assimilated satellite observations in CAMS*i*RA



1628

Area	Coordinates
North America	165°W–55°W, 25°N–75°N
Europe	10°W–45°E, 38°N–70°N
East Asia	90°E–150°E/10°N–55°N
South America	82°W–30°W/40°S–15°N
Tropical Africa	15°W–55°E/10°S–20°N
Northern Africa	15°W–55°E/20°N–35°N
Maritime South East Asia	90°E–150°E/10°S–10°N
Tropics	23°S–23°N
Arctic	60°N–90°N
Antarctica	90°S–60°S
NH mid latitudes	30°N–60°N
SH mid-latitudes	60°S–30°S

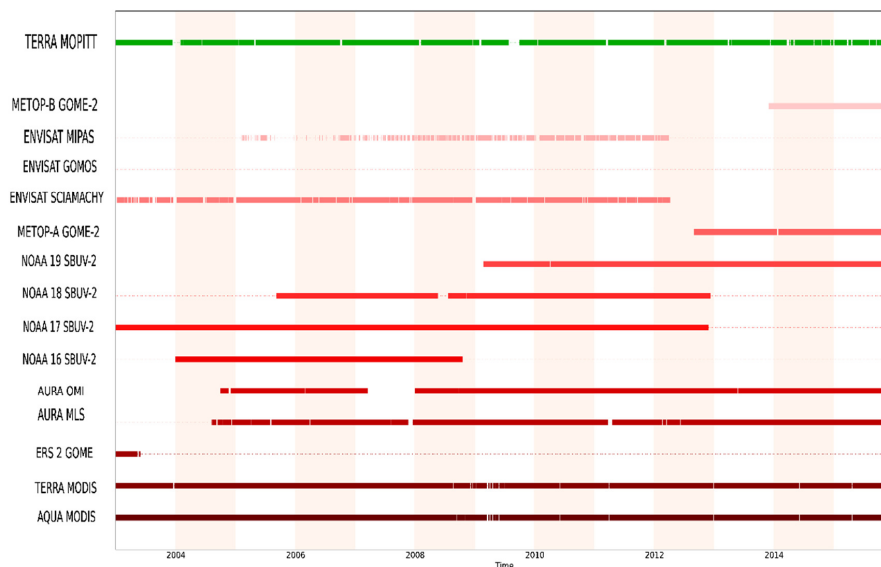
1629

*Table 3 Coordinates of regions*

1630

1631

1632



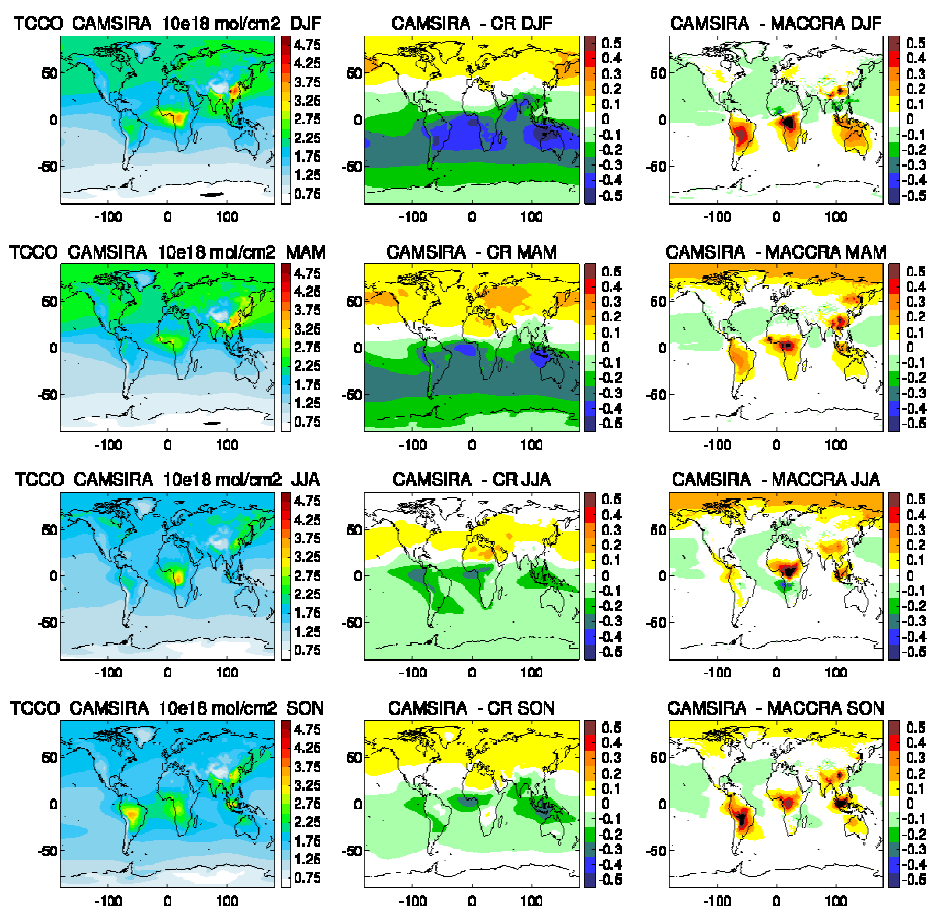
1633

1634

1635

*Figure 1 Time line of assimilated AC satellite retrievals from different instruments assimilated in CAMSiRA (see Table 2)*

1636



1637

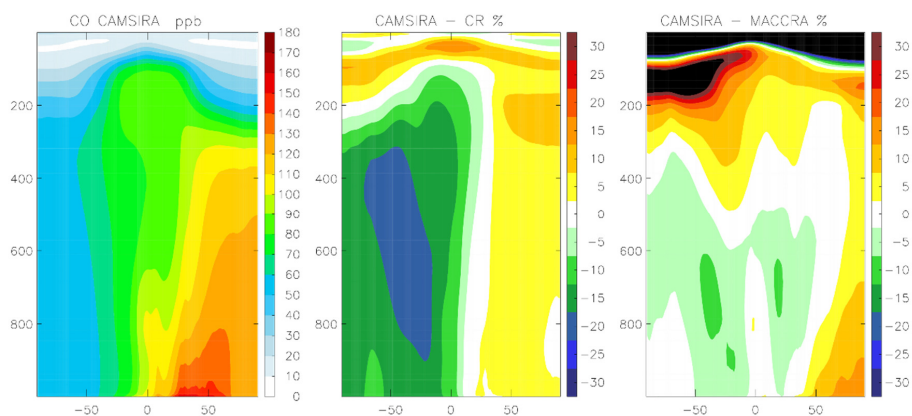
1638

1639

1640

Figure 2 Average TC CO ( $10^{18}$  molecules/cm<sup>2</sup>) of CAMSiRA (2003–2015, left) and difference against CR (2003–2015, middle) and MACCRA (2003–2012, right) for the seasons DJF (row 1), MAM (row 2), JJA (row 3) and SON (row 4).

1641



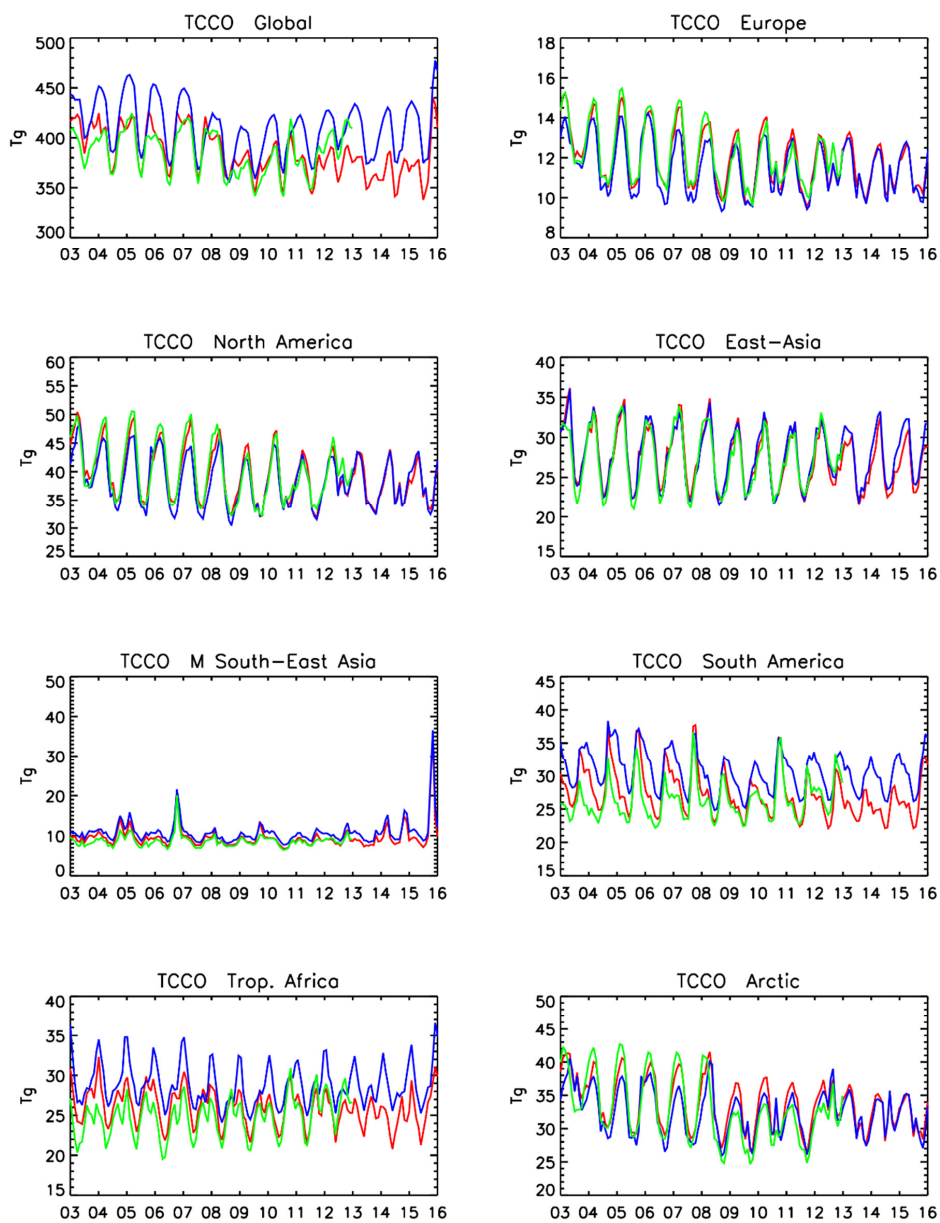
1642

1643

1644

*Figure 3 Zonally averaged CO cross section of CAMSiRA (ppb) (2003–2015, left) and relative difference (%) against CR (2003–2015, middle) and MACCRA (2003–2012, right).*

1645



1646

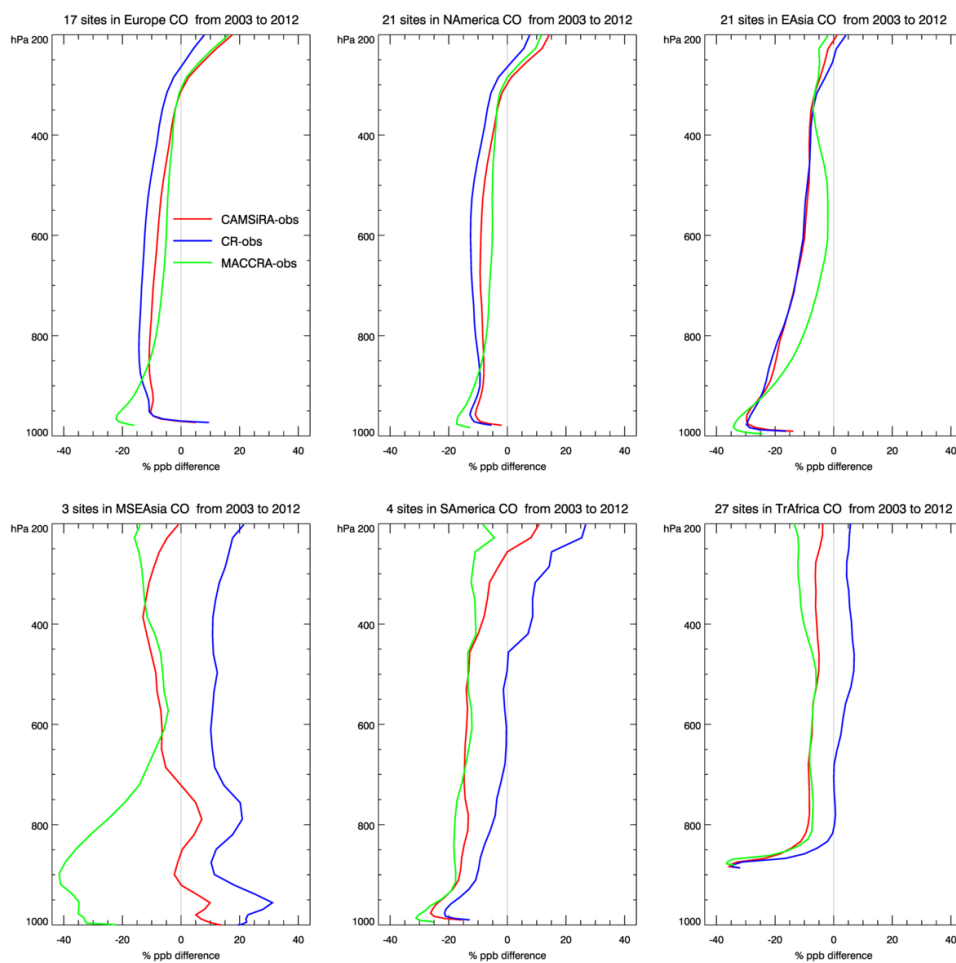
1647

1648

1649

Figure 4 Time series of monthly mean CO burden ( $T_g$ ) over different regions (see Table 3) for the period 2003–2015 from CAMSiRA (red), CR (blue) and MACCRA (green, 2003–2012).

1650



1651

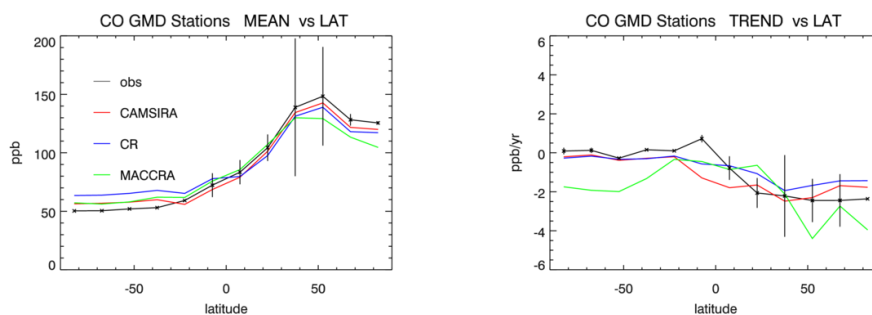
1652

1653

1654

*Figure 5 Average relative bias (%) in CO of CAMSiRA, MACCRA and CR against MOZAIC / IGAOS flight profiles averaged over different regions (see Table 3) for the period 2003–2012.*

1655



1656

1657

1658

1659

1660

*Figure 6 Zonal average of mean surface CO in ppb observed at NOAA-GMD stations (2003–2014) and values from CAMSiRA, CR and MACCRA (2003–2012) (left) and zonal median of linear trend in ppb/yr (right). The error bars indicate the range of the observed values.*

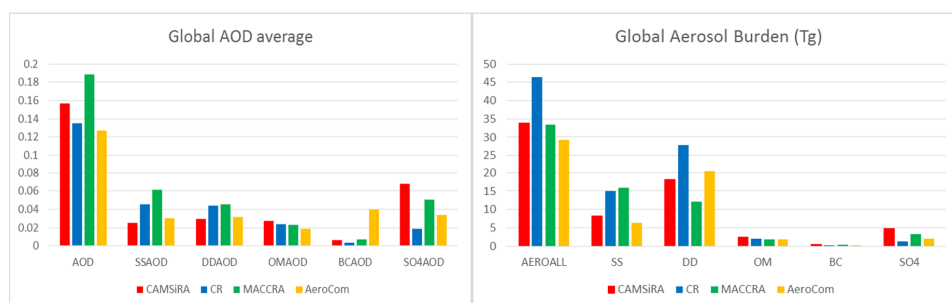
1661





1662

1663



1664

1665

1666

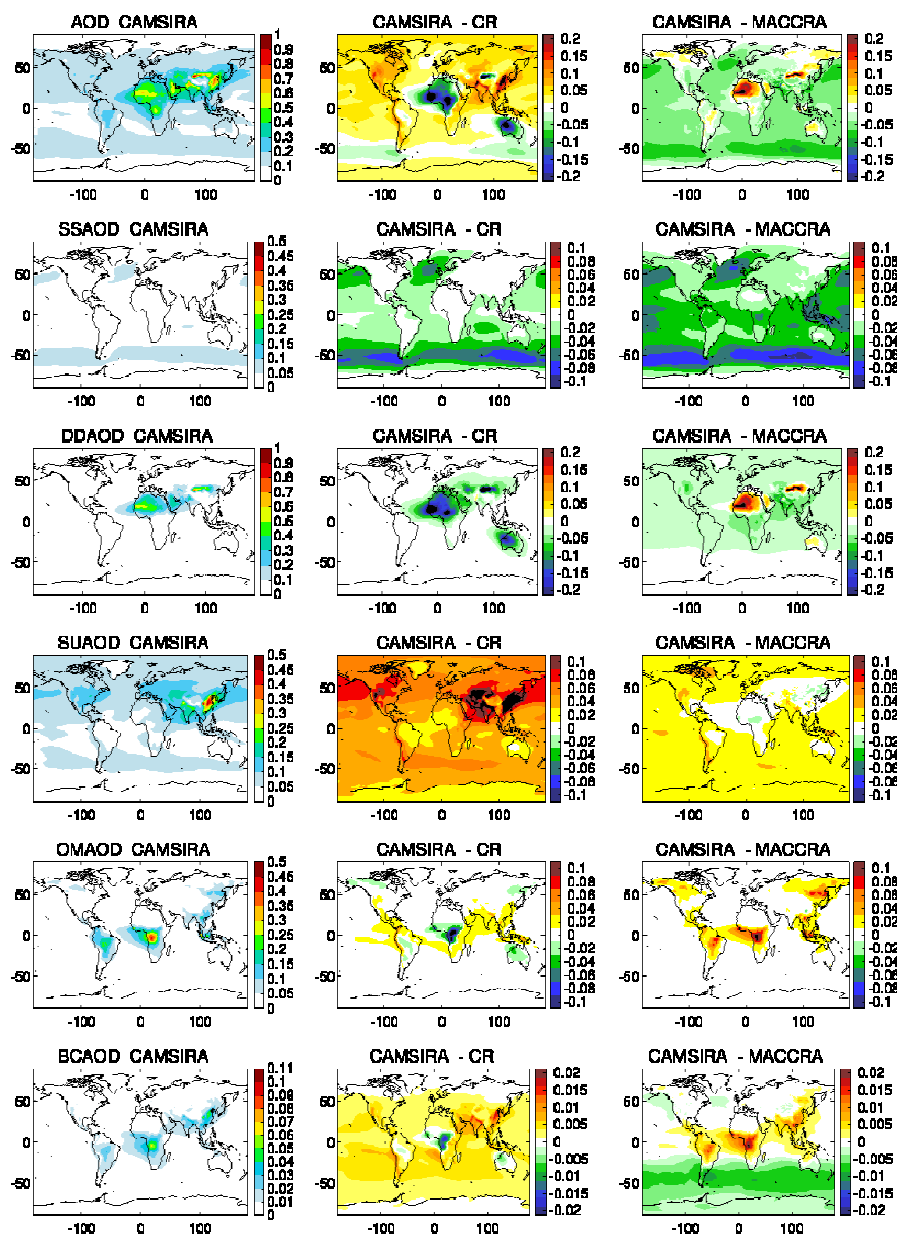
1667

1668

1669

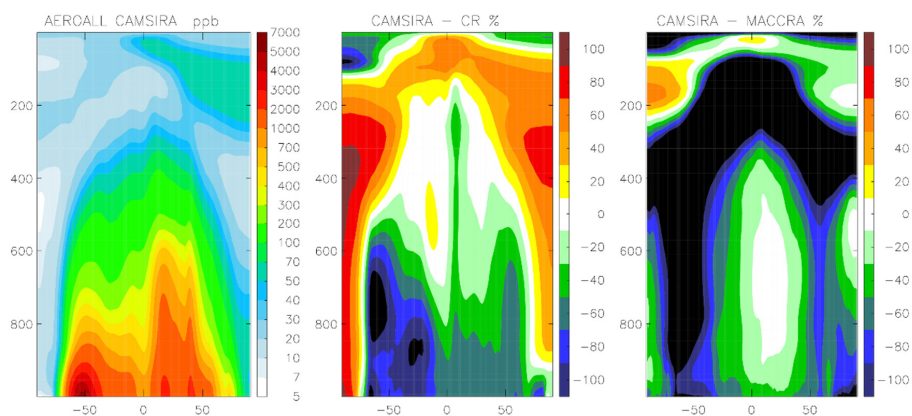
*Figure 7 Globally average of total AOD (550 nm) and species AOD (left) and global total and species and burden in Tg (right) of sea salt (SS), desert dust (DD), organic matter (OM), black carbon (BC) and sulphate aerosol (SO<sub>4</sub>) for CAMSiRA (red), CR (blue) and MACCRA (green) and the median of the AeroCom model inter-comparison (yellow, Kinne et al., 2006 and Textor et al., 2006).*

1670



1671  
 1672  
 1673  
 1674  
 1675

Figure 8 Total average AOD (row 1, scale max 1.0), AOD of desert dust (row 2, 1.0), sea salt (row 3, 0.5), sulphate (row 4, 0.5), organic matter (row 5, 0.5) and black carbon (row 6, 0.11) of CAMSiRA (average 2003–2015, left) and differences against CR (average 2003–2015, middle) and MACCRA (average 2003–2012, right).



1676

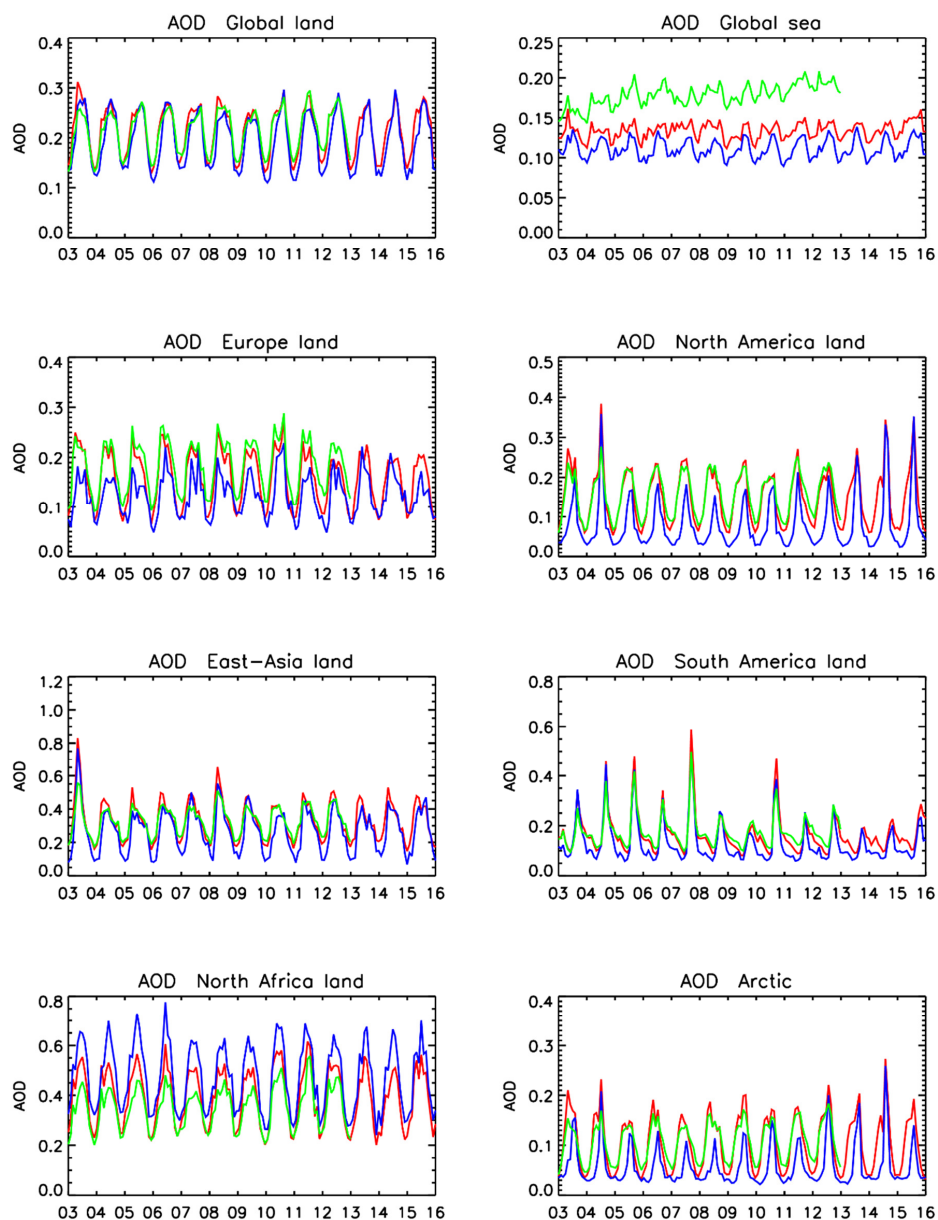
1677

1678

1679

*Figure 9 Zonally averaged total aerosol mass mixing ratio ( $10^{-9}$  kg/kg) of CAMSiRA (2003–2015, left) and relative difference (%) against CR (2003–2015, middle) and MACCRA (2003–2012, right).*

1680



1681

1682

1683

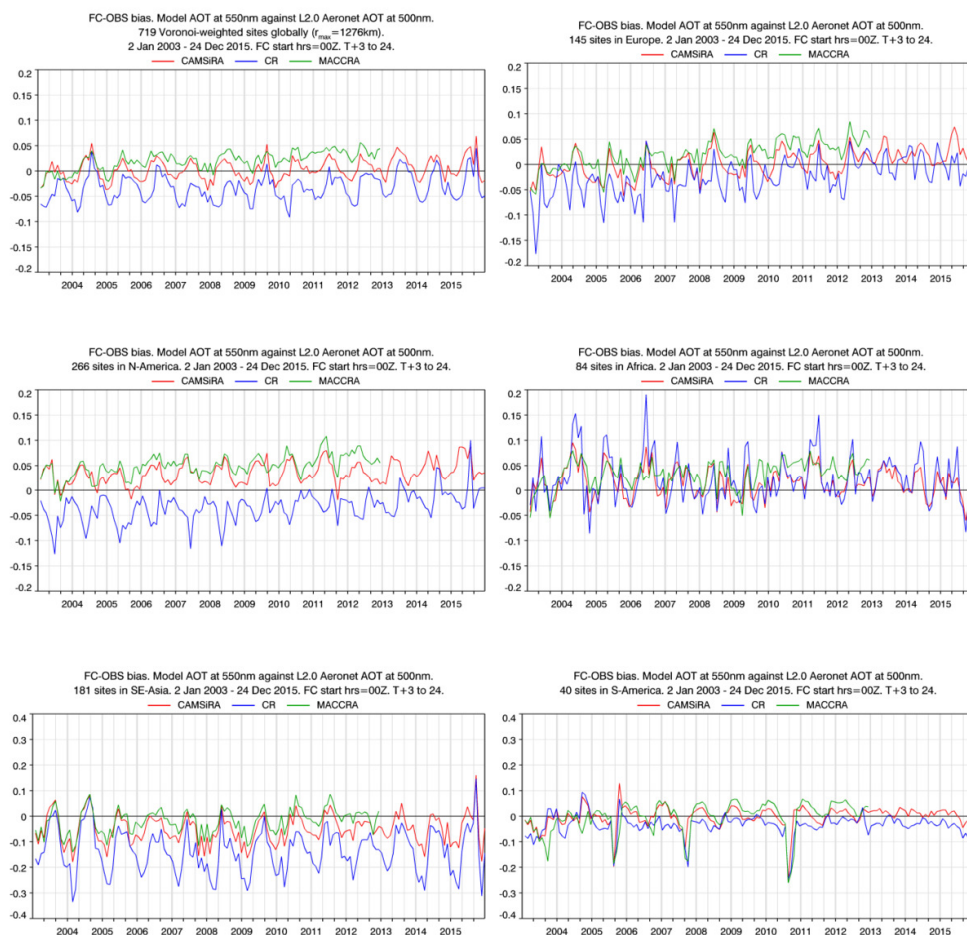
1684

*Figure 10 Time series of monthly mean AOD over the whole globe (land or seas points) and for different regions (see Table 3) for the period 2003–2015 from CAMSiRA (red), CR (blue) and MACCRA (green, 2003–2012).*

1685



1686



1687

1688

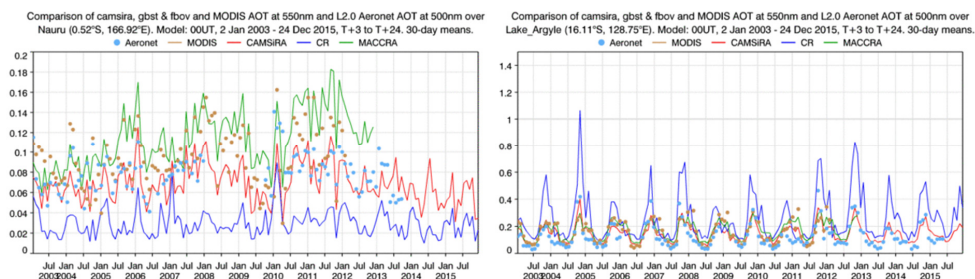
1689

1690

1691

*Figure 11 Time series of monthly mean bias against AERONET AOD observations averaged over the whole globe (top left), Europe (top right), North America (middle left), Africa (middle right), South East Asia (bottom left) and South America (bottom right) for CAMSiRA (red), CR (blue) and MACCRA (green).*

1692



1693

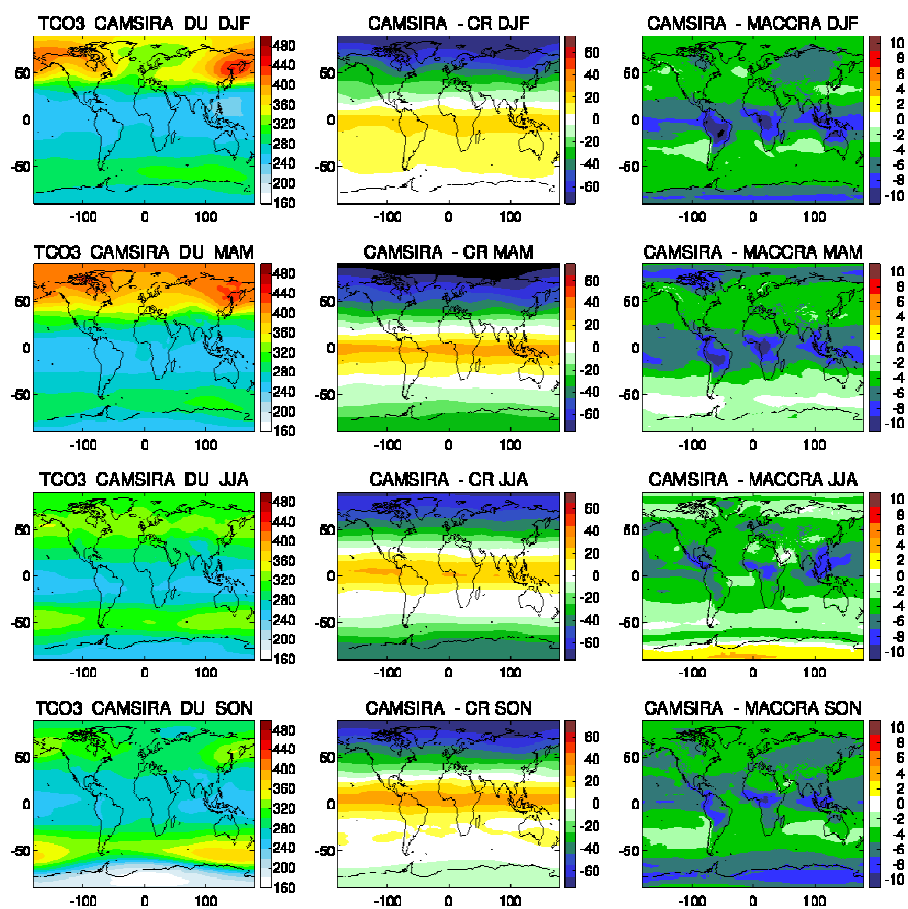
1694

1695

1696

*Figure 12 Time series of monthly mean AOD from AERONET observations (light blue dots), MODIS retrievals (brown dots) and from CAMSIRA (red), CR (blue) and MACCRA (green) at Nauru (left) and Lake Argyle (right).*

1697



1698

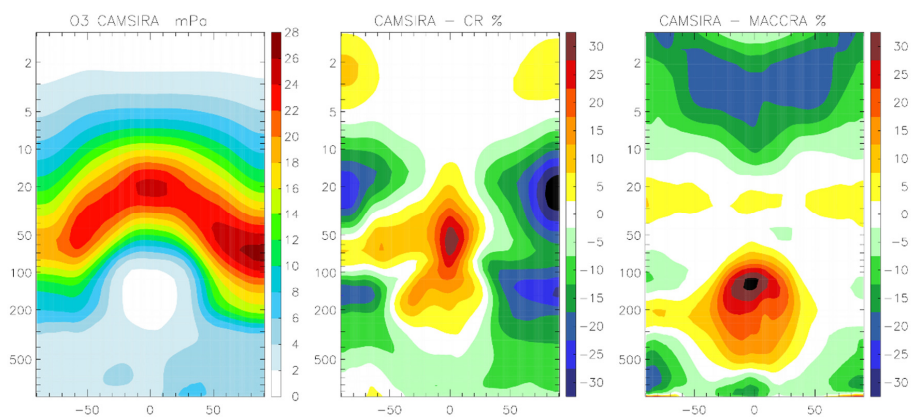
1699

1700

1701

*Figure 13 Seasonal averaged TC ozone (DU) from CAMSiRA (left), difference between CAMSiRA and CR (middle) and CAMSiRA and MACCRA (right, 2003–2012, different scale) for the seasons DJF (row 1) MAM (row 2), JJA (row 3) and SON (row 4).*

1702



1703

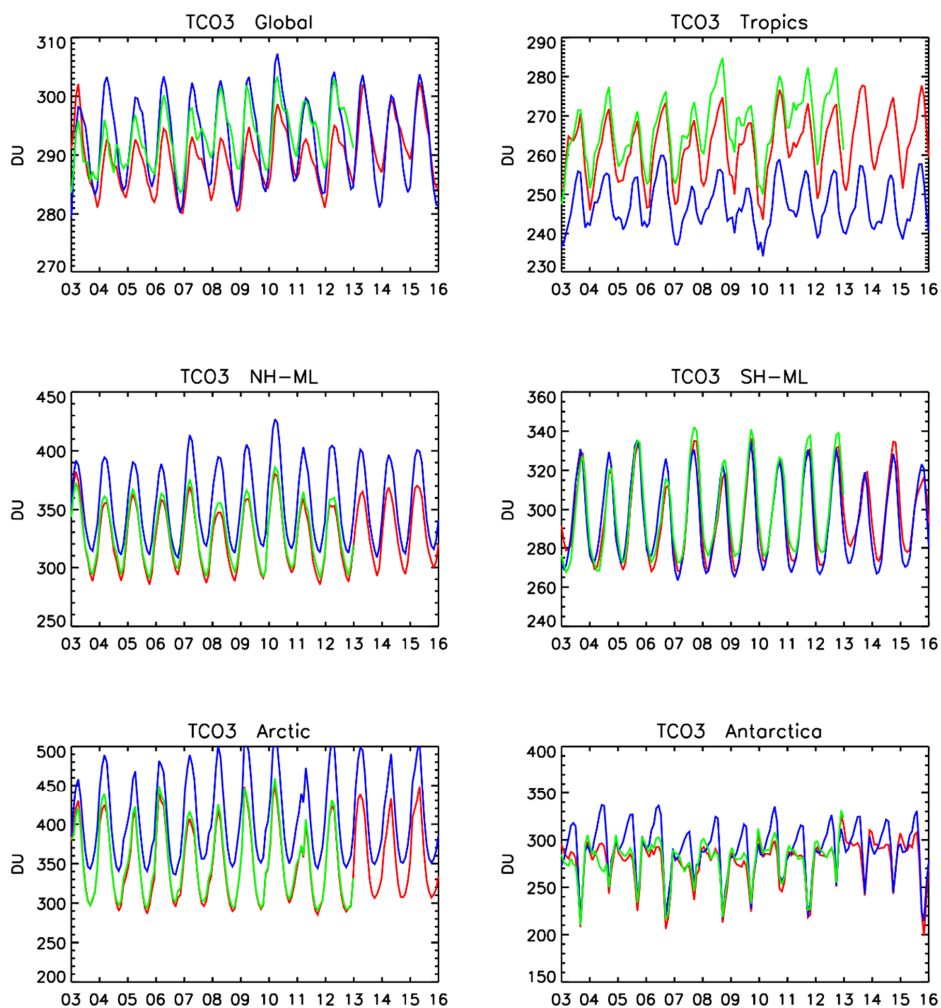
1704

1705

*Figure 14 Zonally averaged ozone partial pressure (mPa) of CAMSIRA (2003–2015, left) and relative difference (%) against CR (2003–2015, middle) and MACCRA (2003–2012)*

1706





1707

1708

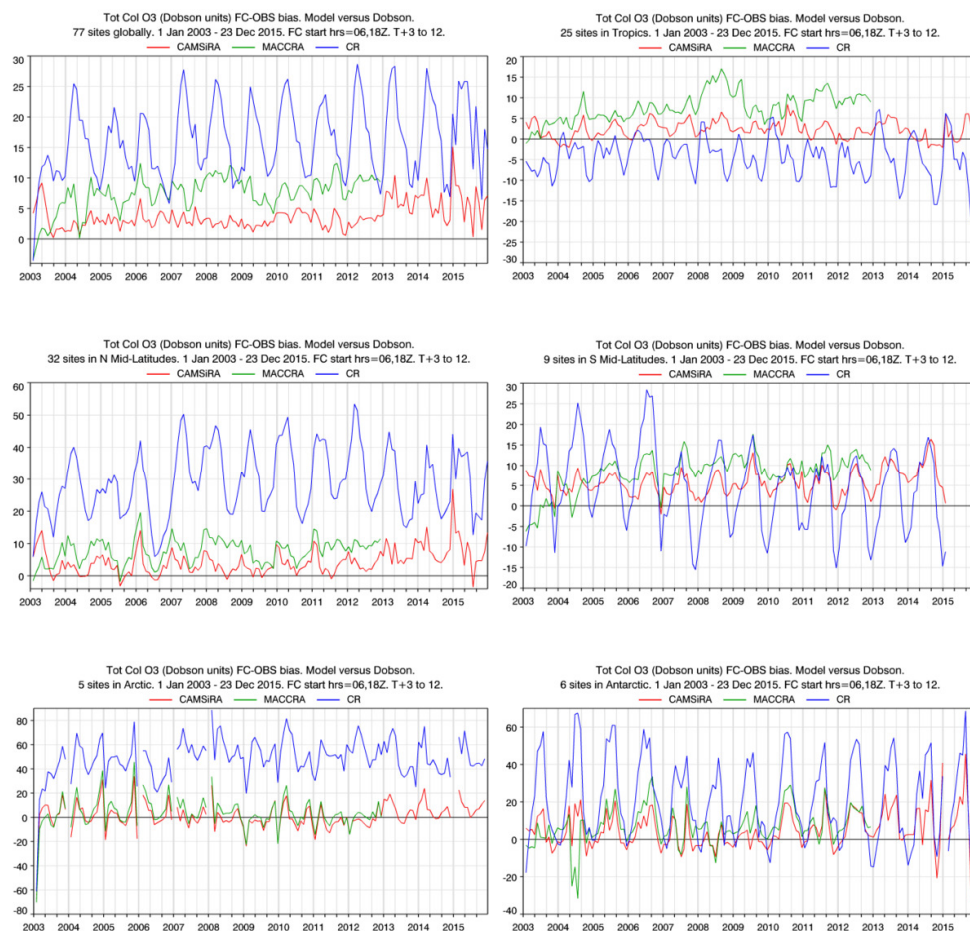
1709

Figure 15 Monthly ozone TC (DU) area averaged over different regions (see Table 3) from CAMSiRA (black), CR (blue) and MACCRA (green) for 2003–2015.

1710



1711



1712

1713

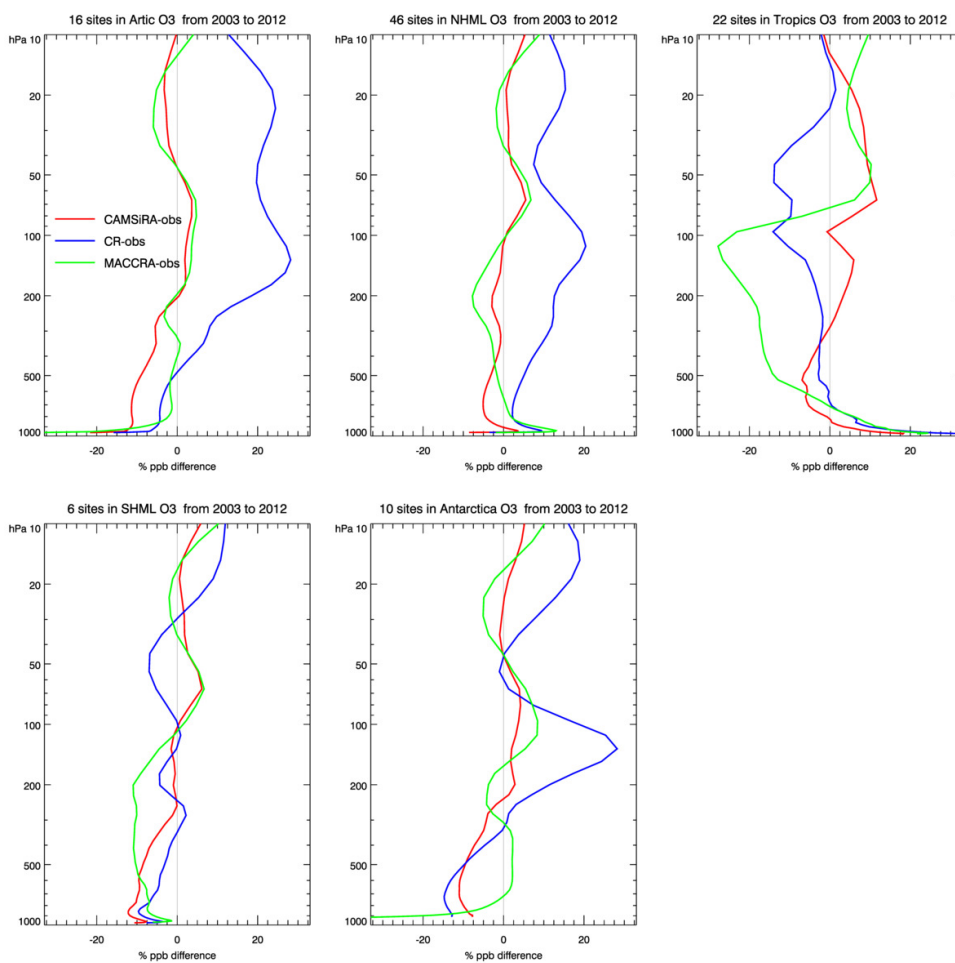
1714

1715

1716

*Figure 16 Time series of monthly mean bias in DU against WOUDC Dobson sun photometers for the globe (top left), the tropics (top right), NH mid-latitudes (middle left), SH mid-latitudes (middle right), the Arctic (bottom left) and Antarctica (bottom right) for CAMSiRA (red), CR (blue) and MACCRA (green).*

1717



1718

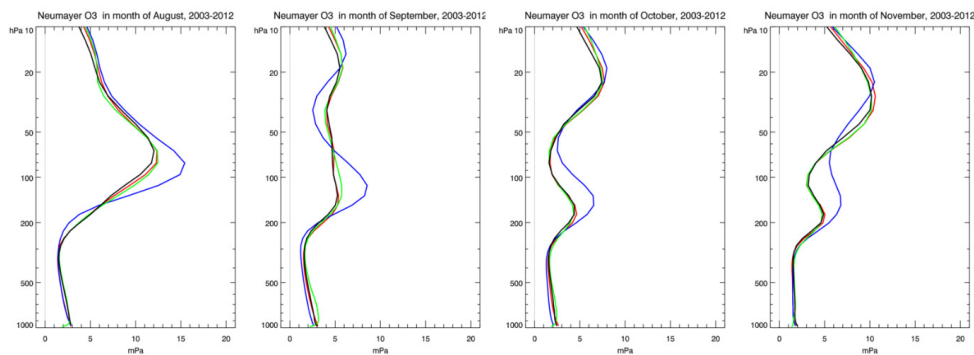
1719

1720

1721

*Figure 17 Mean relative bias of CAMSiRA (red), MACCRA (green) and CR (blue) against ozone sondes in the Arctic (top left), NH mid-latitudes (top middle), Tropics (top right), SH-mod-latitudes (bottom left) and Antarctica (bottom middle) for the period 2003–2012.*

1722



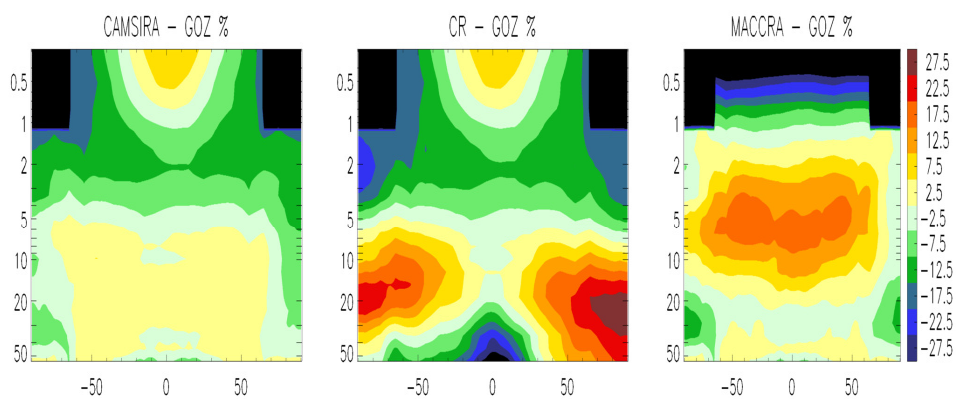
1723

1724

1725

*Figure 18 Monthly mean ozone profiles (mPa) at Neumayer Station from ozone sondes, of CAMSiRA (red), MACCRA (green) and CR (blue) for August to November (2003–20012).*

1726



1727

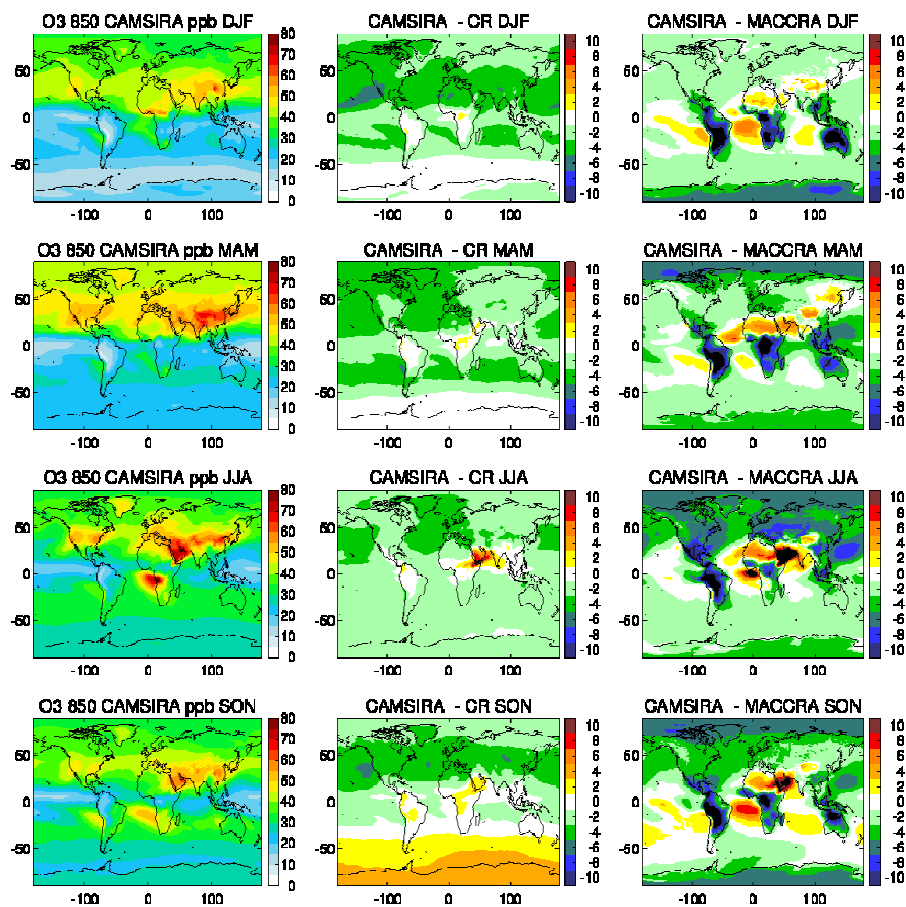
1728

1729

1730

*Figure 19 Cross sections (50–0.3 hPa) of the relative biases of zonally averaged ozone (%) of CAMSiRA (left), CR (middle) and MACCRA (right) against the GOZCARDS product (GOZ) for the period 2005–2012.*

1731



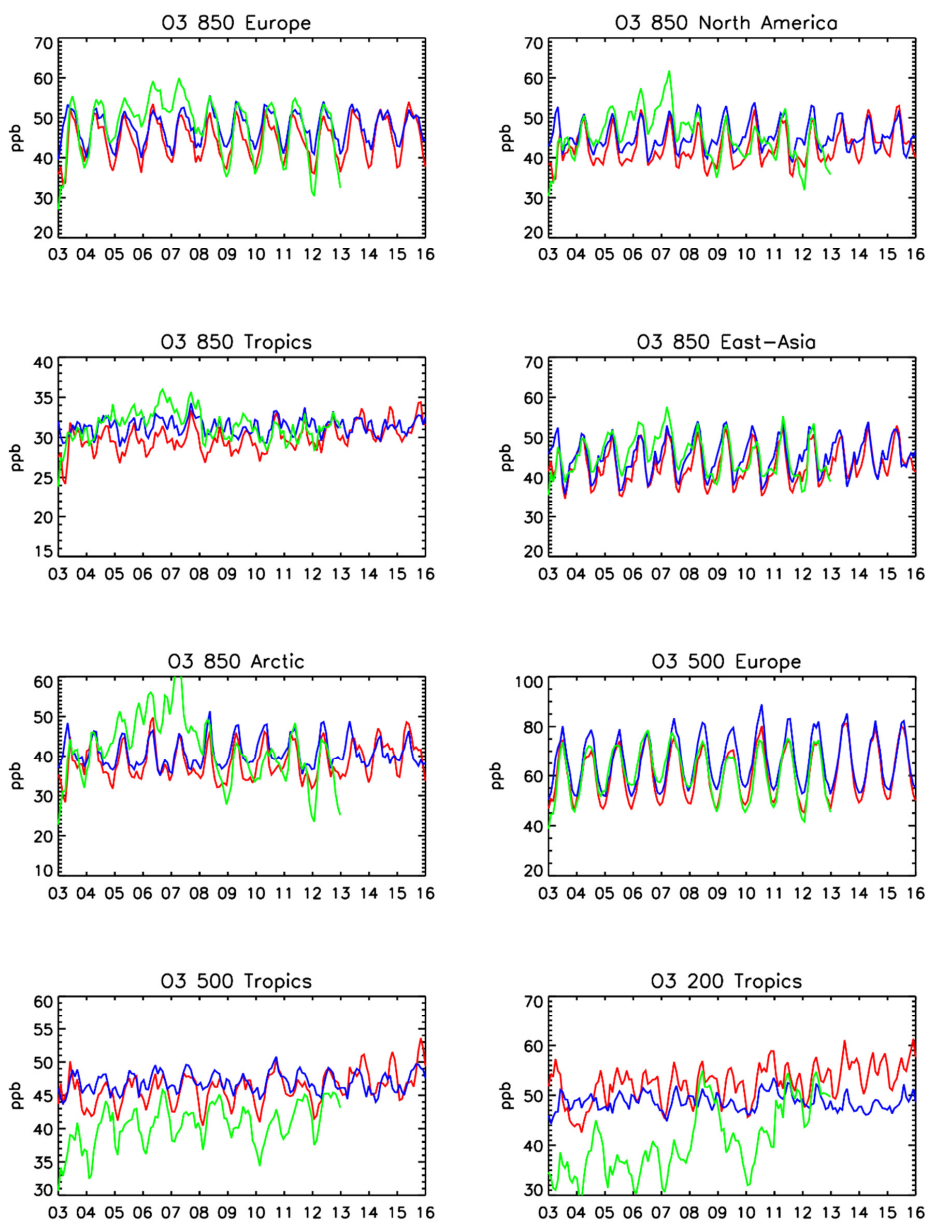
1732

1733

1734

1735

*Figure 20 Seasonal averaged ozone at 850 hPa (ppb) from CAMSiRA (left), difference between CAMSiRA and CR (middle) and CAMSiRA and MACCRA (right, 2003–2012) for the season DJF (row 1), MAM (row 2), JJA (row 3) and SON (row 4).*



1736

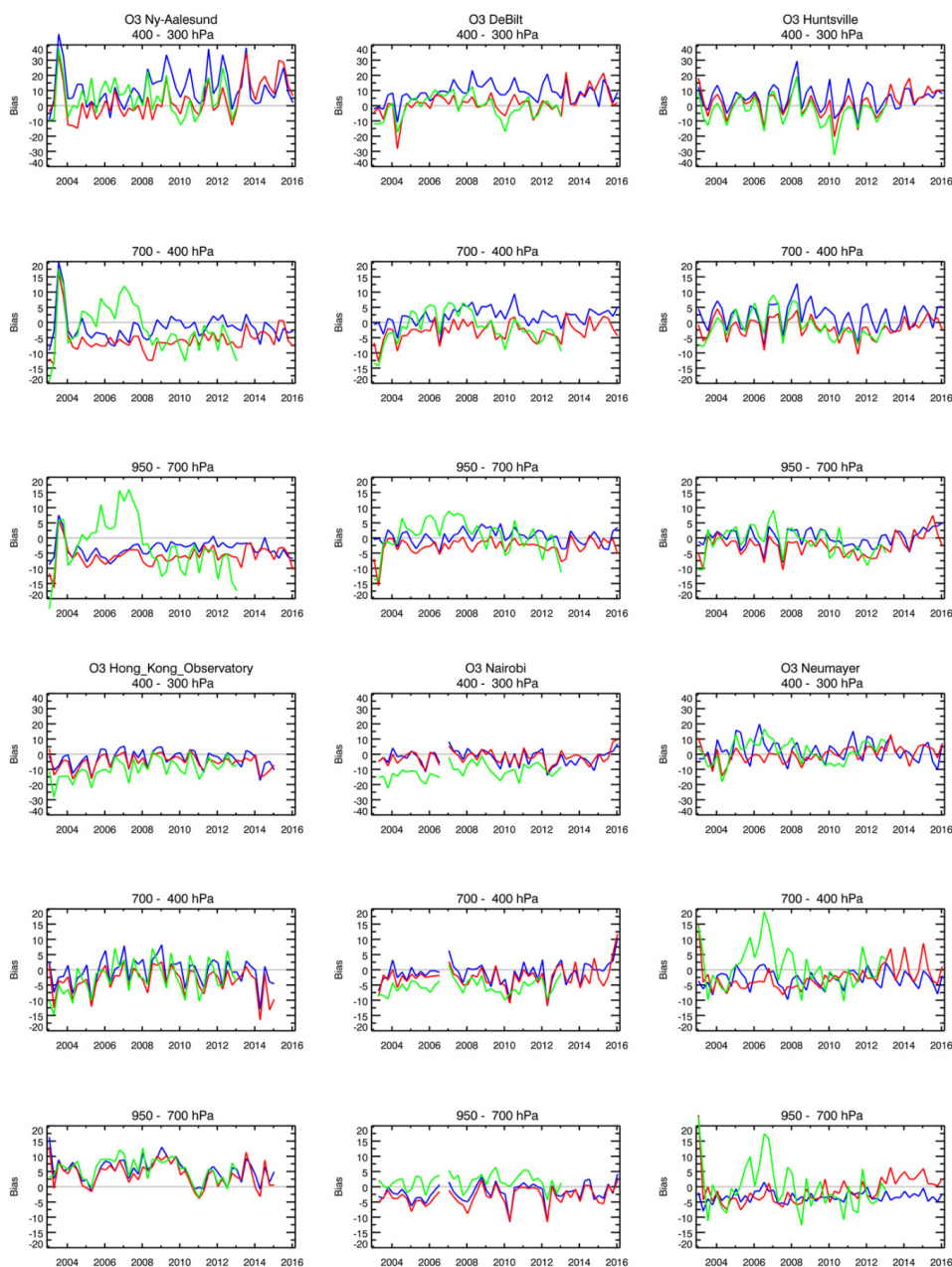
1737

1738

1739

Figure 21 Monthly ozone volume mixing ratio at 850, 500 and 200 hPa over different regions (see Table 3) from CAMSiRA (red), CR (blue) and MACCRA (green) for 2003–2015.

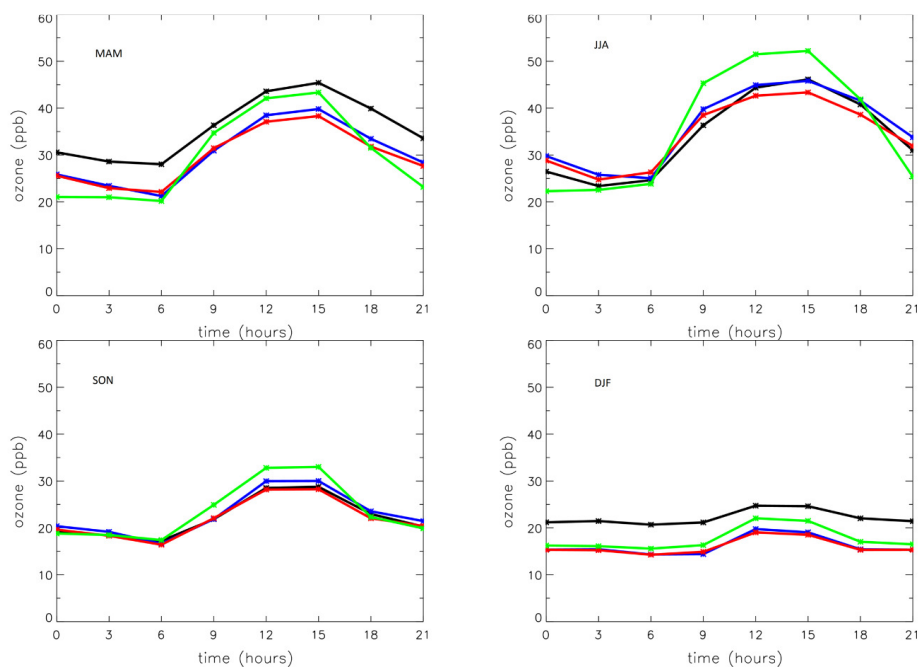
1740



1741  
1742  
1743  
1744  
1745

*Figure 22 Time series of seasonal mean ozone bias in ppb in the pressure ranges 950-700, 700-400 and 400-300 hPa against ozone sondes at Ny-Ålesund, DeBilt, Huntsville, Hong Kong Observatory, Nairobi and Neymayer station for CAMSiRA (red), CR (blue) and MACCRA (green).*





1746

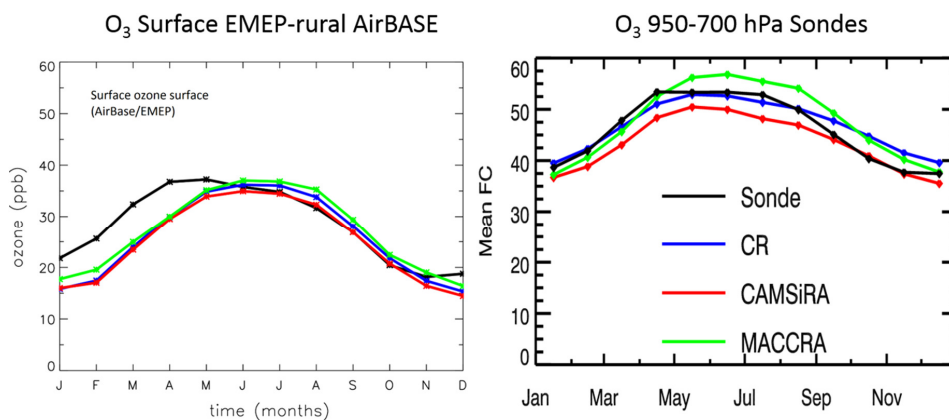
1747

1748

1749

*Figure 23 Average diurnal cycle of ozone at EMEP-AirBase stations in Europe (black) for the seasons MAM (top left), JJA (top right), SON (bottom left) and DJF (bottom right) for CAMSiRA (red), CR (blue) and MACCRA (green).*

1750



1751

1752

1753

1754

*Figure 24 Average seasonal cycle of surface ozone at EMEP-AirBase stations (left) and at European ozone sonde sites in the pressure range (950–700 hPa) for CAMSiRA (red), CR (blue) and MACCRA (green).*